GEMS & GEMOLOGY

SPRING 2012

VOLUME XLVIII

THE QUARTERLY JOURNAL OF THE GEMOLOGICAL INSTITUTE OF AMERICA

Emeralds from Northeastern Brazil

Diamantine: Coated Cubic Zirconia

Precision Measurement of Facet Angles

Vallerano Diamond from Ancient Rome

Radioactive Morganite

Because Public Education Happens At The Counter.

GIA's Retailer Support Kit and website

Download the GIA 4Cs App - Retailer Edition for iPad

New 4Cs app for retailers.
Download today at retailer.gia.edu

A $97.00 value, shipping and handling extra.

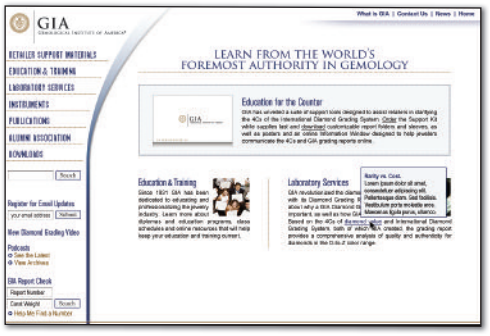

GIA's Retailer Support Kit has been developed to help sales associates educate the public about diamonds, the 4Cs, and thoroughly explain a GIA grading report. Take full advantage of all that GIA has to offer by visiting www.retailer.gia.edu

To order your FREE kit, log on to www.retailer.gia.edu

GIA®

GEMS & GEMOLOGY

Spring 2012
VOLUME 48, No. 1

pg. 3

pg. 29

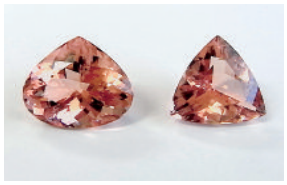

pg. 42

Editorial Staff

Editor-in-Chief
Jan Iverson
jan.iverson@gia.edu

Editor and Technical Specialist
Brendan M. Laurs
blaurs@gia.edu

Managing Editor
Justin Hunter
justin.hunter@gia.edu

Associate Editor
Stuart D. Overlin
soverlin@gia.edu

Editorial Assistant
Brooke Goedert

Editors, Lab Notes
Thomas M. Moses
Shane F. McClure

Editors, Book Reviews
Susan B. Johnson
Jana E. Miyahira-Smith

Contributing Editors
James E. Shigley
Andy Lucas

Editor-in-Chief Emeritus
Alice S. Keller

Customer Service
Norine Honea
(760) 603-7306
nhonea@gia.edu

Production Staff

Creative Director
Faizah Bhatti

Image Specialist
Kevin Schumacher

Multimedia Specialists
Joseph Kaus
Juan Zanahuria

Senior Illustrator
Peter Johnston

Production Supervisor
Richard Canedo

Video Producer
Pedro Padua

Editorial Review Board

Ahmadjan Abduriyim
Tokyo, Japan

Shigeru Akamatsu
Tokyo, Japan

Edward W. Boehm
Chattanooga, Tennessee

James E. Butler
Washington, DC

Alan T. Collins
London, UK

John L. Emmett
Brush Prairie, Washington

Emmanuel Fritsch
Nantes, France

Jaroslav Hyršl
Prague, Czech Republic

A. J. A. (Bram) Janse
Perth, Australia

E. Alan Jobbins
Caterham, UK

Mary L. Johnson
San Diego, California

Anthony R. Kampf
Los Angeles, California

Robert E. Kane
Helena, Montana

Lore Kiefert
Lucerne, Switzerland

Michael S. Krzemnicki
Basel, Switzerland

Thomas M. Moses
New York, New York

Mark Newton
Coventry, UK

George R. Rossman
Pasadena, California

Kenneth Scarratt
Bangkok, Thailand

James E. Shigley
Carlsbad, California

Christopher P. Smith
New York, New York

Wuyi Wang
New York, New York

Christopher M. Welbourn
Reading, UK

GEMS & GEMOLOGY

gia.edu/gandg

Subscriptions
Copies of the current issue may be purchased for $29.95 plus shipping. Subscriptions are $79.99 for one year (4 issues) in the U.S. and $99.99 elsewhere. Canadian subscribers should add GST. Discounts are available for group subscriptions, renewals, GIA alumni, and current GIA students. For institutional rates, contact the Managing Editor. Subscriptions include *G&G*'s monthly gemological e-newsletter, the *G&G eBrief*.

To purchase subscriptions and single issues (print or PDF), visit store.gia.edu or contact Customer Service.

PDF versions of individual articles and sections from Spring 1981 forward can be purchased at gia.metapress.com for $12 each. Visit gia.edu/gandg for free online access to the 1934–2011 subject and author indexes and all 1934–1980 issues.

Database Coverage
Gems & Gemology's five-year impact factor (for 2005–2009) is 1.737, according to the 2010 Thomson Reuters Journal Citation Reports (issued June 2011). *Gems & Gemology* is abstracted in Thomson Reuters products (Current Contents: Physical, Chemical & Earth Sciences and Science Citation Index—Expanded, including the Web of Knowledge) and other databases. For a complete list of sources abstracting *G&G*, go to gia.edu/gandg.

Manuscript Submissions
Gems & Gemology welcomes the submission of articles on all aspects of the field. Please see the Guidelines for Authors at gia.edu/gandg or contact the Editor. Letters on articles published in *Gems & Gemology* are also welcome.

Copyright and Reprint Permission
Abstracting is permitted with credit to the source. Libraries are permitted to photocopy beyond the limits of U.S. copyright law for private use of patrons. Instructors are permitted to photocopy isolated articles for noncommercial classroom use without fee. Copying of the photographs by any means other than traditional photocopying techniques (Xerox, etc.) is prohibited without the express permission of the photographer (where listed) or author of the article in which the photo appears (where no photographer is listed). For other copying, reprint, or republication permission, please contact the Editor.

Gems & Gemology is published quarterly by the Gemological Institute of America, a nonprofit educational organization for the gem and jewelry industry.

Postmaster: Return undeliverable copies of *Gems & Gemology* to GIA, The Robert Mouawad Campus, 5345 Armada Drive, Carlsbad, CA 92008.

Our Canadian goods and service registration number is 126142892RT.

Any opinions expressed in signed articles are understood to be opinions of the authors and not of the publisher.

About the Cover

For decades, Brazil has been one of the world's major sources of fine emerald. In this issue, Dr. J. C. Zwaan and coauthors characterize the emerald produced in the Fazenda Bonfim region of northeastern Brazil since 2006. The jewelry shown on the cover features Brazilian emerald with diamond accents, set in 18K platinum. The necklace contains 26.60 total carats of emeralds, the bracelet 6.50 carats, and the earrings 5.22 carats combined. Courtesy of Real Gems Inc., New York. Photo by Robert Weldon.

Printing is by Allen Press, Lawrence, Kansas.
GIA World Headquarters The Robert Mouawad Campus 5345 Armada Drive Carlsbad, CA 92008 USA

© 2012 Gemological Institute of America All rights reserved.

ISSN 0016-626X

FSC www.fsc.org MIX Paper from responsible sources FSC® C006300

TURNING A NEW PAGE
IN THE DIGITAL AGE

Spring is a time of rebirth and renewal, and that certainly holds true for the Spring 2012 issue of *G&G*. With this edition, we are launching a free application for iPad tablets. This app will complement our print quarterly with enhanced digital content. You can tap on interviews with industry experts, videos spanning the world of gems, detailed slideshows, and other online exclusives. To download the app, go to the iTunes App Store at www.apple.com/ipad/from-the-app-store.

Other tablet apps and a desktop version will be introduced over the next 12 months, so that we deliver this new content to as many devices as possible. Stay tuned.

We think this is an ideal issue to showcase the new app. It leads with Dr. J. C. "Hanco" Zwaan's feature on emeralds from a recently discovered deposit in northern Brazil. As a special supplement to that article, Andy Lucas overviews the Brazilian emerald industry. Next, Dr. Jim Shigley and coauthors test the properties and durability of a recent diamond imitation, coated colorless cubic zirconia. A team led by Dr. Andy Shen finds new applications for a classic two-circle reflecting goniometer. Continuing the theme of old versus new are studies of a diamond ring from ancient Rome and artificially irradiated morganites. The issue contains another full slate of Lab Notes and Gem News International dispatches, including *G&G*'s coverage of this year's Tucson shows.

Inside you'll also find two of our annual reader participation features: the *G&G* Challenge quiz, where you can test your gemological knowledge, and the results of this year's Dr. Edward J. Gübelin Most Valuable Article Awards.

Download G&G's new iPad app to see interviews, videos spanning the world of gems, slideshows, and more.

Because access to *G&G*'s new app is completely free, we will no longer sell print + online subscriptions. That means a one-year print subscription is now available for only $79.99 in the U.S. and $99.99 elsewhere, with a $10 discount for renewals and GIA students and alumni. If you recently paid for a print + online subscription, we will reimburse you the difference—or apply it toward a renewal—on a prorated basis. There's never been a better time to subscribe.

I urge you to download the free app and see our new digital content for yourself. And be sure to tell us what you think.

Cheers,

Jan Iverson | Editor-in-Chief | jan.iverson@gia.edu

EMERALDS FROM THE FAZENDA BONFIM REGION, RIO GRANDE DO NORTE, BRAZIL

J. C. (Hanco) Zwaan, Dorrit E. Jacob, Tobias Häger, Mário T. O. Cavalcanti Neto, and Jan Kanis

In 2006, emeralds were discovered in the Fazenda Bonfim region of northeastern Brazil. Emerald mineralization occurs in association with small recrystallized pegmatitic bodies hosted by metamorphosed ultramafic rocks within the Santa Monica Shear Zone. Prospecting and exploration have been carried out in a few small pits and tunnels, producing emerald crystals with transparent areas that typically range between 2 and 5 mm. Polished samples typically show a saturated bluish green color with a medium-light to medium tone. The most common internal features are partially healed fissures with two-phase (liquid-gas) fluid inclusions and a variety of fine, parallel-oriented growth tubes. The emeralds contain moderate amounts of the chromophore elements Cr and Fe, and traces of V; they also show relatively high K and low Li. FTIR spectroscopic features are consistent with alkali-bearing emeralds that contain considerable CO_2 and a small amount of deuterated water. Emeralds from Fazenda Bonfim can be distinguished from those of other schist- and pegmatite-related commercial deposits.

Brazil is an important emerald producer. Well-known deposits occur in the states of Minas Gerais (Belmont, Piteiras, and Capoeirana—see Hänni et al., 1987; Epstein, 1989; Souza et al., 1992; Kanis, 2002; Rondeau et al., 2003); Bahia (Socotó and Carnaíba—see Schwarz 1990b; Eidt and Schwarz, 1988; Giuliani et al., 1990; Giuliani et al., 1997); and Goiás (Santa Terezinha—see Cassedanne and Sauer, 1984; Schwarz 1990a; Giuliani et al., 1990 and 1997). In the northeastern part of Brazil, emeralds are known from near Tauá in Ceará State, but they are not of high quality (Schwarz et al., 1988).

In Rio Grande do Norte State, rare-element mineralized granitic pegmatites have been known since the pioneering work of Johnston (1945) and Rolff (1946) in the Borborema Pegmatitic Province. In 2006, a team led by one of the present authors discovered emeralds in the Fazenda Bonfim region (figure 1; Cavalcanti Neto and Barbosa, 2007). The team was hired by Emprogeo Ltd. (Natal, Brazil) to explore for chromium, nickel, and platinum mineralization associated with ultramafic rocks, which were known to be present but had never been properly mapped. Emeralds were found in an area where geologists had previously focused on gold and rare-element mineralization. Several mines in this region (near the municipality of Lajes) had produced beryl and/or columbite-tantalite from pegmatites, but without any attention to the potential of ores related to ultramafic rocks.

After the discovery of emeralds in the Fazenda Bonfim region, Mineração Vale Verde Ltd. (registered in June 2006) acquired the mining rights from Emprogeo Ltd. Exploration of the area, which comprises nearly 656 hectares, started in August 2006. Mineração e Comércio Itaobi Ltda. also owns several licenses close to this area, and Mineração Santo Expedito Ltda. is the holder of a nearby gold, tungsten, and bismuth mining concession. All have invested heavily in mineral exploration (sampling, drilling, mapping, and geochemical surveys). Despite these efforts and promising early results, the emerald mine has not yet begun production.

See end of article for About the Authors and Acknowledgments.
GEMS & GEMOLOGY, Vol. 48, No. 1, pp. 2–17,
http://dx.doi.org/10.5741/GEMS.48.1.2.
© 2012 Gemological Institute of America

Figure 1. A limited amount of emeralds have so far been produced from the Fazenda Bonfim region in Brazil's Rio Grande do Norte State. The faceted stones shown here weigh 1.29–1.92 ct, and the cabochon weighs 3.89 ct. Photo by Robert Weldon.

Gemological properties of faceted light to dark green emeralds weighing up to 10 ct that were reportedly from this area were briefly described by Milisenda (2007). The present article characterizes the gemological properties of the emeralds from Fazenda Bonfim in detail and introduces chemical data. Information on the geology and mining was gathered by authors JCZ and JK over the course of a seven-day visit to the Fazenda Bonfim mining area in July 2009, and updated information on the situation at the deposit was supplied by Mineração Vale Verde Ltd.

LOCATION AND ACCESS

The Fazenda Bonfim region lies west of Natal, the state capital of Rio Grande do Norte, between the municipalities of São Tomé, Caiçara do Rio do Vento, and Lajes. The emerald deposit is located near the Bonfim gold-tungsten mine (figure 2), at coordinates 05°50.45′S, 036°07.10′W and an elevation of ~420 m. From Natal, the workings can be reached by driving about 95 km west to Caiçara do Rio do Vento, then another 6 km west on a paved road. A dirt track then proceeds about 18 km south to the mining area.

Figure 2. The emerald deposit in the Fazenda Bonfim region is located southwest of the village of Caiçara do Rio do Vento.

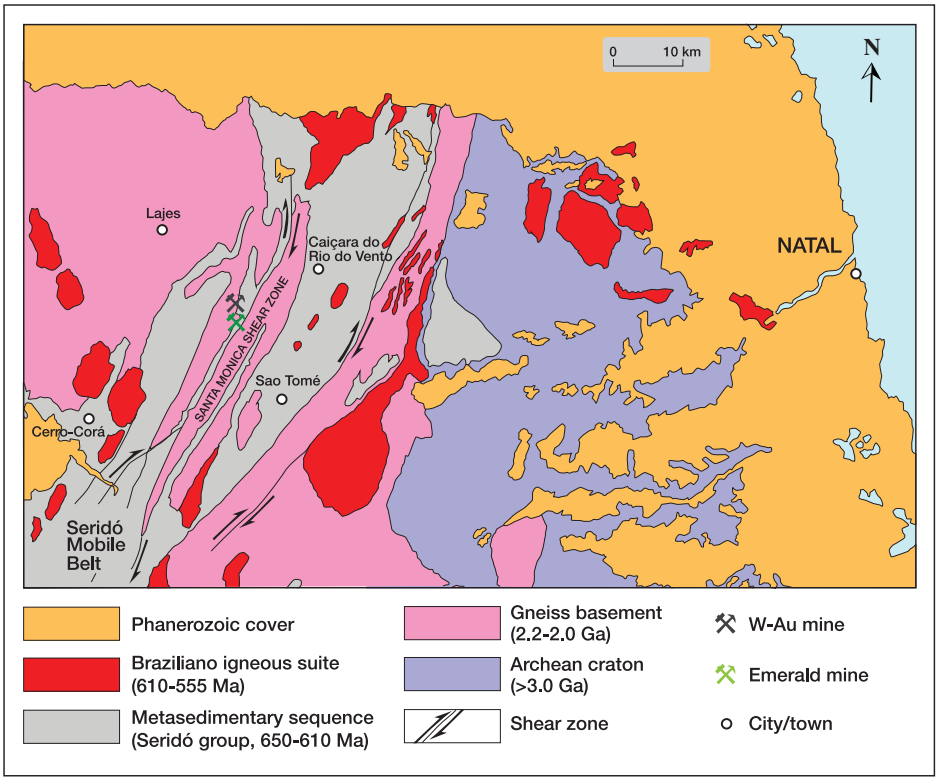

Figure 3. This simplified geological map shows the Seridó Mobile Belt in the northern segment of the Borborema Province, northeastern Brazil. The emerald deposit is located in the basement gneiss, close to the Bonfim gold-tungsten mine, which is hosted by metasedimentary rocks. Modified after Angelim et al. (2006) and Souza Neto et al. (2008).

GEOLOGY

The emerald deposit is situated in the Seridó Mobile Belt (figure 3), which is dominated by continental-scale strike-slip shear zones trending northeast to north-northeast. The rocks consist of basement gneiss, a metasedimentary sequence called the Seridó Group, and the Brasiliano igneous suite (Souza Neto et al., 2008). The basement gneiss comprises metamorphosed (migmatitic) igneous rocks of tonalitic to granitic composition and minor metabasic lenses. The Seridó Group consists of marble, gneiss, quartzite, metaconglomerate, and mica schist. The Brasiliano igneous suite includes porphyritic and fine-grained granites with minor aplites and pegmatites that are widely distributed. The granitoid rocks have U-Pb zircon ages of 610–555 Ma and were intruded during the Brasiliano orogeny (610–530 Ma), while the pegmatite bodies are constrained by ages between 510–480 Ma (U-Pb dating of uraninite and columbite) and 523 Ma (average Ar/Ar date of biotite from the pegmatites; Souza Neto et al., 2008).

Figure 4. Emeralds at the Fazenda Bonfim deposit occur in association with recrystallized pegmatitic bodies that intruded a sheared succession of talc, talc-amphibole, and biotite±amphibole schists, adjacent to a granitic gneiss (the strongly weathered unit at the top). A small recrystallized pegmatite is visible on the left side, in the biotite schist. Photo by J. C. Zwaan.

In the Seridó Mobile Belt, more than 700 mineralized granitic pegmatites occur in an approximately 15,000 km^2 area. These pegmatites comprise the northern part of the Borborema Province, which is known for rare-element mineralization including tantalite-columbite (tantalum-niobium), beryl (beryllium), and cassiterite (tin; Da Silva et al., 1995). Other commodities exploited from the region since the 1940s include gold (found in skarns together with tungsten) and quartz veins, both occurring in the metasedimentary Seridó Formation (Souza Neto et al., 2008).

Figure 5. Emeralds commonly occur near the contact between recrystallized pegmatite and biotite schist, as shown in the 15-cm-wide specimen on the left. The recrystallized pegmatitic rocks, mainly consisting of sodium-rich feldspar and quartz veins, show a saccharoidal texture and may also contain emeralds (right, image width 11.5 cm). Photos by J. C. Zwaan.

Emerald mineralization is associated with ultramafic to mafic rocks (metamorphosed into amphibolites) within the Santa Monica Shear Zone. These rocks are located at relatively higher altitude (>400 m) in the resistant granite gneiss basement. Adjacent to the amphibolites is a succession of talc, talc-amphibole, and biotite±amphibole schists, with a sharp contact between biotite schist and granitic gneiss (figure 4). The biotite schist layers range from 0.2 m to more than 3 m thick, and dip northwest rather steeply at 38°–56°. Small recrystallized pegmatitic bodies are present in the schist, near the contact with the granitic gneiss. Emeralds occur in and around those bodies, particularly within the biotite schist.

The recrystallized pegmatitic veins have a saccharoidal texture and are generally homogeneous, mainly consisting of sodium-rich plagioclase, though they also contain narrow quartz veins (typically up to a few centimeters wide). The emeralds within the recrystallized pegmatites are often small (<1 cm) and light-medium to medium bluish green (figure 5). The better-color emeralds appear to be associated particularly with the narrow quartz veins within the recrystallized pegmatites.

The recrystallized nature of the pegmatitic veins (compare, e.g., Giuliani et al., 1990; Zwaan, 2006) clearly indicates that metasomatic reactions with the schist played an important role in bringing the vital elements together to form emerald (Cr from the ultramafic rocks, and Be, Al, and Si from the veins). Detailed study of the area's geology is being undertaken to better understand the mechanisms and conditions of emerald formation.

EXPLORATION AND MINING

Prospecting is hindered by dense vegetation, which also limits the use of satellite imagery. A geochemical survey of soil samples (Scholz, 2008) revealed that Cr and Be anomalies follow the orientation of the Santa Monica Shear Zone. The highest values of both elements were found in the central part of the Fazenda Bonfim deposit, in the same area that has been worked so far. Anomalies also have been found farther north and northeast. A core drilling program of the mining area consisted of 33 holes (47 mm diameter) for a total length of 1,115 m. Further exploration has been carried out, using hand tools, in a few small pits and adits along the ultramafic/granitic gneiss contact (figure 6). The surface exposure showing potential for new mineralization extends no more than 700 m, and additional tunneling along the contact is needed to further explore the downward extension of the narrow zone of emerald mineralization.

Figure 6. This overview of the emerald mining area shows small pits and adits along the ultramafic/granitic gneiss contact. Photo by J. C. Zwaan.

Figure 7. A basic processing plant has been used onsite to wash and sort the mined material in search of emeralds. Photos by J. C. Zwaan.

Material from the pits dug so far has been processed with a basic washing and sorting plant, built onsite (figure 7). Part of this material also was transported to Caiçara do Rio do Vento, where more than 20 women sorted through 2.5 tonnes/day of ore, collecting 100–150 grams of beryl/emerald daily (J. Amancio Nery, pers. comm.; e.g., figure 8); this averages 50 grams per tonne. An internal report by Mineração Vale Verde Ltd. (Scholz, 2008) stated a figure of 10.5 kg/tonne, but this was based on testing of only 127.8 kg of mineralized rock. The production on the day of our visit to the sorting area was particularly low, but material of better quality and quantity from previous days was presented at the company's offices.

Mineração Vale Verde Ltd. has invested in the infrastructure necessary for a well-organized mining operation, such as running water, electricity, housing, an explosives magazine, and a repair shop. However, a dispute over the ownership rights has temporarily suspended activities. The case was resolved in November 2011, and operations are expected to resume in early 2012, after the rainy season.

The discovery of emeralds has stimulated additional geologic studies of the Lajes region, through a collaboration between the Federal University of Rio Grande do Norte, the Geological Survey of Brazil and other governmental parties, and Mineração Vale Verde Ltd. The Geological Survey is mapping the area around Lajes on a 1:100,000 scale to locate other ultramafic and recrystallized pegmatitic bodies. The aim is to obtain a detailed geologic map of this region and finally to create a prospecting guide for mining entrepreneurs.

DESCRIPTION OF THE ROUGH

Fazenda Bonfim emeralds typically consist of crystal fragments with homogeneous color. Well-formed crystals showing hexagonal prisms are rarely recovered as broken segments that commonly lack flat (pinacoidal) terminations. Transparent fragments and crystals (figure 9) typically range between 2 and 5 mm, though larger

Figure 8. Some of the emerald obtained from material processed in the washing plant is shown here. The large crystals on the lower right are 5 cm long. Courtesy of Mineração Vale Verde Ltd.

included crystals measuring a few centimeters long have been found.

The color of the emeralds ranges from light slightly bluish green to medium-dark bluish green. Very pale green beryl is also found.

MATERIALS AND METHODS

For this study, we examined 41 samples from Fazenda Bonfim, including 11 pieces of emerald rough that were transparent and suitable for faceting and 15 thin sections made from emerald-bearing rock; all of this material was collected by author JCZ during his visit to the mine. Parallel plates were cut and polished from three of the rough pieces for spectroscopy, whereas the thin sections were used only for studying inclusions in the emerald grains. In addition, 14 faceted and one cabochon-cut emerald, ranging from 0.17 to 3.89 ct, were obtained from Mineração Vale Verde Ltd. for this investigation.

Figure 9. The emerald fragments and crystals recovered from the Fazenda Bonfim deposit are typically small but of homogeneous color. The piece at the front-left is 10 mm wide. Photo by Dirk van der Marel.

Analyses done at the Netherlands Gemmological Laboratory included standard gemological testing and UV-Vis-NIR, FTIR, and Raman spectroscopy. A Rayner refractometer (yttrium aluminum garnet prism) with a near sodium–equivalent light source was used to measure refractive index and birefringence, specific gravity was determined hydrostatically, a calcite dichroscope revealed pleochroic colors, long- and short-wave UV lamps were used in a darkened room to observe fluorescence, and absorption spectra were visualized with a System Eickhorst M9 spectroscope with a built-in light source. Internal features were observed with a standard gemological microscope and a Nikon Eclipse E600 POL polarizing microscope.

Inclusions in 15 samples were analyzed by Raman spectroscopy using a Thermo DXR Raman microscope with 532 nm laser excitation. UV-Vis-NIR absorption spectra of six representative samples (one cabochon, two faceted, and three parallel plates) were taken with a Unicam UV 540 spectrophotometer in the 280–850 nm range. Mid-IR spectra of 16 representative samples (one cabochon, 14 faceted, and one parallel plate) were collected using a Thermo Nicolet Nexus FT-IR-NIR spectrometer.

Quantitative chemical analyses (46 spots) were carried out on 15 faceted emeralds at the electron microprobe facility of the Institute of Earth Sciences, Free University of Amsterdam, using a JEOL model JXA-8800M instrument. Analyses were performed at 15 kV, with a beam current of 25 nA and a spot size of 3 µm. The count time was 25 seconds for major elements and 36 seconds for most trace elements (50 seconds for V, Cr, and Rb).

Trace-element chemical data of 24 samples (15 faceted and 9 rough) were measured quantitatively by laser ablation–inductively coupled plasma–mass spectrometry (LA-ICP-MS) at the Johannes Gutenberg University's Institute of Geosciences using an Agilent 7500ce quadrupole ICP-MS coupled with a New Wave Research NWR-193 laser ablation system (193 nm wavelength). Ablation was carried out with helium as the carrier gas at an energy density of 2.77 J/cm^2, a pulse rate of 10 Hz, and a 50 µm crater size. NIST SRM 610 and 612 glass reference materials were used as external standards, and

TABLE 1. Physical properties of emeralds from Fazenda Bonfim, Rio Grande do Norte, Brazil.

Color	Very light to medium-dark slightly bluish green to strongly bluish green; typically a saturated bluish green with a light-medium to medium tone
Clarity	Very slightly to heavily included
Refractive indices	n_o = 1.587–1.591; n_e = 1.578–1.583
Birefringence	0.008–0.009
Specific gravity	2.72–2.74
Pleochroism	Distinct to strong; (light) yellowish green (o-ray), and bluish green to greenish blue (e-ray)
Fluorescence	Inert to long- and short-wave UV radiation
Chelsea filter	Pink to red (stones with saturated colors) or no reaction
Visible spectrum	Distinct lines at ~636, 662, and 683 nm; partial absorption between 580 and 630 nm; and complete absorption <430 nm
Internal features	• Often homogeneous color distribution, but moderate color zoning may occur as planar zones oriented parallel to the prism faces • Partially healed fissures with two-phase inclusions—typically square, rectangular, or comma-like • Negative crystals, forming CO_2-rich two-phase inclusions • Partially decrepitated inclusions • Parallel growth tubes • Extremely fine unidentified fiber-like inclusions • Mineral inclusions: rounded crystals of sodic plagioclase, platelets of phlogopite, thin flakes of hematite, and clusters of minute grains of quartz

^{29}Si was the internal standard. Data reduction was carried out using GLITTER 4.0 software (Macquarie University, Sydney, Australia). An average SiO_2 concentration of 63.5 wt.% was used, based on electron microprobe data. For comparison with the Fazenda Bonfim emeralds, we also collected LA-ICP-MS data on emeralds from two additional pegmatite-related deposits: Kafubu, Zambia (21 samples) and Sandawana, Zimbabwe (16 samples). The data reduction process for these localities used average SiO_2 concentrations of 63.0 and 62.8 wt.%, respectively (based on published electron microprobe and PIXE data; e.g., Zwaan et al., 1997, 2005; Calligaro et al., 2000). Detection limits were typically in the lower parts per billion range, and analytical uncertainties were generally between 5% and 15%, based on the external reproducibility of the reference materials (Jacob, 2006).

Figure 10. The polished emeralds studied for this report represented a range of sizes, from 0.17 to 3.89 ct, and were an attractive saturated light to medium-dark bluish green. Photo by Dirk van der Marel.

GEMOLOGICAL PROPERTIES

The gemological properties are summarized in table 1, with details described below.

Visual Appearance. The polished emeralds ranged from slightly bluish green to strongly bluish green, with a very light to medium-dark tone. Many were an attractive saturated bluish green with a light-medium to medium tone. The samples were very slightly to heavily included, and most of them were small (<0.20 ct). However, some of the faceted stones weighed nearly 2 ct and a 3.89 ct cabochon was also examined (figure 10). The color was evenly distributed, though moderate color zoning was observed in some rough fragments and polished material.

Physical Properties. Refractive indices were n_o = 1.587–1.591 and n_e = 1.578–1.583, yielding a birefringence of 0.008–0.009. Specific gravity varied between 2.72 and 2.74. The emeralds were inert to long- and short-wave UV radiation. All of the samples with more saturated colors appeared pink to red under the Chelsea filter, while the others showed no reaction. Dichroism was distinct to strong, in (light) yellowish green and bluish green to greenish blue.

The visible spectra of most of the emeralds had distinct lines at ~636, 662, and 683 nm, partial absorption between 580 and 630 nm, and complete absorption in the violet range (<430 nm). Small, light-colored emeralds showed a weaker spectrum with a clear line at 683 nm.

Microscopic Characteristics. The most commonly encountered inclusions were partially healed fissures with two-phase fluid inclusions (aquo-carbonic fluid

and gas) that were typically square, rectangular or comma-like (figure 11). Many of the emeralds had fine growth tubes oriented parallel to the c-axis. Occasionally observed were hexagonal-shaped negative crystals with a large bubble containing CO_2 (determined by Raman microspectroscopy; figure 12). Some fluid inclusions had an irregular shape with signs of shrinkage

In Brief

- Emerald mineralization at Fazenda Bonfim occurs in association with small recrystallized pegmatitic bodies and biotite schist.
- Exploration activities have produced a small amount of material from shallow pits and tunnels.
- The emeralds are typically small but show attractive color with moderate Cr and Fe, and low V. Relatively high K and Cs and low Li and Na separate them from other pegmatite-associated emeralds.
- Two-phase fluid inclusions and fine growth tubes are common, and FTIR spectra show characteristics of alkalis, CO_2, and deuterated water.

or were partially decrepitated and empty (figure 13). Unidentified extremely fine curved fiber-like inclusions, more or less parallel-oriented, also occurred in a few samples. Six stones showed evidence of clarity enhancement (three minor, three moderate).

Figure 11. Arrays of square or rectangular two-phase inclusions were widespread in the Fazenda Bonfim emeralds. Fine parallel-oriented growth tubes were also observed in many of the samples. Photomicrograph by J. C. Zwaan; image width 1.4 mm.

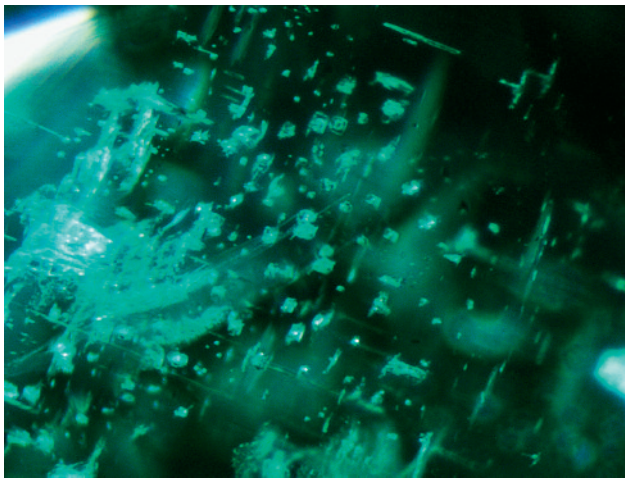

Figure 12. Raman microspectroscopy showed the presence of CO_2 within large gas bubbles in hexagonal-shaped negative crystals. Photomicrograph by J. C. Zwaan; image width 0.8 mm.

Solid inclusions were uncommon. Inclusions of plagioclase (figure 14) had Raman spectra consistent with albite or oligoclase. Platelets of phlogopite (figure 15, left) and hematite were also observed, as well as minute inclusions of quartz (figure 15, right). Occasionally, fluid inclusions contained captured minerals that were doubly refractive under crossed polarizers. In one case, the captured minerals were identified by Raman analysis as carbonate and mica (probably magnesite and muscovite), and also bertrandite (figures 16 and 17).

Figure 13. These irregular fluid inclusions show signs of shrinkage; on the left side is a decrepitated and empty inclusion. Photomicrograph by J. C. Zwaan; image width 0.35 mm.

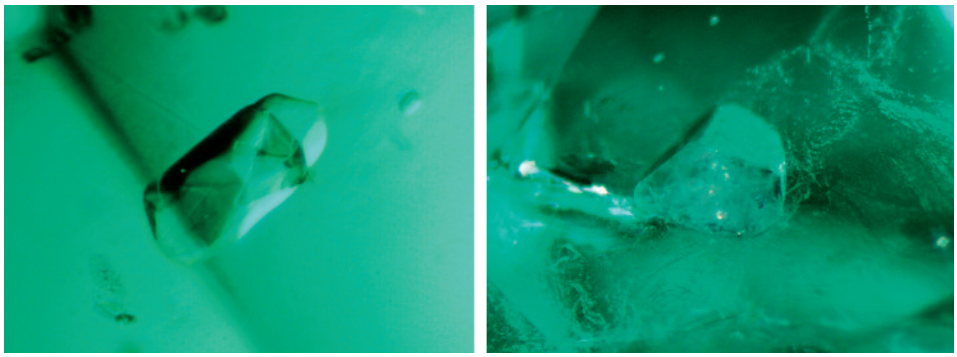

Figure 14. Slightly rounded grains of sodic plagioclase were identified in the emeralds. The crystal on the left is shown in transmitted light (image width 0.3 mm), while the larger one on the right is photographed in darkfield illumination (image width 1.4 mm). Photomicrographs by J. C. Zwaan.

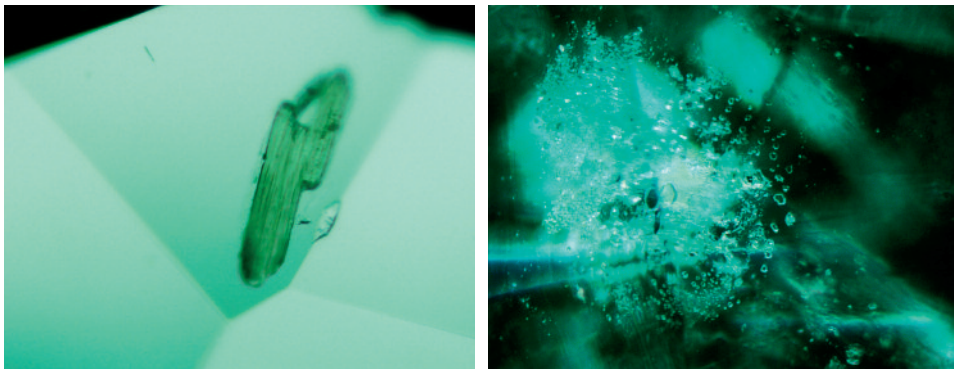

Figure 15. Platelets of phlogopite (left, image width 0.7 mm) and clusters of minute inclusions of quartz (right, image width 1.5 mm) were observed in some of the emeralds. Photomicrographs by J. C. Zwaan.

CHEMICAL COMPOSITION

Table 2 presents chemical analyses for representative samples of Fazenda Bonfim emeralds. A complete listing of all analyses, including ions calculated for the microprobe data, is available in the *G&G* Data Depository at gia.edu/gandg. The most important chromophore in the emeralds was Cr, which averaged 0.32 wt.% Cr_2O_3 and ranged from 0.16 wt.% in light bluish green samples to 0.72 wt.% in a medium bluish green stone. Vanadium concentrations were consistently low, averaging 0.03 wt.% V_2O_3. The other chromophore was Fe, which averaged 0.82 wt.% FeO and showed a maximum of 1.04 wt.% FeO.

The emeralds contained relatively high concentrations of Mg (average 2.27 wt.% MgO) but rather low Na (average 0.66 wt.% Na_2O). Traces of Ca, K, Cs, Li, P, Sc, Ti, Mn, Co, Ni, Zn, Ga, and Rb were detected in all of the samples. Potassium values were consistently high (average of 764 ppm), whereas Li contents were rather low (average of 106 ppm).

Table 3 summarizes the trace-element ranges obtained from LA-ICP-MS data for emeralds from Fazenda Bonfim, Kafubu, and Sandawana (see Discussion for comparison).

SPECTROSCOPY

The UV-Vis-NIR spectra were typical for emeralds with considerable iron content. The ordinary ray (E⊥c; figure 18) showed broad bands at approximately 438 and 605 nm, a weaker peak at 478 nm, and a doublet at 680 and

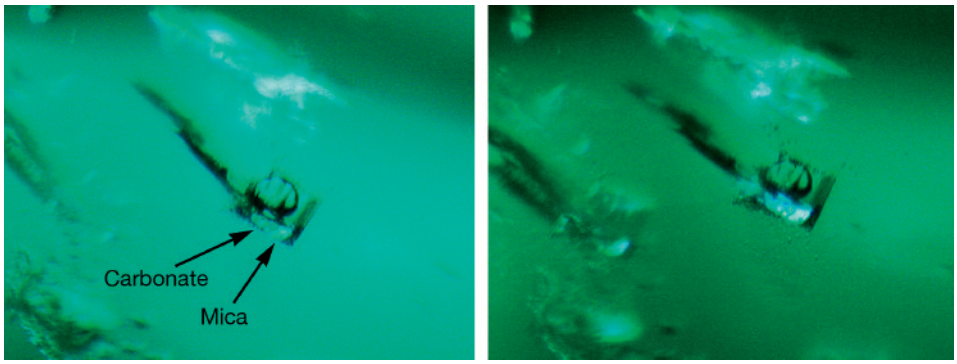

Figure 16. This fluid inclusion in an emerald contains doubly refractive captured minerals, mainly carbonate and mica along with bertrandite in the carbonate. Photomicrographs by J. C. Zwaan, transmitted light (left) and between crossed polarizers (right); image width ~0.3 mm.

TABLE 2. Average chemical composition of representative emeralds from Fazenda Bonfim.[a]

Sample	N1	N2	N3	N4	N5	N6	N7	N8	N9	N10	N11	N12	N13	N14	N15
Weight (ct)	3.89	1.92	1.29	1.26	0.15	0.18	0.19	0.20	0.23	0.19	0.19	0.19	0.21	0.19	0.17
Color	Med-dk. bG	Med. bG	Med. bG	Med.-lt. bG	Int. lt. sl. bG	Med. bG	Med.-lt. bG	Med.-lt. bG	Med. v.st. bG	Med-lt. bG	Med.-lt. bG	Med.-lt. bG	Med.-lt. bG	Med.-lt. bG	Lt. bG
Oxides (wt.%)[b]															
SiO_2	63.30	63.51	63.03	63.23	63.20	63.39	63.56	63.33	63.15	63.71	62.85	63.37	63.79	63.70	62.98
Al_2O_3	14.49	14.41	14.41	14.30	13.90	14.52	13.80	14.48	14.48	14.62	13.82	14.69	14.58	14.76	14.02
Sc_2O_3	bdl	0.02	bdl	bdl	0.02	bdl	0.03	bdl	bdl	0.03	0.02	bdl	bdl	bdl	0.02
V_2O_3	0.03	0.02	0.04	0.03	0.03	0.03	0.03	0.02	0.03	0.03	0.03	0.03	0.03	0.04	0.03
Cr_2O_3	0.32	0.25	0.18	0.23	0.42	0.57	0.35	0.31	0.49	0.44	0.36	0.29	0.20	0.25	0.16
BeO (calc)[c]	13.08	13.09	13.07	13.05	13.04	13.10	13.09	13.07	13.04	13.14	12.99	13.13	13.12	13.15	13.00
FeO	0.82	0.76	0.90	0.75	0.87	0.75	0.93	0.66	1.01	0.71	0.97	0.74	0.48	0.74	0.94
MgO	2.22	2.23	2.37	2.24	2.53	2.07	2.54	2.24	1.72	2.13	2.51	2.26	2.25	2.25	2.49
CaO	0.04	0.05	0.05	0.04	0.06	0.03	0.07	0.04	0.03	0.03	0.07	0.05	0.04	0.04	0.07
Na_2O	0.59	0.62	0.91	0.81	0.68	0.64	0.81	0.52	0.79	0.52	0.68	0.81	0.38	0.43	0.56
K_2O	0.05	0.06	0.07	0.06	0.06	0.07	0.08	0.04	0.03	0.04	0.07	0.06	0.04	0.05	0.07
Rb_2O	bdl	bdl	bdl	bdl	bdl	bdl	bdl	bdl	bdl	bdl	bdl	bdl	bdl	bdl	bdl
Cs_2O	0.02	bdl	0.04	0.03	0.04	0.05	0.04	0.05	0.03	0.04	0.04	0.02	0.02	bdl	0.04
Minor and trace elements (ppm)[d]															
Li	128	99	116	113	104	108	105	84	88	107	122	74	108	82	109
B	1.1	bdl	bdl	bdl	1.3	bdl	bdl	bdl	bdl	1.0	bdl	bdl	bdl	2.0	1.4
P	89	90	85	94	88	96	95	99	96	104	98	97	94	112	87
K	792	903	1212	1024	922	902	1098	626	496	626	1245	665	777	724	1088
Ca	416	444	734	418	479	250	543	385	194	227	620	377	344	439	497
Sc	96	72	138	66	104	53	101	45	122	145	169	81	45	91	114
Ti	6.9	4.4	7.0	4.9	3.3	7.0	4.1	4.2	3.2	3.2	7.0	3.9	3.3	5.6	7.0
V	123	121	146	116	136	175	139	90	171	140	150	114	97	117	144
Cr	2164	1637	1409	2006	2744	4222	2525	1504	2916	2995	2365	1946	1547	1768	1748
Mn	9.6	11	15	12	11	15	12	9.6	19	12	14	9.2	10	11	14
Co	2.5	2.2	2.4	2.4	2.3	2.2	2.4	2.2	2.1	2.0	2.4	2.2	2.1	2.3	2.6
Ni	16	15	15	16	16	21	16	15	19	18	16	15	15	16	16
Cu	bdl	bdl	bdl	bdl	bdl	bdl	bdl	bdl	bdl	bdl	0.54	0.61	0.79	29	bdl
Zn	25	20	17	20	18	44	19	19	78	44	20	17	18	49	20
Ga	20	19	19	18	19	17	21	18	47	31	22	18	19	17	20
Ge	bdl	bdl	bdl	bdl	bdl	0.83	bdl	bdl	0.72	0.76	bdl	bdl	bdl	bdl	bdl
Rb	67	69	80	68	82	65	81	62	52	60	85	66	67	66	83
Sr	0.06	0.05	0.10	0.06	0.04	bdl	0.07	0.04	bdl	bdl	0.15	0.03	0.06	0.78	0.05
Y	0.05	0.05	0.07	bdl	0.06	0.04	0.06	0.03	bdl	0.04	0.09	bdl	0.05	0.06	0.06
Zr	0.10	0.07	0.13	0.10	0.11	bdl	0.10	0.09	bdl	bdl	0.23	0.09	0.09	0.13	bdl
Nb	bdl	bdl	bdl	bdl	bdl	bdl	bdl	bdl	bdl	0.03	bdl	bdl	bdl	0.17	bdl
Mo	bdl	bdl	bdl	bdl	bdl	bdl	bdl	bdl	bdl	bdl	bdl	bdl	bdl	bdl	bdl
Sn	bdl	bdl	1.1	bdl	0.77	bdl	bdl	bdl	0.79	bdl	1.3	bdl	bdl	2.1	1.1
Cs	273	252	375	241	311	494	303	222	340	408	380	233	217	238	392
Ba	bdl	bdl	bdl	bdl	0.22	bdl	bdl	bdl	0.26	bdl	bdl	bdl	bdl	1.2	bdl
La	bdl	bdl	0.02	bdl	bdl	bdl	bdl	bdl	0.03	bdl	bdl	bdl	bdl	0.04	bdl
Ta	0.06	0.06	0.08	0.05	0.06	bdl	0.06	0.06	bdl	bdl	0.07	0.05	bdl	0.05	0.11
Au	bdl	bdl	bdl	bdl	bdl	bdl	bdl	bdl	bdl	bdl	bdl	bdl	bdl	bdl	bdl
Pb	bdl	bdl	bdl	bdl	0.07	bdl	bdl	bdl	bdl	bdl	0.12	bdl	bdl	1.7	0.11
Bi	bdl	bdl	bdl	bdl	0.06	bdl	0.04	bdl	bdl	bdl	0.07	bdl	bdl	0.04	0.07

[a] Abbreviations: bdl = below detection limit; bG = bluish green, lt. = light, med. = medium, dk. = dark, Int. = intense, sl. = slightly, v.st. = very strongly.
[b] Oxides analyzed by electron microprobe; average of three analyses per sample on different spots (four analyses of sample N3). For complete electron microprobe analyses, including the calculated ions per formula unit, see the G&G Data Depository.
[c] BeO was calculated based on an assumed stoichiometry of 3 Be atoms per formula unit.
[d] Trace elements analyzed by LA-ICP-MS; average of three analyses per sample on different spots (two analyses of sample N7).

683 nm, all indicating the presence of Cr^{3+}. A band at about 835 nm pointed to the presence of Fe^{2+}, whereas the peak at about 371 nm demonstrated Fe^{3+} (compare Wood and Nassau, 1968; Schmetzer et al., 1974; Platonov et al., 1978).

FTIR measurements yielded spectra consistent with alkali-bearing emeralds (figure 19). A peak at around 7095 cm^{-1} indicated the presence of type II water (i.e.,

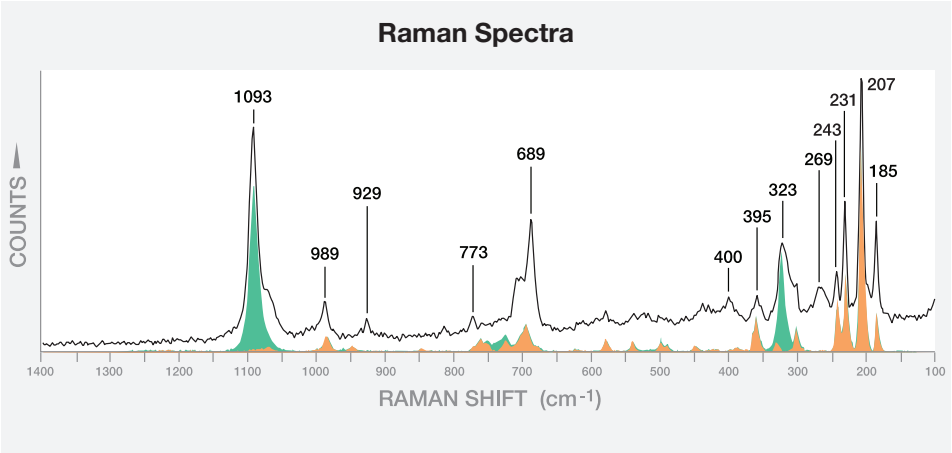

Figure 17. The doubly refractive minerals in figure 16 gave a Raman spectrum that could be resolved into a mixture of carbonate (magnesite, green spectrum) and bertrandite (orange spectrum). The remaining peak at 689 cm^{-1} and the shoulder around 1070 cm^{-1} can be attributed to beryl, the inclusion host.

water molecules associated with alkali ions in the channels of the beryl structure; Wood and Nassau, 1968). The alkali ions in these emeralds were mainly Na^+, K^+, Cs^+, and Li^+. As non-polarized spectra were obtained from faceted and cabochon-cut specimens, the 5272 cm^{-1} peak could not be confirmed as a type II water absorption band; this can only be proven when a polarized spectrum is taken perpendicular to the c-axis (Schmetzer et al., 1997). A smaller peak at 3234 cm^{-1} was related to either type II H_2O or to $(OH)^-$ oriented parallel to the c-axis (Banko, 1995, 1997). The broad band between about 3900 and 3400 cm^{-1} was due to type II and type I water molecules (type I are not linked to other ions).

The FTIR spectra consistently showed a strong band at 2357 cm^{-1}, indicating the presence of CO_2. This band is strongly dichroic, with greater absorption for the ordinary ray, a feature related to the orientation of CO_2 within the channel of the beryl structure (Wood and Nassau, 1968). Very weak peaks at ~2671 and 2640 cm^{-1} can be assigned to type I and type II HOD molecules (de Donato et al., 2004), indicating the presence of deuterium next to hydrogen in some of the water molecules ("deuterated water").

None of our spectra indicated a resin in any of the samples, nor did we see any green fillers. Stones with fractures containing a near-colorless filler showed a higher peak around 2925 cm^{-1}, as well as lower peaks around 2854 and 2955 cm^{-1} that are typical for an oil (e.g., Johnson et al., 1999; Kiefert et al., 1999).

Figure 18. A representative absorption spectrum of an emerald from Fazenda Bonfim, in the direction of the ordinary ray (E⊥c), shows the presence of Cr^{3+}, Fe^{2+}, and Fe^{3+}. The approximate path length of the beam is 5 mm.

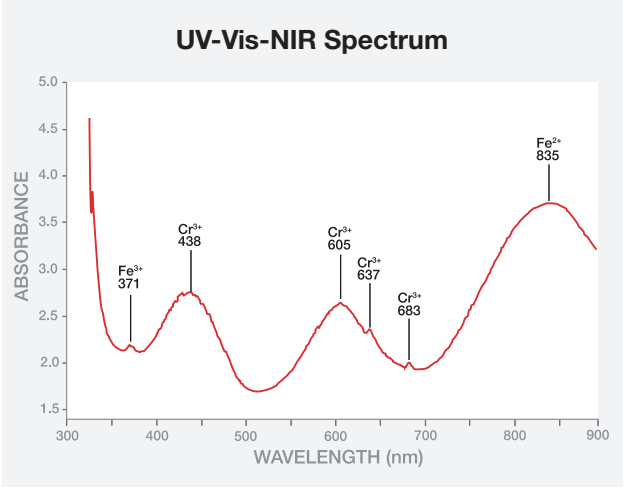

DISCUSSION

Physical Properties. The relatively high refractive indices of Fazenda Bonfim emeralds are typical for emeralds from schist- and pegmatite-related deposits. These high RIs are caused by the presence of alkali ions, water, and substantial Mg and Fe (Wood and Nassau, 1968; Černý and Hawthorne, 1976). Zwaan et al. (2005) compared other commercially available emeralds with similar RI, birefringence, and SG values. Based on that comparison, the distinguishing internal features of Fazenda Bonfim emeralds (prominent fluid inclusions, parallel growth tubes, and few solid inclusions) differ considerably. Although many of their internal features are comparable to those encountered in emeralds from the Itabira District of Minas Gerais (compare Hänni et al., 1987; Souza, 1988; Souza et al., 1992; Zwaan, 2001; and Rondeau et al., 2003), the absence of amphibole in the Fazenda Bonfim emeralds is distinctive. Amphibole inclusions are common in emeralds from many other

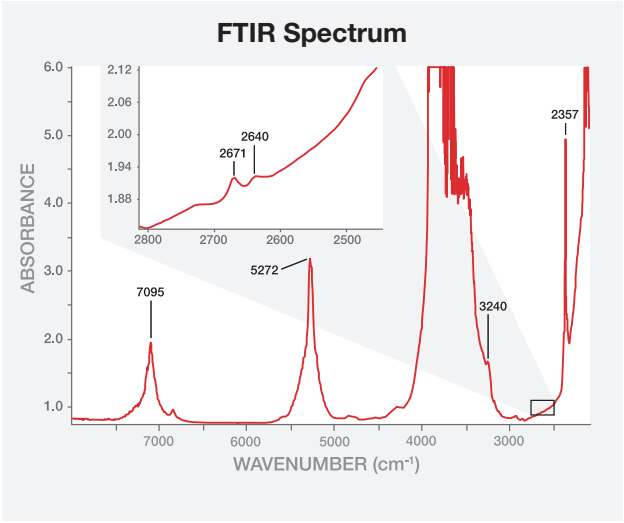

Figure 19. This representative mid-FTIR spectrum of a Fazenda Bonfim emerald shows a 7095 cm^{-1} peak caused by vibrations of water molecules adjacent to alkali ions in the channel sites. Those same water molecules and unassociated water molecules caused the broad band between 3900 and 3400 cm^{-1}. The peak at 2357 cm^{-1}, due to CO_2, was consistently high in the samples. The inset shows very weak peaks at ~2671 and 2640 cm^{-1} that indicate the presence of deuterated water. The approximate path length of the beam is 5 mm.

schist-related emerald deposits (e.g., Schwarz, 1998; Zwaan et al., 2005).

Chemical Properties. Using Schwarz's (1990a) empirical subdivision of low, medium, and high concentrations of elements in emerald, the Fazenda Bonfim stones show low Na and V, and moderate Cr, Fe, and Mg. Notable are the relatively high K and low Li contents compared to most emeralds from Zambia and Zimbabwe, which also come from schist-type deposits related to pegmatitic intrusions (table 3 and figure 20). Only some Zambian emeralds show very high K values combined with lower Li. A better separation between the three localities can be made by plotting Ga versus Li (figure 21). The Fazenda Bonfim emeralds have low Li values and moderate-to-high Ga.

A clear separation between the three localities can also be made by plotting data for K, Li+Cs, and Rb in a ternary diagram (figure 22). The Fazenda Bonfim emeralds show intermediate K and Li+Cs contents, and stand out clearly from Sandawana emeralds and most Zambian emeralds that show high Li+Cs, and from some Zambian stones that are K-dominant. The Zimbabwean emeralds can be distinguished from Zambian material by their higher Rb content. When a beryl is Li-rich, Cs typically appears in higher concentrations as well (Bakakin and Belov, 1962). Generally speaking, extremely fractionated rare-element granitic pegmatites

TABLE 3. Trace-element concentrations (ppm) of emeralds from three pegmatite-related deposits.[a]

Deposit	Fazenda Bonfim, Brazil	Kafubu, Zambia	Sandawana, Zimbabwe
Samples	24	21	16
Trace element (ppm)			
Li	63–221 (106)	84–868 (514)	225–764 (492)
B	bdl–3.4	bdl–10.7	bdl–1.6
P	70–132 (96)	92–167 (118)	76–128 (109)
K	398–1306 (764)	30–2728 (671)	134–431 (263)
Ca	161–966 (360)	65–782 (314)	46–727 (131)
Sc	22–170 (89)	2.7–349 (108)	13–109 (43)
Ti	1.8–8.7 (4.8)	1.8–25 (8.5)	2.5–179 (60)
V	60–180 (128)	34–333 (108)	101–379 (257)
Cr	887–4976 (2277)	374–4507 (1835)	1363–7821 (4752)
Mn	6.0–21 (11.4)	6.5–80 (27)	3.2–1714 (66)
Co	1.5–2.7 (2.1)	0.99–5.9 (3.0)	1.6–7.6 (2.5)
Ni	8.8–22 (15)	9.8–50 (19)	9.9–84 (19)
Cu	bdl–29	bdl–0.57	bdl–4.4
Zn	14–110 (26)	12.7–129 (39)	30–294 (82)
Ga	14–49 (20)	6.8–18 (12)	19–44 (28)
Ge	bdl–1.0	bdl–1.6	bdl–0.84
Rb	52–101 (72)	12.4–223 (76)	120–328 (222)
Sr	bdl–0.78	bdl–0.21	bdl–0.23
Y	bdl–0.13	bdl–0.06	bdl–0.14
Zr	bdl–0.33	bdl–0.19	bdl–3.0
Nb	bdl–0.17	bdl–0.06	bdl–0.65
Mo	bdl	bdl–0.21	bdl–0.26
Sn	bdl–2.1	bdl–14.8	bdl–14.1
Cs	213–557 (345)	131–1927 (739)	251–1315 (654)
Ba	bdl–1.2	bdl–6.9	bdl–0.5
La	bdl–0.06	bdl–0.04	bdl–0.16
Ta	bdl–0.57	bdl–0.06	bdl–0.74
Au	bdl–0.12	bdl	bdl
Pb	bdl–1.7	bdl–4.5	bdl–5.7
Bi	bdl–0.12	bdl–0.06	bdl–0.07

[a] *Element ranges are shown, with average values in parentheses. Abbreviation: bdl = below detection limit.*

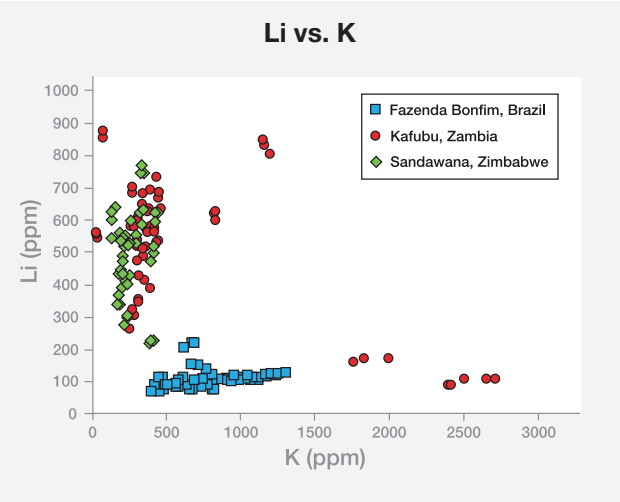

Figure 20. This plot shows the relatively high K and low Li concentrations in Fazenda Bonfim emeralds compared to those in Sandawana (Zimbabwe) and Kafubu (Zambia) samples.

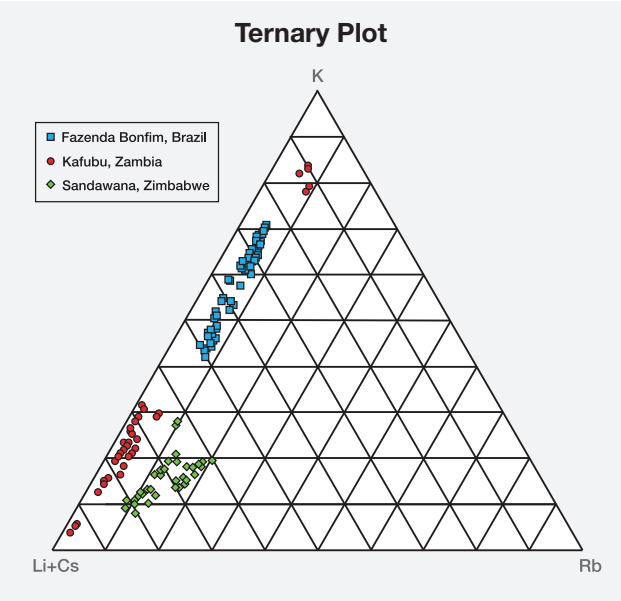

Figure 22. The concentrations of K, Li+Cs, and Rb in emeralds from Fazenda Bonfim, Zambia, and Zimbabwe are plotted in this ternary diagram. The Fazenda Bonfim emeralds show intermediate K and Li+Cs content and are clearly distinguished from Zimbabwean emeralds and most Zambian emeralds that show enriched Li+Cs. The Zimbabwean emeralds have relatively higher Rb.

of the LCT association (lithium, cesium, tantalum) are enriched in Li and Cs (e.g., Černý et al., 1985; Simmons, 2007). Emeralds from Zambia and Zimbabwe are found in close connection to highly evolved pegmatites (e.g., Seifert et al., 2004; Zwaan, 2006) and indeed show high Li and Cs. In Rio Grande do Norte, the pegmatites of the Borborema Pegmatitic Province are not considered among the most evolved, and they are classified under Černý's (1989) "beryl-columbite-phosphate" subtype (Da Silva et al., 1995). This is consistent with the lower Li and Cs in the associated emeralds from Fazenda Bonfim.

Figure 21. A plot of Li versus Ga separates Fazenda Bonfim emeralds, which have low Li values and moderate-to-high Ga, from Zambian stones (lower Ga with higher Li) and Zimbabwean emeralds (higher Li and Ga).

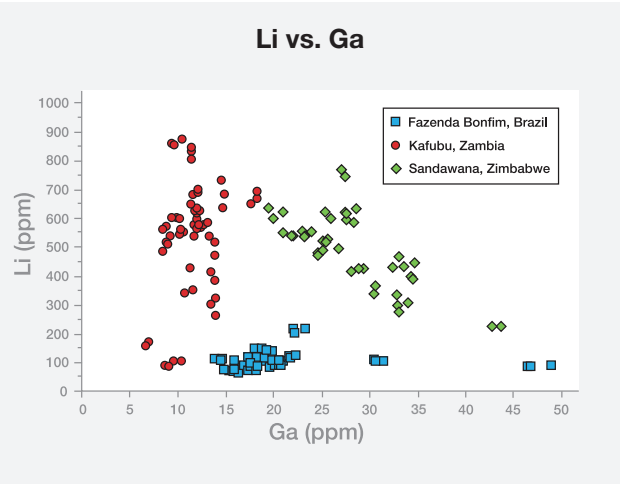

Compared to our LA-ICP-MS results (table 3), analyses of emeralds from Kafubu and Sandawana by Abduriyim and Kitawaki (2006) show similar trends for most elements, although they reported higher Li values for Zambian emeralds (320–1260 ppm). They also gave higher upper limits for Li in Sandawana emeralds (1370 ppm), as well as very high Cs in those samples (up to 0.30 wt.% Cs_2O). In Zambian emeralds, they reported higher upper limits for Zn (up to 970 ppm) and for Ga (up to 55 ppm). Because average values were not listed by those authors, it is difficult to assess the significance of these differences in results. Zwaan et al. (2005) showed that in one emerald crystal from Zambia, cesium ranged from 0.05 to 0.23 wt.% Cs_2O (microprobe analyses), with the highest concentration in the outer portion of the crystal. So variations in trace-element concentration may depend highly on the precise locations chosen for spot analyses.

Figure 23. Emeralds from Fazenda Bonfim are somewhat similar to those from Itabira, Brazil. Shown here are loose Fazenda Bonfim emeralds—the faceted stones weigh 1.29 and 1.92 ct, the cabochon is 3.89 ct, and the crystal section (courtesy of Nature's Geometry, Laguna Beach, California) measures 5.5 mm—along with jewelry featuring Brazilian emeralds. The ring contains a 3.20 ct Capoeirana emerald center stone and the necklace is set with Bahia emeralds; the pear shapes weigh ~0.4 ct each. Jewelry courtesy of ABC Gems Inc., Los Angeles; photo by Robert Weldon.

From chemical data reported in the literature, it can be deduced that emeralds from the Itabira District of Minas Gerais show overlapping values but generally higher Na_2O content, up to 1.93 wt.%. The average Na_2O content reported for emeralds from the Belmont, Capoeirana, and Piteiras mines are 0.97, 0.99, and 1.52 wt.%, respectively (Schwarz, 1990c; Zwaan, 2001). Rondeau et al. (2003) analyzed two representative samples from Piteiras and gave Na_2O values of 1.43 and 1.58 wt.%, respectively. LA-ICP-MS analyses also gave high Na_2O contents, between 1.33 and 2.18 wt.%, for Itabira emeralds (Abduriyim and Kitawaki, 2006). Additionally, emeralds from Itabira contain less Cs than those from Fazenda Bonfim; Cs_2O was below the detection limit of the electron microprobe (Schwarz, 1990c; Zwaan, 2001) and up to only 0.01 wt.% by LA-ICP-MS (Abduriyim and Kitawaki, 2006).

CONCLUSION

Emerald mineralization at Fazenda Bonfim occurs in association with ultramafic rocks in the Seridó Mobile Belt, within the Santa Monica Shear Zone. Small recrystallized pegmatitic bodies lie in a succession of talc, talc-amphibole, and biotite±amphibole schists, and emeralds occur in and around those bodies, particularly in the adjacent biotite schist near the contact with granitic gneiss.

The polished emeralds studied for this report typically displayed a saturated bluish green color with a medium-light to medium tone, and were very slightly to heavily included. Their relatively high refractive indices are typical for emeralds from schist-related deposits. The most commonly encountered inclusions were partially healed fissures with two-phase fluid inclusions (typically square, rectangular or "comma-like") and fine, parallel-oriented growth tubes. The emeralds' chemical composition is characterized by relatively high K; moderate Cr, Fe, and Mg; and low Na, V, and Li. FTIR spectra showed characteristics of alkali-bearing emeralds with considerable CO_2, as well as the presence of deuterated water.

The Fazenda Bonfim emeralds can be distinguished from those of other commercially important schist- and pegmatite-related localities by careful comparison of physical and chemical properties, as well as internal features. Their properties show the most overlap with emeralds from the Itabira District of Brazil (e.g., figure 23), but they can still be differentiated by their significantly higher Cs and generally lower Na.

Future emerald production from Fazenda Bonfim will depend on the extent of mineralization along the shear zone, both laterally and down the contact.

ABOUT THE AUTHORS

Dr. Zwaan (zwaanj@naturalis.nl) is head of the Netherlands Gemmological Laboratory and a researcher at Naturalis, the national museum of natural history in Leiden, the Netherlands. Drs. Jacob and Häger are researchers at the Johannes Gutenberg University's Institute for Geosciences in Mainz, Germany. Dr. Cavalcanti Neto is a geologist at the Federal Institute for Education, Science and Technology of Rio Grande do Norte in Natal, Brazil. Mr. Kanis is a consultant based in Veitsrodt, Germany.

ACKNOWLEDGMENTS

The authors thank Mineração Vale Verde Ltd. (Caiçara do Rio do Vento, Brazil) for providing valuable information on the exploration and mining operation, granting full access to the deposit, and supplying samples for examination. We are grateful to Mr. J. Amancio Nery for logistical support. Dirk van der Marel (Netherlands Gemmological Laboratory) is thanked for his general assistance. Facilities for electron microprobe analyses were provided by the Free University of Amsterdam and by NWO, the Netherlands Organisation for Scientific Research. LA-ICP-MS analyses were performed at the Johannes Gutenberg University's Institute for Geosciences.

REFERENCES

Abduriyim A., Kitawaki H. (2006) Applications of laser ablation–inductively coupled plasma–mass spectrometry (LA-ICP-MS) to gemology. *G&G*, Vol. 42, No. 2, pp. 98–118, http://dx.doi.org/10.5741/GEMS.42.2.98.

Angelim L.A.A., Medeiros V.C., Nesi J.R. (2006) Programa Geologia do Brasil – PGB. Projeto Geológico e Recursos Minerais do Estado do Rio Grande do Norte. Mapa Geológico do Estado do Rio Grande do Norte. Escala 1:500.000. CPRM/FAPERN, Recife.

Araújo M.N.C., Vasconcelos P.M., Alves da Silva F.C., Jardim de Sá E., Sá J.M. (2005) $^{40}Ar/^{39}Ar$ geochronology of gold mineralization in Brasiliano strike-slip shear zone in the Borborema Province, NE Brazil. *Journal of South American Earth Sciences*, Vol. 19, pp. 445–460, http://dx.doi.org/10.1016/j.jsames.2005.06.009.

Bakakin V.V., Belov N.V. (1962) Crystal chemistry of beryl. *Geokhimiya*, Vol. 5, pp. 420–433.

Banko A.G. (1995) Wasser- und Alkaligehaltbestimmung von Beryllen anhand der FTIR-Spektroskopie. *Mitteilungen der Österreichische Mineralogischen Gesellschaft*, Vol. 140, pp. 39–45.

Banko A.G. (1997) FTIR-Spektroskopische Untersuchungen na Beryllen unterschiedlicher Herkunft, sowie die Geologische, Mineralogische und Gemmologische Charakterisierung der Diamanten des Espinhaço-Gebirges (Minas Gerais, Brasilien). Dissertation am Institut für Mineralogie und Kristallografie, Universität Wien.

Calligaro T., Dran J.-C., Poirot J-P., Querré G., Salomon J., Zwaan J.C. (2000) PIXE/PIGE characterisation of emeralds using an external micro-beam. *Nuclear Instruments and Methods in Physics Research B*, Vol. 161–163, pp. 769–774, http://dx.doi.org/10.1016/S0168-583X(99)00974-X.

Cassedanne J.P., Sauer D.A. (1984) The Santa Terezinha de Goiás emerald deposit. *G&G*, Vol. 20, No. 1, pp. 4–13, http://dx.doi.org/10.5741/GEMS.20.1.4.

Cavalcanti Neto M.T.O., Barbosa R.V.N. (2007) As esmeraldas de Lajes, Caiçara do Rio dos Ventos e São Tomé/RN. *Holos*, Ano 23, Vol. 2, pp. 92–104.

Černý P., Hawthorne F.C. (1976) Refractive indices versus alkali contents in beryl: General limitations and applications to some pegmatitic types. *Canadian Mineralogist*, Vol. 14, pp. 491–497.

Da Silva M.R.R., Höll R., Beurlen H. (1995) Borborema Pegmatitic Province: Geological and geochemical characteristics. *Journal of South American Earth Sciences*, Vol. 8, Nos. 3/4, pp. 355–364, http://dx.doi.org/10.1016/0895-9811(95)00019-C.

de Donato P., Cheilletz A., Barres O., Yvon J. (2004) Infrared spectroscopy of OD vibrators in minerals at natural dilution: Hydroxyl groups in talc and kaolinite, and structural water in beryl and emerald. *Applied Spectroscopy*, Vol. 58, No. 5, pp. 521–527, http://dx.doi.org/10.1366/000370204774103336.

Eidt T., Schwarz D. (1988) Die brasilianischen Smaragde und ihre Vorkommen: Carnaíba/Bahia. *Zeitschrift der Deutschen Gemmologischen Gesellschaft*, Vol. 37, No. 1/2, pp. 31–47.

Epstein D.S. (1989) The Capoeirana emerald deposit near Nova Era, Minas Gerais, Brazil. *G&G*, Vol. 25, No. 3, pp. 150–158, http://dx.doi.org/10.5741/GEMS.25.3.150.

Giuliani G., Silva L.J.H.D., Couto P. (1990) Origin of emerald deposits of Brazil. *Mineralium Deposita*, Vol. 25, pp. 57–64.

Giuliani G., Cheilletz A., Zimmermann J-L., Ribeiro-Althoff A.M., France-Lanord C., Féraud G. (1997) Les gisements d'émeraude du Brésil: Genèse et typologie. *Chronique de la Recherche Minière*, Vol. 526, pp. 17–61.

Hänni H.A., Schwarz D., Fischer M. (1987) The emeralds of the Belmont mine, Minas Gerais, Brazil. *Journal of Gemmology*, Vol. 20, No. 7/8, pp. 446–456.

Jacob D.E. (2006) High sensitivity analysis of trace element-poor geological reference glasses by laser-ablation inductively coupled plasma-mass spectrometry (LA-ICP-MS). *Geostandards and Geoanalytical Research*, Vol. 30, No. 3, pp. 221–235, http://dx.doi.org/10.1111/j.1751-908X.2006.tb01064.x.

Johnson M.L., Elen S., Muhlmeister S. (1999) On the identification of various emerald filling substances. *G&G*, Vol. 35, No. 2, pp. 82–107, http://dx.doi.org/10.5741/GEMS.35.2.82.

Johnston W.D. Jr. (1945) Beryl-tantalite pegmatites of northeastern Brazil. *Geological Society of America Bulletin*, Vol. 56, pp. 1015–1070, http://dx.doi.org/10.1130/0016-7606(1945)56[1015:BPONB]2.0.CO;2.

Kanis J. (2002) Piteiras, Brasilien; Erfolgreiche Smaragdsuche mit modernsten Methoden. *Lapis*, Vol. 27, No. 3, pp. 13–18.

Kiefert L., Hänni H.A., Chalain J.P., Weber W. (1999) Identification of filler substances in emeralds by infrared and Raman spectroscopy. *Journal of Gemmology*, Vol. 26, No. 8, pp. 487–500.

Milisenda C.C. (2007) Gemmologie Aktuell – New emerald deposit in Brazil. *Gemmologie: Zeitschrift der Deutschen Gemmologischen Gesellschaft*, Vol. 56, No. 3–4, p. 79.

Platonov A.N., Taran M.N., Minko O.E., Polshyn E.V. (1978) Optical absorption spectra and nature of color of iron-containing beryls. *Physics and Chemistry of Minerals*, Vol. 3, No. 1, pp. 87–88.

Rolff P.A.M.A. (1946) *Minerais dos Pegmatitos da Borborema*. DNPM/DFPM, Rio de Janeiro, Boletim 78, pp. 24–76.

Rondeau B., Notari F., Giuliani G., Michelou J-C., Martins S., Fritsch E., Respinger A. (2003) La mine de Piteiras, Minas Gerais, nouvelle source d'émeraude de belle qualité au Brésil. *Revue de Gemmologie*, No. 148, pp. 9–25.

Schmetzer K., Berdesinski W., Bank H. (1974) Über die Mineralart beryll, ihre farben und Absorptionsspektren. *Zeitschrift der Deutschen Gemmologischen Gesellschaft*, Vol. 23, No. 1, pp. 5–39.

Schmetzer K., Kiefert L., Bernhardt H.J., Zhang B. (1997) Charac-

terization of Chinese hydrothermal synthetic emerald. *G&G*, Vol. 33, No. 4, pp. 276–291, http://dx.doi.org/10.5741/GEMS.33.4.276.
Scholz R. (2008) Preliminary Report on the Economic Potential Evaluation of Emerald Mineralization at Fazenda Bonfim. Mineração Vale Verde, internal report, DNPM – 848.044/2006; 848.057/07; 848.046/06 (in Portuguese, English translation by S. Cuberos Perez).
Schwarz D. (1990a) Die brasilianischen Smaragde und ihre Vorkommen: Santa Terezinha de Goiás/GO. *Zeitschrift der Deutschen Gemmologischen Gesellschaft*, Vol. 39, No. 1, pp. 13–44.
Schwarz D. (1990b) The Brazilian emeralds and their occurrences: Socotó, Bahia. *Journal of Gemmology*, Vol. 22, No. 3, pp. 147–163.
Schwarz D. (1990c) Die Chemische Eigenschaften der Smaragde I. Brasilien. *Zeitschrift der Deutschen Gemmologischen Gesellschaft*, Vol. 39, No. 4, pp. 233–272.
Schwarz D. (1998) The importance of solid and fluid inclusions for the characterization of natural and synthetic emeralds. In D. Giard, Ed. *L'émeraude*, Association Française de Gemmologie, Paris, pp. 71–80.
Schwarz D., Hänni H.A., Martins F.L. Jr., Fischer M. (1988) Die Smaragde der Fazenda Boa Esperança bei Tauá, Ceará, Brasilien: Vorkommen und Charakteristika. *Zeitschrift der Deutschen Gemmologischen Gesellschaft*, Vol. 36, No. 3/4, pp. 133–147.
Seifert A.V., Zacek V., Vrana S., Pecina V., Zacharias J., Zwaan J.C. (2004) Emerald mineralization in the Kafubu area, Zambia. *Bulletin of Geosciences*, Vol., 79, No. 1, pp. 1–40.
Simmons W.B. (2007) Gem-bearing pegmatites. In L.A. Groat, Ed., *Geology of Gem Deposits*, Mineralogical Association of Canada, Short Course Series, Vol. 37, pp. 169–206.
Souza J.L. (1988) Mineralogia e geologia da esmeralda da jazida de Itabira, Minas Gerais. *Revista Escola de Minas*, Vol. 43, No. 2, pp. 31–50.
Souza J.L., Mendes J.C., Silveira Bello R.M., Svisero D.P., Valarelli J.V. (1992) Petrographic and microthermometrical studies of emeralds in the 'garimpo' of Capoeirana, Nova Era, Minas Gerais State, Brazil. *Mineralium Deposita*, Vol. 27, pp. 161–168, http://dx.doi.org/10.1007/BF00197103.
Souza Neto J.A., Legrand J.M., Volfinger M., Pascal M.L., Sonnet P. (2008) W-Au skarns in the Neo-Proterozoic Seridó Mobile Belt, Borborema Province in northeastern Brazil: An overview with emphasis on the Bonfim deposit. *Mineralium Deposita*, Vol. 43, pp. 185–205, http://dx.doi.org/10.1007/s00126-007-0155-1.
Wood D.L., Nassau K. (1968) The characterization of beryl and emerald by visible and infrared absorption spectroscopy. *American Mineralogist*, Vol. 53, pp. 777–800.
Zwaan J.C. (2001) Preliminary study of emeralds from the Piteiras emerald mine, Minas Gerais, Brazil. *28th International Gemmological Conference*, Madrid, Spain, pp. 106–109.
Zwaan J.C. (2006) Gemmology, geology and origin of the Sandawana emerald deposits, Zimbabwe. *Scripta Geologica*, Vol. 131, pp. 1–211.
Zwaan J.C., Kanis J., Petsch E.J. (1997) Update on emeralds from the Sandawana mines, Zimbabwe. *G&G*, Vol. 33, No. 2, pp. 80–100, http://dx.doi.org/10.5741/GEMS.33.2.80.
Zwaan J.C., Seifert A.V., Vrána S., Laurs B.M., Anckar B., Simmons W.B., Falster A.U., Lustenhouwer W.J., Muhlmeister S., Koivula J.I., Garcia-Guillerminet H. (2005) Emeralds from the Kafubu area, Zambia. *G&G*, Vol. 41, No. 2, pp. 116–148, http://dx.doi.org/10.5741/GEMS.41.2.116.

For online access to all issues of GEMS & GEMOLOGY from 1981 to the present, visit:

store.gia.edu

Characterization of Colorless Coated Cubic Zirconia (Diamantine)

James E. Shigley, Al Gilbertson, and Sally Eaton-Magaña

Over the past several years, diamond simulants have entered the market that consisted of colorless cubic zirconia reportedly coated with a thin layer (e.g., represented to be 30–50 nm) of nanocrystalline diamond particles embedded in a matrix. One manufacturer, Serenity Technologies (Temecula, California), has marketed this material as Diamantine. SIMS chemical analysis of samples obtained from Serenity in October 2009 indicated a very thin (~5 nm) film of carbon (along with Al and Ti) on the CZ surface. Durability tests performed in conjunction with SEM imaging demonstrated that the thin coating does not completely withstand typical gemstone cleaning and handling procedures. The only standard gemological technique that could establish the presence of a coating was EDXRF spectroscopy, which detected Ti from the adhesion layer deposited on the CZ during the initial part of the coating process.

Sophisticated techniques used in the semiconductor and optical coating industries are now being applied to the treatment of gemstones. In the past few years, the jewelry industry has witnessed the introduction of several faceted gem materials (diamond, topaz, quartz, cubic zirconia, and others) reportedly coated with thin colored or colorless surface layer(s) of substances such as aluminum oxide, diamond-like carbon (DLC), and nanocrystalline synthetic diamond to change their color or allegedly improve their appearance and/or durability (see, e.g., Henn, 2003; Shen et al., 2007; Ogden, 2008; Schmetzer, 2008; Bennet and Kearnes, 2009). These new coating treatments present several important challenges for the jewelry trade, including their proper description, identification, determination of any visual or physical effects resulting from the coating, and disclosure (see box A).

For the past several years, Serenity Technologies of Temecula, California, has produced and marketed a simulant consisting of faceted cubic zirconia (CZ) coated with what is described as a thin, transparent, colorless layer containing submicroscopic particles of nanocrystalline synthetic diamond embedded in a matrix material (see figure 1 and www.serenitytechnology.com). This product is currently sold under the brand name Diamantine and is distributed only through licensed dealers. The

Figure 1. This cubic zirconia (2.00 ct) has been coated by Serenity Technologies with a proprietary colorless thin layer that is said to consist of "nanocrystalline diamond particles" embedded in a matrix. Photo by Robert Weldon.

Diamantine production process has a capacity of 2,000 carats in each cycle, for a total of 20,000 carats per day (S. Neogi, pers. comm., 2009). Colorless and variously colored thin-film layers can be deposited on CZ by this process. With modifications to the surface-cleaning procedure, similar layers can also be deposited on other gem materials, including emerald, opal, and tanzanite. Colored gemstones coated with diamond-like carbon have been available in the trade for years (Koivula and Kammerling, 1991).

See end of article for About the Authors and Acknowledgments.
Gems & Gemology, Vol. 48, No. 1, pp. 18–30,
http://dx.doi.org/10.5741/GEMS.48.1.18.
© 2012 Gemological Institute of America

BOX A: QUESTIONS SURROUNDING THE IDENTIFICATION AND DISCLOSURE OF THIN-FILM COATINGS ON GEMSTONES

The availability of gemstones and pearls with thin colored or colorless coatings, containing not only synthetic diamond but possibly other materials, poses real challenges for gem identification and treatment disclosure. The jewelry trade needs to consider such questions as:

1. What requirement does a gemological laboratory, gemologist, appraiser, or jeweler have to disclose the presence of a coating that may not be detectable or permanent?
2. What is the requirement to disclose a colorless coating when it does not appear to change the gem material's properties, appearance, or durability?
3. Does a layer on the surface of a polished gem material have a thickness threshold, above which it would be considered a coating (requiring legal disclosure) and below which it would be considered a surface contamination (not requiring disclosure)?
4. What proof is necessary from a producer before making claims that a coating of a given thickness offers protection or improves the underlying gem material's optical characteristics?
5. What responsibility do sellers of gem materials with colorless coatings have to substantiate claims regarding the benefits provided by the coating?
6. What guidelines regarding coating durability and coating permanence should be established for a treated gem material?
7. While advanced gemological testing techniques currently in use are designed to analyze the bulk chemical and spectral properties of a gem material, what techniques will be required now and in the future to detect and identify coatings on the polished surfaces of gem materials?

The present study was undertaken to determine the nature of the colorless coating on Diamantine. Earlier, Eaton-Magaña and Chadwick (2009) examined 14 samples of colorless EternityCZ, marketed by Serenity as "nanocrystalline synthetic diamond coated" cubic zirconia. Since the coating technology may change over time, it is unclear if the material they examined is the same as the product described here. In both instances, the coated samples displayed the gemological properties of cubic zirconia.

WHAT IS DIAMANTINE?

Serenity's website indicates that Diamantine is produced by a proprietary process—which consists of a thorough cleaning of the CZ facet surfaces, followed by a plasma-enhanced ion deposition—to create a coating on the CZ consisting of a dispersion of tiny carbon-containing particles embedded in a matrix. The website indicates this process "involves the development of a coating of nanocrystalline diamond particles of size below 60 nm uniformly on all cut surfaces of the gem material utilizing Serenity's proprietary nanodiamond technology… The average size of these particle clusters varies between 5–30 nm." An illustration on Serenity's website shows the Diamantine coating consisting of three portions, as seen in cross-section: an "adhesion layer" deposited directly on the surface of the CZ to help the carbon-containing particles adhere to the substrate, a thicker intermediate layer containing "nanocrystalline diamond" particles embedded randomly in a more abundant matrix material, and a "protective outer layer."

A study of the structure of the coating layer was commissioned by Serenity in February 2009 and was performed by Evans Analytical Group (EAG) in Santa Clara, California. The full results compiled by EAG may be found on Serenity's website. High-resolution transmission electron microscopy (HRTEM) produced high-magnification (>100,000×) images showing the combined thickness of the coating was on the order of 50 nm. In these HRTEM images, the coating did not appear to be evenly distributed, which suggests that it may be thinner or even absent from small regions of the gem's surface. Additional images at 138,000× magnification obtained using scanning electron microscopy (SEM) clearly showed the presence of nanocrystalline particles in the size range of 5–20 nm. Chemical analysis of selected areas of the coating on two Diamantine samples by energy-dispersive X-ray spectroscopy (EDS) detected the following elements in varying concentrations: Al, Ti, Si, O, Zr, and C. Some spots showed high Zr and low C concentrations, which suggests that the coating was either absent or present only as an extremely thin layer on the substrate CZ.

The Serenity-EAG 2009 study also included an electron diffraction pattern image that was obtained

by passing an electron beam through a very thin vertical cross-section of the coating and the CZ substrate. Within the coating layer were small regions of crystalline material (with a regular arrangement of distinct layers of atoms) in an otherwise structurally amorphous matrix (with randomly arranged atoms) that appeared to constitute most of the coating. The (hkl) spacings between atomic layers within the small crystalline regions corresponded to the lattice spacings in diamond (111), as well as those in metallic Al (002) and Ti (102), as stated on Serenity's website. The lattice spacings in another coating corresponded only to diamond, with no Al and Ti, which Serenity representatives interpreted as indirect evidence of "nanocrystalline diamond" particles in the coating.

We did not have the opportunity to examine the coated CZ samples studied by EAG. As with the results by Eaton-Magaña and Chadwick (2009) on Serenity-coated CZ, we can only assume that those samples were similar to the ones examined here.

MATERIALS AND METHODS

Materials. The Diamantine product uses CZ starting material that is cut and polished to higher standards than most cubic zirconia in the market. We also obtained very well-cut CZ samples for Serenity to coat for us. These samples did not exhibit the typical poor symmetry and facet polish seen in commercial CZ, but instead were cut to precise angles so their face-up appearance pattern mimicked that of the best cut-grade ranges for round brilliant-cut diamonds.

Sixty-five cubic zirconia samples were initially used in the study; all were standard round brilliants weighing 1.41–2.08 ct. Of these samples, 39 were coated by Serenity in the fall of 2009 and early 2010 to create their colorless Diamantine product, while the remaining 26 were left uncoated for comparison. Each of these 65 samples was first laser-inscribed on the girdle surface with a project identification number. Each was examined with 10× magnification by experienced GIA laboratory staff who plotted any minor surface imperfections using standard diamond clarity grading procedures.

In addition to the coated faceted samples, one of two flat polished CZ plates measuring ~7.5 mm in diameter was "thickly" coated (~100 nm) by Serenity for this study in October 2009.

As mentioned above, in the Diamantine material that is sold commercially, a thin layer is applied as a protective surface on top of the layer containing the carbon nanoparticles. To assist GIA in analyzing the underlying carbon-containing layer, in April 2010 Serenity provided five additional coated faceted CZ samples (1.69–2.01 ct) that did not include the adhesion and protective layers.

Six additional faceted samples (1.74–2.03 ct) of Diamantine were purchased through a third party in July 2011.

In Brief

- Diamantine (like uncoated CZ) is easily distinguished from diamond on the basis of thermal conductivity.
- When imaged by SEM, the coating contains nanocrystalline particles that appear consistent with diamond. However, testing by methods available to us could not confirm their identity.
- These nanocrystalline particles did not completely remain on the CZ after simple durability tests (such as cleaning with a polishing cloth, with or without alcohol).
- Serenity is reportedly planning to release a new version of Diamantine, along with a testing device that can detect the coating.

Gemological Examination and Advanced Data Collection at GIA. Samples of the coated CZ were subjected to standard gemological testing methods to detect any evidence of the coating, its effects, and differences between the coated and uncoated material. For this examination we used a Nikon Eclipse LV100 polarizing microscope with Nomarski differential interference contrast illumination and 1,000× magnification capability.

Representative samples of the coated CZ were also tested with more advanced spectroscopy instrumentation (although Serenity officials maintain that such techniques cannot effectively characterize thin-film coatings). Spectroscopic analyses were performed on both the coated and uncoated polished plates and on 10 coated and several uncoated CZ samples. Infrared absorption spectroscopy was done on carefully cleaned samples in the mid-infrared (6000–400 cm^{-1}, 1 cm^{-1} resolution) and reflective near-infrared (up to 11000 cm^{-1}, 4 cm^{-1} resolution) ranges at room temperature with a Thermo Scientific Nicolet 6700 Fourier-transform infrared (FTIR) spectrometer. A total of 512 scans per spectrum were collected to improve the signal-to-noise ratio. Ultraviolet-visible–near infrared (UV-Vis-NIR, 250–1000 nm) absorption spectra were measured with a PerkinElmer Lambda 950 spectrometer using a 1.0 nm bandpass. Photoluminescence (PL) and Raman

spectra were obtained with a Renishaw InVia Raman confocal microspectrometer. Four lasers with five excitation wavelengths were employed to activate optical defects in the coating: an Ar-ion laser at 488 and 514.5 nm, an He-Ne laser at 633 nm, a diode laser at 830 nm, and an He-Cd metal-vapor laser at 325 nm. Raman spectra (typically 2500–500 cm^{-1}, and 1600–1200 cm^{-1} for high-accumulation runs) were collected using all five excitation wavelengths. To observe the characteristic diamond Raman peak at 1332 cm^{-1} we also tried several experimental variations, including the use of liquid-nitrogen temperatures to cool the samples, high magnification during spectra collection, both standard and confocal operating modes, up to 60 accumulations to improve the signal-to-noise ratio, and applying a thin gold layer to the coated surface to facilitate a modified technique known as surface-enhanced Raman spectroscopy (SERS; see Huang et al., 2000; Prawer and Nemanich, 2004).

Qualitative energy-dispersive X-ray fluorescence (EDXRF) data were collected using a Thermo ARL Quant'X EDXRF analyzer to see if Al and Ti could be detected in the coating on five samples. These were selected from the initial study group of 39 samples; on each one, the table surface was analyzed. Two data acquisition conditions were used to optimize the detection of these elements: (1) for Al—4 kV voltage, 1.62 mA current, no filter, and 100 second count time, under vacuum; (2) for Ti—12 kV voltage, 1.98 mA current, Al filter, and 100 second count time, under vacuum. Note that laser ablation–inductively coupled plasma–mass spectrometry (LA-ICP-MS) analysis was not attempted because the coating layer is too thin to be sampled sufficiently by the ablation procedure for analysis.

Coating Characterization at Commercial Analytical Facilities. A second EAG study was commissioned by GIA in October 2009 to investigate the chemical composition of the coating layer. Analyses were carried out by dynamic secondary ion mass spectrometry (SIMS) using a Physical Electronics 6650 quadrupole-based system (figure 2). Because of the high cost of SIMS, only two samples were analyzed: a commercial Diamantine (sample CZ105) and a coated specimen that did not include the adhesion and protective layers; both of these were coated and obtained directly from Serenity.

With the SIMS technique, the sample is bombarded under vacuum conditions with a finely focused, ~50 mm diameter beam of cesium ions (1 kV, 135 nA), which results in the ejection and ionization of atoms from the sample. These secondary ions are accelerated into a double-focusing mass spectrometer, where they are separated according to their energy and mass/charge ratio and detected. Continued exposure of the sample to the beam of cesium ions gradually erodes the target area (~600 × 600 µm) layer-by-layer to form a flat-bottomed crater. Over time, data can be obtained at progressively greater depths below the surface to produce a depth profile of the changing chemical composition through the coating down into the substrate CZ. The actual depths of the pits created by SIMS analysis of the Serenity samples were subsequently measured. The elemental concentrations and sputter rates were determined using a calibrated diamond-like carbon test sample. From the pit depth, beam parameters, and milling time, EAG determined the depth of each element in the coating. Several positions on the table facet of each sample were analyzed to ensure the data were representative.

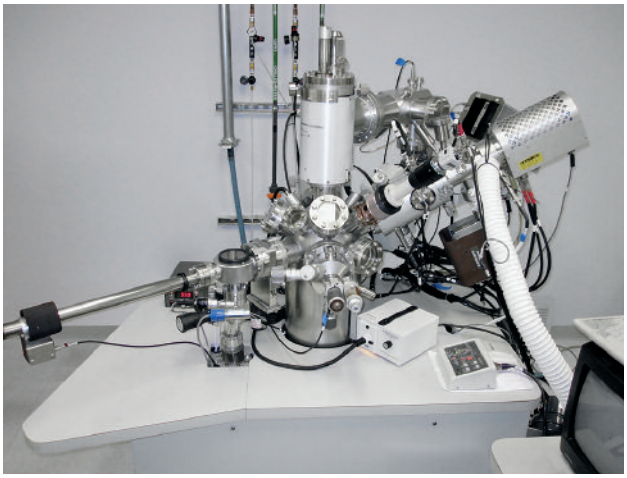

Figure 2. The uncoated and coated CZ samples were analyzed by dynamic secondary ion mass spectrometry (SIMS) at Evans Analytical Group in Santa Clara, California. Photo by Tim Thomas.

The elements analyzed by SIMS included H, C, N, O, Al, Ti, and Zr. The results were quantified using the Rayleigh backscattering method on two reference samples, each consisting of a thin layer (30.5 and 150 nm) of diamond-like carbon (DLC). This quantification provided a means to convert the signal intensity of ions removed from the sample to element concentration values. The detection limit was 1×10^{19} atoms/cm^3 for H, and 1×10^{18} atoms/cm^3 for C, N, and O. The rate of removal (or sputtering) of atoms from the surface by the cesium-ion beam can also provide information on coating composition (since the rate varies with the type of material), and this was also quantified on the

DLC reference samples. Also analyzed by this method were an amorphous carbon reference standard and a silicon sample coated with microcrystalline synthetic diamond.

Additionally, scanning electron microscopy (SEM) and energy-dispersive X-ray spectroscopy (EDS) was performed on two occasions to examine several coated and uncoated samples at the California Institute of Technology (Caltech) in Pasadena. The instrument consisted of a high-resolution analytical scanning electron microscope (LEO 1550 VP FESEM) equipped with an Oxford INCA Energy 300 EDS system, operated with an accelerating voltage of 10 kV and electron beam current of 10 nA. On the first occasion (December 2010), three faceted Diamantines (two obtained in 2009 and one in 2010), the "thickly" coated CZ plate, and one uncoated faceted CZ were imaged by SEM, and then the EDS spectra were collected. Due to the amount of charging on these nonconductive samples, we deposited 10 nm of conductive carbon using a turbo-carbon evaporator and reimaged the samples at higher magnification (up to 150,000×). On the second occasion (July 2011), we examined five Diamantine samples that had just been purchased through a third party (with a specific request from us to not handle them in any way). We deposited 10 nm of conductive carbon on the samples and imaged them with SEM.

After SEM analysis, these later five samples were then subjected to durability testing to see how well the coating adhered to the CZ substrate. (Note that the conductive carbon coating that we applied to these samples would not affect the adhesion of Serenity's coating.) Five tests, each one carried out on a different Diamantine sample, consisted of:

A. Cleaning for 30 seconds with a gem cloth
B. Cleaning for 30 seconds with a gem cloth and alcohol
C. Application of adhesive tape across the table facet
D. Rubbing the table facet for 30 seconds against a slurry of aluminum oxide powder and water on an aluminum oxide-impregnated polishing lap (followed by cleaning with a gem cloth and alcohol)
E. Rubbing the table facet for 30 seconds against 60,000 diamond grit in oil on a polishing lap (followed by cleaning with a gem cloth and alcohol)

We then recoated the five samples with 10 nm of conductive carbon and reimaged them with the SEM. The durability tests and SEM imaging were completed within four hours after the Diamantine package was initially opened.

Additional Testing. Our initial visual observation and jewelry manufacturing testing experiments are briefly described in box B. The results of these investigations became questionable after our second SEM examination revealed that the coating could be partially removed from Diamantine by simple cleaning procedures. We therefore became concerned that the coatings on the earlier samples used in this testing

BOX B: INITIAL VISUAL OBSERVATION AND JEWELRY MANUFACTURING TESTING

Visual Observation Testing. We conducted two rounds of visual observation tests to compare the face-up appearance of the Diamantine product with that of colorless round-brilliant CZs and diamonds based on GIA's cut-grade parameters (Moses et al., 2004). Our goal was to see if the coating improved the appearance of these CZ samples, producing a stronger resemblance to diamond.

In general, our observers could not distinguish between the face-up appearance of diamond, coated CZ, and uncoated CZ.

Testing of Jewelry Manufacturing Procedures. On its website, Serenity warns customers not to have a Diamantine sample polished, recut, or subjected to heat from a jeweler's torch. We conducted two tests to check the durability of the Diamantine product using typical manufacturing and repair procedures. These consisted of (1) casting a CZ in place in a ring and (2) finishing a gold ring set with CZ by filing and finishing the four metal prongs.

We found no difference in the behavior of the coated and uncoated CZ samples in the two repair procedures.

TABLE 1. Comparison of physical properties of two carbon allotropes (graphite and diamond) and some intermediate carbon-based thin-film coating materials.

	Graphite	Diamond-like carbon	Nanocrystalline diamond	Single-crystal diamond
Description	Crystalline carbon (graphite) with a hexagonal structure and sp^2 bonding (and weak bonding between the hexagonal layers)	Amorphous carbon with significant sp^2 bonding in an sp^3 network, but without long-range crystallinity	Uniform distribution of diamond crystallites (3–15 nm) with sp^2 carbon bonding along grain boundaries	Cubic crystalline carbon (diamond) with pure sp^3 bonding
Approximate amount of sp^3 (i.e., diamond) bonding	0%	33%[a], 40%[b]	90%[a,c]	100%
Density (g/cm^3)	2.02–2.23	2.9[d]	3.5[b]	3.53
Refractive index	1.8[e]	1.75[f]; 1.85–1.95[a]	2.0–2.1[a]; 2.34[g]	2.418
Vickers hardness (GPa)	0.14[h]	5–49[b]; 6.5–37[f]	40–75[b]	55–113[b]

Sources: [a] Mednikarov et al., 2005; [b] Gielisse, 1998a; [c] Gruen, 1999; [d] Herrera-Gomez et al., 2010; [e] Willis, 1970; [f] Gielisse, 1998b; [g] Potocky et al., 2009; [h] Patterson et al., 2000.

had been accidentally removed by such cleaning, so the results will not be described here and further study will be needed to address these subjects.

RESULTS

Gemological Examination. We suspect that during the coating deposition process, one or more carbon-containing materials—including diamond, diamond-like carbon, and carbon (graphite)—could be produced, depending on the deposition conditions. Table 1 provides a comparison of these carbon materials' physical properties.

We found no differences in gemological properties between Diamantine and standard CZ samples. The coating could not be seen in reflected light with a standard gemological microscope, or in polarized transmitted light at 1,000× magnification. Diamantine was not misidentified as diamond using, for example, a standard thermal conductivity probe.

With the exception of Raman spectroscopy, standard analytical methods and instruments used in major gemological laboratories are unlikely to detect a very thin, colorless, carbon-containing coating on a polished CZ or other gem material—or, if such a coating is detected, to confirm that the carbon is in the crystalline form of diamond. Raman spectroscopy is the most established method for determining the type of carbon present in a material. The diamond Raman peak (produced by sp^3 bonding of carbon atoms) is located at 1332 cm^{-1}, while the graphite-related Raman feature (where the carbon has sp^2 bonding) is a broad band centered at ~1550 cm^{-1} (see Zaitsev, 2001, pp. 69–70, 111–112). Our Raman spectroscopy investigation was unable to detect the 1332 cm^{-1} or the ~1550 cm^{-1} peak (figure 3, top), even with a 325 nm UV laser at liquid-nitrogen temperatures on the CZ plate represented as having a "thick" coating (figure 3, bottom).

We also were unable to establish the presence of the coating using the other spectroscopic techniques available in GIA's laboratory. The results from reflective NIR and UV-Vis-NIR spectra were inconclusive; mid-FTIR and PL spectroscopy showed only features consistent with the underlying CZ.

EDXRF chemical analysis detected a weak X-ray fluorescence peak characteristic of Ti in the coating of the tested Diamantine samples. This feature was not detected in the uncoated CZ, thus providing evidence for identifying the presence of one component of the Diamantine coating (figure 4).

SEM Characterization. Two sets of samples were analyzed by SEM to look for visual evidence of the nanocrystalline particles. These tests were an attempt to reproduce Serenity's SEM images at the same or higher magnification.

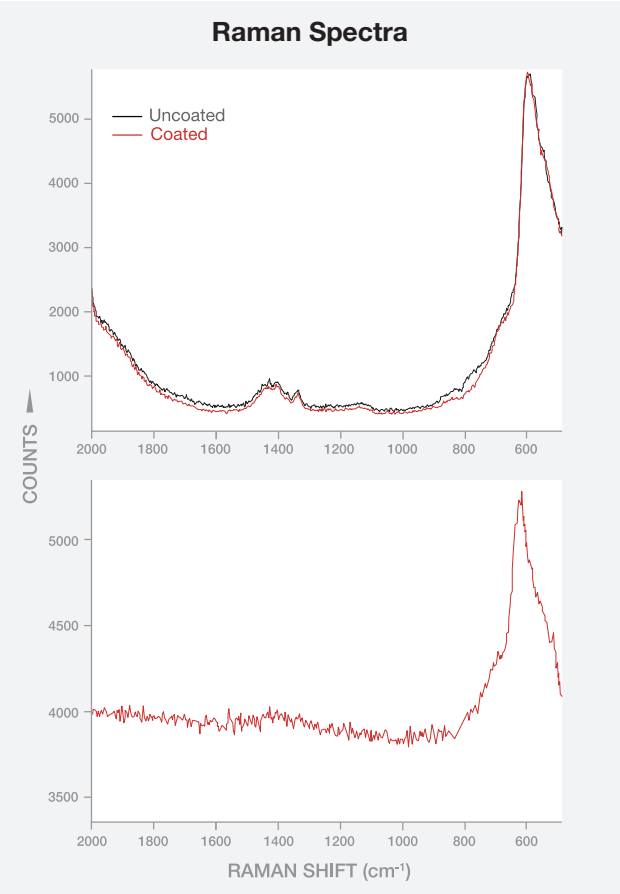

Figure 3. Raman spectra were collected with a 325 nm laser from a CZ plate before and after a "thick" coating was applied by Serenity Technologies (top). The spectrum for the coated sample overlays that of the uncoated sample, and showed no significant differences in the regions associated with carbon—neither the 1332 cm^{-1} peak characteristic of diamond nor the ~1550 cm^{-1} peak associated with graphitic carbon. As shown on the bottom, Raman spectra of the coated sample at liquid-nitrogen temperature collected using a 325 nm laser at 50× magnification and 60 accumulations could not detect the 1332 cm^{-1} peak in the coating.

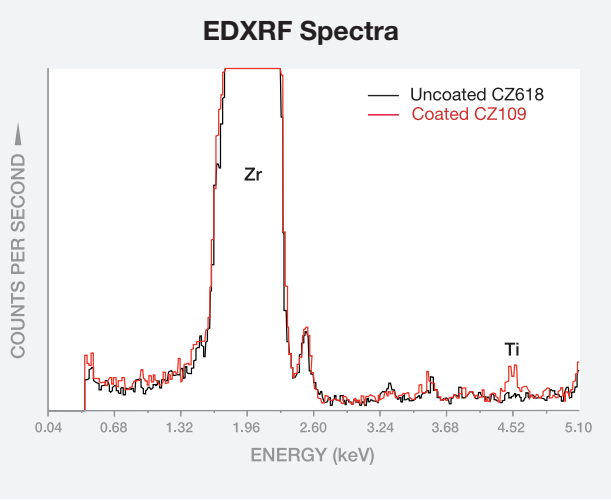

Figure 4. This EDXRF spectrum of a Diamantine sample shows a weak emission peak due to Ti, which is absent from the spectrum of the uncoated CZ. The dominant feature in both spectra is the large peak due to Zr.

The first study was comprised of samples used in other tests that had been in GIA's possession for 7–18 months. During this time, these samples had been subjected to standard procedures of cleaning with isopropyl alcohol and handling with tweezers on numerous occasions. The SEM images of these "coated" samples generally showed no indication of a coating. Even at very high magnification (150,000×), we were unable to observe any nanocrystalline particles. The notable exception was the "thickly" coated plate (figure 5). We observed some small remnants of what appeared to be nanoparticles (figure 5B and 5C), though these images were not entirely consistent with the manufacturer's SEM image of the same disk just after coating (figure 5A). The vast majority of the images obtained from surveying the surface of the coated samples were, in contrast, more consistent with the uncoated sample (compare figures 5D and 5E). Very little carbon was detected, generally, and the carbon signature increased with the deposition of the 10 nm conductive carbon coating.

Unable to observe the coating on these samples, we decided to procure some new, untouched samples and study the conditions that might remove the Diamantine coating. The second SEM study was conducted in July 2011 using samples acquired through the trade, and the packaging was not opened until minutes before the samples were placed in the SEM. In all five samples, we consistently observed crystallites with a grain size of about 50–100 nm (left images in figures 6A–E). However, significant changes were seen in most of the images collected after durability testing. The Serenity coating was somewhat able to withstand the first test (rubbing with a gem cloth), but the other four tests removed the larger crystallites from the CZs (right images in figures 6A–E). Some smaller, low-relief grains underneath the larger crystallites still remained, but most of the "nanocrystalline" component (presumably synthetic diamond) was gone.

These SEM images and EDS spectra clearly indicated that the coating is not durable enough to withstand normal use. The majority of the coating was gone after

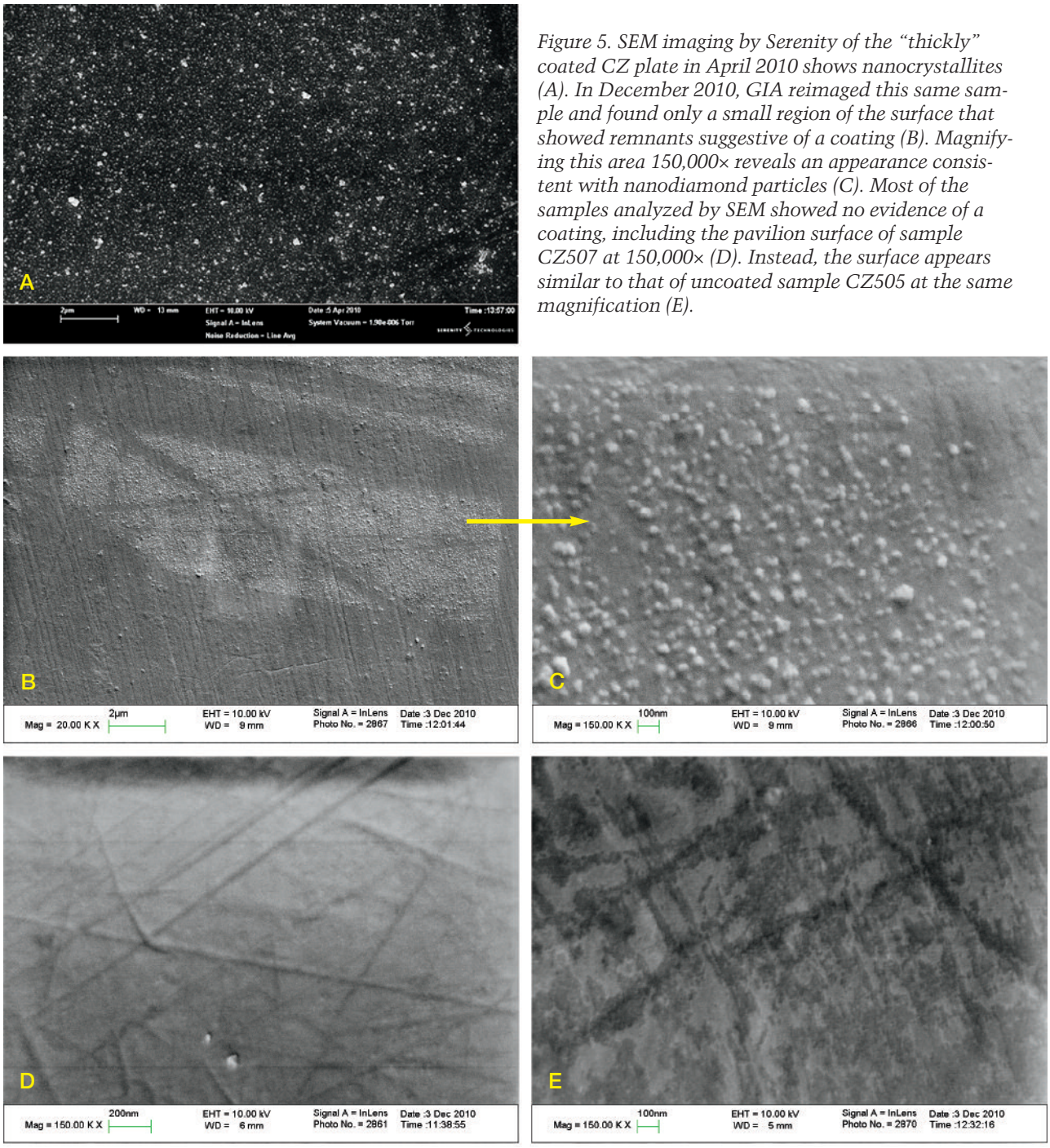

Figure 5. SEM imaging by Serenity of the "thickly" coated CZ plate in April 2010 shows nanocrystallites (A). In December 2010, GIA reimaged this same sample and found only a small region of the surface that showed remnants suggestive of a coating (B). Magnifying this area 150,000× reveals an appearance consistent with nanodiamond particles (C). Most of the samples analyzed by SEM showed no evidence of a coating, including the pavilion surface of sample CZ507 at 150,000× (D). Instead, the surface appears similar to that of uncoated sample CZ505 at the same magnification (E).

30 seconds of deliberate cleaning or other abrasion (with the exception of simply rubbing the sample with a gem cloth). When subjected to longer periods of standard use—handling with tweezers, gemological testing, and cleaning with a gem cloth or isopropyl alcohol—the coating seems to disappear entirely; even the small low-relief grains observed in the "after" images of the durability study are no longer present. These results call into question the stability of this coating in real-world applications. Because the coating is colorless, it would be difficult (if not impossible) for a gemologist or consumer to verify the continued existence of the

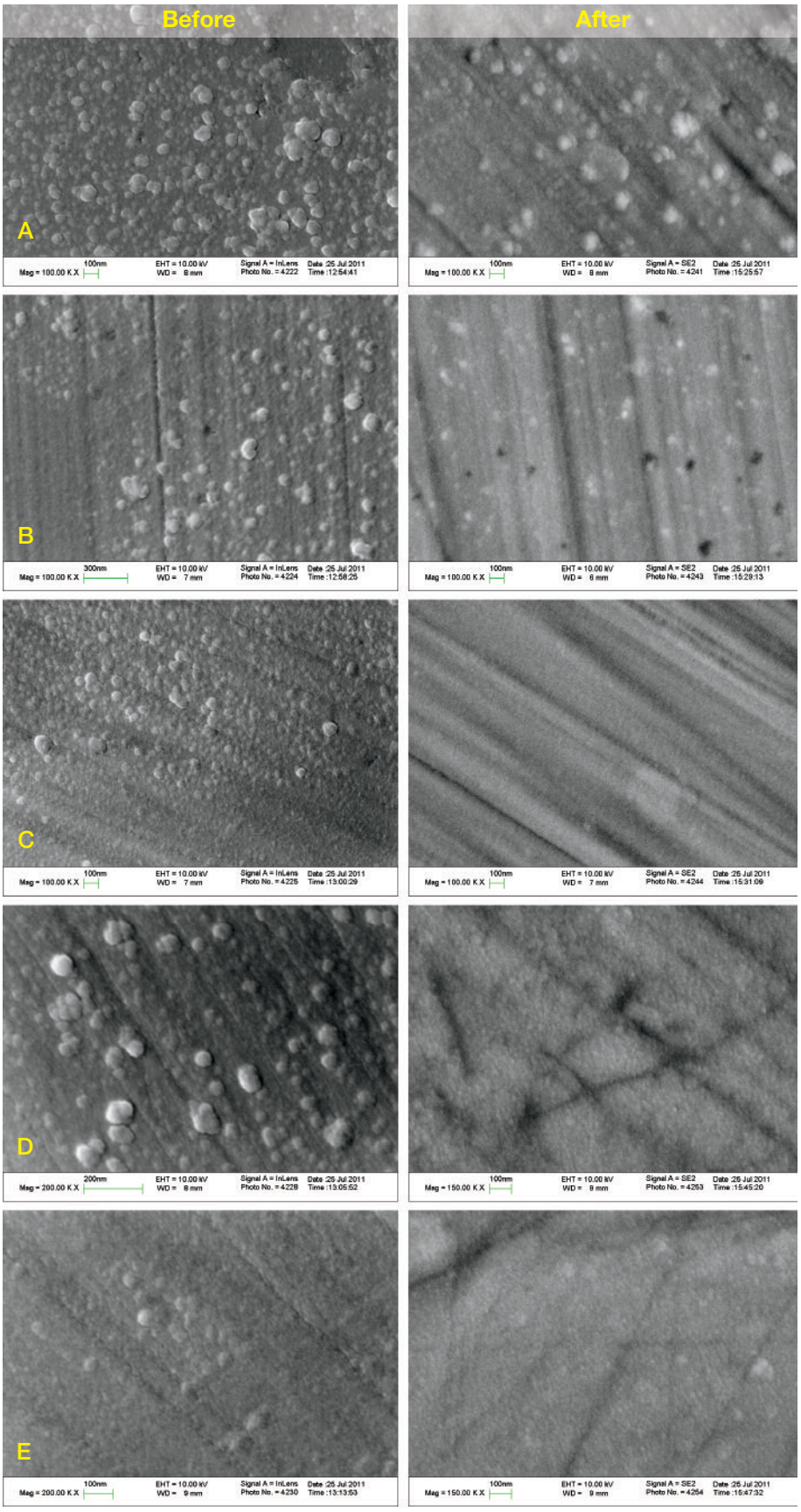

Figure 6. This series of before-and-after SEM images (magnified 100,000×–200,000×) showcases the effects of various durability tests on a set of never-handled Diamantine samples acquired in July 2011. All of the "before" images show crystallites, most of which were removed by the durability tests. The five "after" images correspond to durability tests A through E, respectively, that are described in the Materials and Methods section. These 30-second tests did not remove the coatings entirely, as the "after" images show some small, low-relief remnants of material.

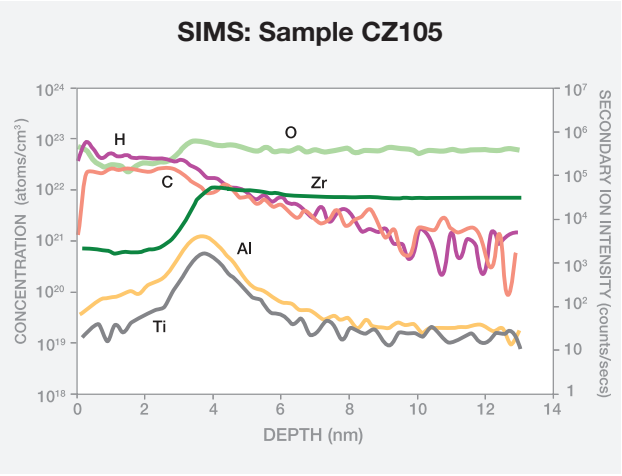

Figure 7. This SIMS depth profile of Diamantine sample CZ105 shows concentrations of C and H to depths of about 5 nm, and concentrations of Ti and Al with highest values at about this same depth. These results suggest that the carbon-containing coating is about 5 nm thick. The presence of Zr and O directly on the sample surface when sputtering begins indicates that some areas of the CZ surface lack the coating layer.

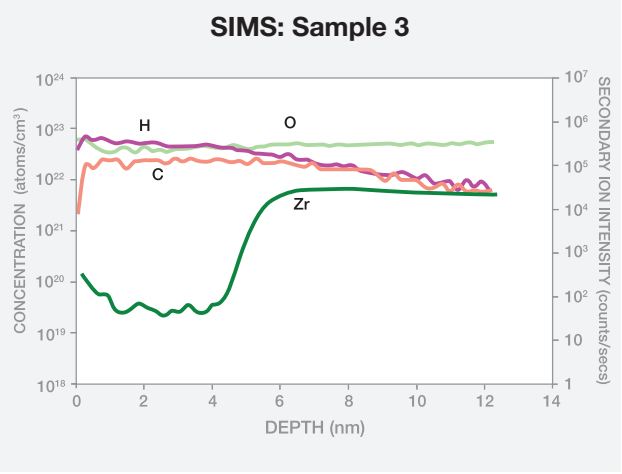

Figure 8. This SIMS depth profile is similar to the one shown in figure 7, except the sample was not coated with the metallic adhesion layer or protective outer layer. As a result, the Ti and Al concentration profiles seen in figure 7 are absent here.

reported nanocrystalline synthetic diamond component of the Diamantine coating; such a finding would require SEM examination.

SIMS Characterization. Concentration depth profiles through the coating layer into the CZ substrate are presented for commercial Diamantine sample CZ105 (figure 7) and for CZ sample 3, a coated specimen that did not include the adhesion and protective layers (figure 8). As both figures show, C and H were detected at the surface, and their concentrations decreased by about a factor of 100 within approximately 5 nm of the surface. The Al and Ti concentrations of CZ105 peaked at about the same depth, suggesting that the carbon-containing layer above the adhesion layer is only about 5 nm thick. It is unclear if the coating layer has a similar thickness on all facets of the CZ. The rate of sputtering by the beam was more consistent with amorphous carbon than with diamond, which indicates that amorphous carbon likely comprises a portion of the coating's content.

It should be noted that the coating thickness of approximately 5 nm documented by the SIMS analyses of these two samples does not match the ~30–50 nm coating reported on the Serenity website (TEM image no. 4 indicates 30 nm). Explanations for this discrepancy could include: (1) inconsistent application of the coating from one sample to another (or within a given sample); (2) inadvertent removal of the coating by standard cleaning and handling, as in the "after" images of figure 6; (3) the possibility that the coating had been removed entirely and the detected carbon was simply due to contamination; and (4) the possibility that the SIMS analysis under-represented the true thickness. The detection of Zr and O at the surface of the samples immediately upon sputtering suggests there may be areas where no coating was present, which agrees with the HRTEM images on Serenity's website that appear to show a nonuniform deposition of the coating.

As stated above, Serenity's website describes the coating as consisting of three layers—an adhesion layer, a layer containing the "nanocrystalline diamond" particles, and a protective outer layer. Based on our SIMS results, we could not chemically differentiate these three layers.

DISCUSSION

According to the determination made in the October 2009 EAG study, both coated samples tested by SIMS showed a carbon concentration of 2.5×10^{22} atoms/cm^3 in the coating layer (again, see figures 7 and 8). This value is a fraction of the reported density for nanocrystalline diamond (1.74×10^{23} atoms/cm^3 or 3.5 g/cm^3) and diamond-like carbon (1.46×10^{23} atoms/cm^3 or 2.9 g/cm^3), which likely indicates that a lower-density matrix material forms the dominant portion of the coating on Diamantine.

From the reported thickness of 30 nm provided by Serenity, we determined the maximum amount of

carbon that could be deposited in the coating. These values can be combined with the surface area of the CZ to calculate the volume of carbon added to the entire stone. For a representative round brilliant CZ with a weight of 1.76 ct (6.49 × 6.52 × 3.88 mm), we estimated a total coating surface area of 86.5 mm^2. If the entire coating were composed of nanocrystalline synthetic diamond, which we know is not the case, the 30 nm carbon coating would add a weight of ~9.0 µg or approximately 0.000045 ct. The added weight of the actual nanocrystalline synthetic diamond particles would be less than this value because they appear to be a small component of a non-diamond matrix, and they would likely be removed by handling.

To put a coating thickness of 30 nm into perspective, consider that if this coating consisted of nanocrystalline synthetic diamond (assuming a lattice spacing of 0.357 nm), it would only be 84 atoms thick. As our results show, this coating—regardless of the actual form of the carbon—does not add to the durability of the CZ, nor does it appear to be stable to normal wear and cleaning. Therefore, it is difficult to ascertain the gemological value added by these thin-film colorless coatings.

The absence of any Raman peaks associated with diamond is not surprising, given the extreme thinness of these coatings and the likelihood that carbon is not the dominant component of the thin film. Also, it is likely that we were unable to detect the diamond Raman peak because the coating was no longer present on the CZ. The Raman spectrum provided for the coating on the Serenity website was collected using a different substrate material; CZ was not used in that instance due to its background signal (S. Neogi, pers. comm., 2009). To our knowledge, then, the characteristic Raman peak for diamond has not been observed from any nanocrystalline synthetic diamond–coated CZ.

Previous studies of Serenity-coated colored diamonds (see Shen et al., 2007) with coatings as thick as 40 nm were unable to observe any coating-related peaks using PL spectroscopy. Most gemological laboratories are not equipped to measure or identify such thin coatings, and much of the equipment needed for such a surface analysis is time-consuming, prohibitively costly, or destructive. If such coatings become more prevalent within the gem trade and require identification, instrumentation and testing techniques may need to be added to the gemological laboratory repertoire.

Our SEM results strongly suggest that the Diamantine coating is not durable and does not reliably adhere to the underlying CZ. The SEM results appear to explain the thinness of the carbon layer measured by SIMS (~5 nm), as this value is closer to the typical thickness of adventitious carbon (i.e., contamination of ~1 nm by hydrocarbon species covering most surfaces that are exposed to air) than the thickness of the nanocrystalline synthetic diamond layer reported by Serenity.

Other studies have described nanocrystalline and polycrystalline synthetic diamond as a coating on materials such as silicon carbide (i.e., synthetic moissanite). Fan et al. (1996) used an interlayer of titanium carbide to improve the adhesion between the synthetic diamond crystals and the silicon carbide, and the lattice mismatch between diamond (0.357 nm) and silicon carbide (0.308 nm) is much lower than between diamond and cubic zirconia (0.517 nm). Those researchers reported polycrystalline synthetic diamond film thicknesses of 500–1000 nm, nearly 10 times thicker than those reported by Serenity for their coatings. Due to the synthetic diamond films' greater thickness and strong adhesion, Fan et al. easily characterized them with Raman spectroscopy and SEM.

Although the exact details of the coating process performed by Serenity are unknown to us, it is likely that the CZ is heated to a high temperature (during CVD synthetic diamond growth, the substrate is typically heated to 800–900°C). Alternatively, one U.S. patent application describes a procedure in which a stone is immersed in a nanodiamond slurry and then dried in inert gas; the nanodiamonds adhere to the surface through van der Waals forces (Neogi and Neogi, 2010). This does not appear to be the method employed by Serenity on Diamantine. Nevertheless, our SEM results indicate that the coating lacks long-term durability and may have even disintegrated in the course of our testing. The most enduring effect of the coating process might be the annealing of the cubic zirconia and the continued presence of the metals used in the "adhesion layer," although more tests would be necessary to confirm this.

The reported thickness of these films (30–50 nm) contributes very little carbon to the coated stone. The films' thinness probably stems from the fact that the coating material likely contains nanocrystalline synthetic diamond, and is not made up of single-crystal synthetic diamond. A non-single-crystal coating that is too thick would limit transparency. Additionally, the RI of nanocrystalline diamond (no higher than 2.34) is lower than that of diamond (2.418), so the visual effect of having a higher-RI coating material is not as great as if it were single-crystal diamond.

FURTHER DEVELOPMENTS

As this article was being prepared in the fall of 2011, Serenity representatives informed us that they had developed a newer version of Diamantine. They said they had stopped distributing the older version to their vendors in the spring of 2011, though we had no difficulty purchasing this product in July. This older material still exists in the trade and among consumers, and a version of Diamantine is currently being marketed by a major retail jewelry chain in India.

Serenity officials also told us they had developed a handheld testing instrument for commercial sale that would detect the presence of the Diamantine coating. In June 2011, the company posted an online video that showed the operation of this new instrument, which has tweezer-like probes that make contact with two points on the stone being tested. The instrument's screen displays the word "Diamantine" only when it detects the coating; when a diamond, uncoated CZ, or other type of material is tested, the screen simply reads "Serenity Technologies."

So far we have been unable to obtain further information on the new instrument or have the opportunity to examine it. We assume the instrument detects the presence of metal components in the coating (e.g., Al and Ti, or possibly another metal in the "new" version of this product) by testing for electrical conductivity. Such metallic components appear to have better adhesion to the CZ surface (as demonstrated by our EDXRF detection of Ti after the "diamond" coating may have been removed by our routine handling of Diamantine samples over a period of months). Since a diamond tests negatively on this device, the instrument apparently does not indicate whether the coating contains "nanoparticles of synthetic diamond."

Figure 9. Several samples of uncoated CZ (left, 1.48–1.84 ct) are shown here, together with Diamantine (right, 1.70–2.07 ct). Photo by Robert Weldon.

CONCLUSION

Cubic zirconia that is coated with a thin surface layer of "nanocrystalline diamond" to allegedly improve its appearance and/or durability has been marketed by Serenity Technologies as Diamantine (figure 9). We could not observe the thin colorless coating on Diamantine with the optical microscope, or with most standard analytical techniques used by major gemological laboratories. SEM imaging detected a nanocrystalline coating on newly purchased Diamantine samples, but the coating on these gems was subsequently largely removed by rudimentary cleaning and handling. Therefore, the SEM images called into question the long-term durability of this coating. The only technique that could establish whether the coating had ever existed was EDXRF, which detected the Ti from the metallic adhesion layer. Of course, this criterion is not useful for testing for coatings on Ti-bearing substrates.

We detected C, Ti, and Al using the SIMS technique, but we could not confirm that the carbon was in the form of diamond. The inability of Raman spectroscopy to detect the characteristic diamond peak at 1332 cm^{-1}, assuming the actual presence of diamond, is likely due to the thinness and instability of the coating. The SIMS data indicated that the carbon-containing coating was only about 5 nm thick on the two samples that were analyzed.

Coatings of "synthetic diamond" deposited on diamond simulants should not be confused with synthetic diamonds in which the entire weight and volume of the gemstone is actually diamond. Advanced gemological testing is sometimes needed to distinguish synthetic diamond from natural diamond. However, like uncoated CZ, Diamantine is easily separated from diamond (natural or synthetic) on the basis of thermal conductivity, weight-to-diameter ratio, and specific gravity.

Techniques for use in gemological laboratories for detecting coatings on gems will need to be refined in the future. Useful methods could include scanning electron microscopy (SEM) for high-magnification imaging and Nomarski differential interference contrast microscopy for investigating the flatness of a surface. When a difference in refractive index is suspected between the coating and substrate, the ellipsometry technique may be useful.

ABOUT THE AUTHORS

Dr. Shigley (jshigley@gia.edu) is a distinguished research fellow, Mr. Gilbertson is a research associate, and Dr. Eaton-Magaña is a research scientist, at GIA in Carlsbad.

ACKNOWLEDGMENTS

The authors thank Jayant Neogi and Dr. Suneeta Neogi of Serenity Technologies for supplying samples of their Diamantine product, and for coating several CZ samples provided by GIA. Jerry Golech, an instructor in the Jewelry Manufacturing Arts program at GIA in Carlsbad, assisted with the durability tests. Dr. Troy Blodgett of GIA helped analyze the visual observation test results. Tim Thomas of GIA organized the study of the coated CZ samples at commercial analytical facilities. Dr. Chi Ma collected the SEM images and EDS spectra at Caltech. Karen Chadwick (formerly at GIA in Carlsbad) assisted with the gemological characterization.

REFERENCES

Bennet K.E., Kearnes R.H. (2009) Azotic® thin-film surface enhancement of gemstones. *Canadian Gemmologist*, Vol. 30, No. 1, pp. 20–34.

Eaton-Magaña S., Chadwick K.M. (2009) Lab Notes: Cubic zirconia reportedly coated with nanocrystalline synthetic diamond. *G&G*, Vol. 45, No. 1, pp. 53–54.

Fan W.D., Jagannadham K., Goral B.C. (1996) Multilayer diamond coatings on silicon carbide. *Surface and Coatings Technology*, Vol. 81, No. 2/3, pp. 172–182, http://dx.doi.org/10.1016/0257-8972(95)02476-X.

Gielisse P.J. (1998a) Mechanical properties of diamond, diamond films, diamond-like carbon, and like-diamond materials. In M.A. Prelas, G. Popovici, and L.K. Bigelow, Eds., *Handbook of Industrial Diamonds and Diamond Films*, Marcel Dekker, New York, pp. 49–88.

——— (1998b) Mechanical properties of diamond films. In P.J. Gielisse, V.I. Ivanov-Omskii, G. Popovici, and M. Prelas, Eds., *Diamond and Diamond-Like Film Applications*, Technomic Publishing Co., Lancaster, PA, pp. 281–296.

Gruen D.M. (1999) Nanocrystalline diamond films. *Annual Review of Materials Science*, Vol. 29, pp. 211–259, http://dx.doi.org/10.1146/annurev.matsci.29.1.211.

Henn U. (2003) Gemmologische Kurzinformationen: Edelsteine met aufgedampften, hauchdünnen Metallschichten [Gemmological short notes: Gemstones sputtered with metallic thin films]. *Gemmologie—Zeitschrift der Deutschen Gemmologischen Gesellschaft*, Vol. 52, No. 1, pp. 41–44.

Herrera-Gomez A., Sun Y., Aguirre-Tostado F.-S., Hwang C., Mani-Gonzalez P.-G., Flint E., Espinosa-Magaña F., Wallace R.M. (2010) Structure of ultra-thin diamond-like carbon films grown with filtered cathodic arc on Si(001). *Analytical Sciences*, Vol. 26, No. 2, pp. 267–272, http://dx.doi.org/10.2116/analsci.26.267.

Huang B.R., Chen K.H., Ke W.Z. (2000) Surface-enhanced Raman analysis of diamond films using different metals. *Materials Letters*, Vol. 42, No. 3, pp. 162–165, http://dx.doi.org/10.1016/S0167-577X(99)00176-7.

Koivula J.I., Kammerling R.C., Eds. (1991) Gem News: Faceted gems coated with diamond-like carbon. *G&G*, Vol. 27, No. 3, p. 186.

Mednikarov B., Spasov G., Babeva T., Pirov J., Sahatchieva M., Popov C., Kulisch W. (2005) Optical properties of diamond-like carbon and nanocrystalline diamond films. *Journal of Optoelectronics and Advanced Materials*, Vol. 7, No. 3, pp. 1407–1413.

Moses T.M., Johnson M.L., Green B., Blodgett T., Cino K., Geurts R.H., Gilbertson A.M., Hemphill T.S., King J.M., Kornylak L., Reinitz I.M., Shigley J.E. (2004) A foundation for grading the overall cut quality of round brilliant cut diamonds. *G&G*, Vol. 40, No. 3, pp. 202–228, http://dx.doi.org/10.5741/GEMS.40.3.202.

Neogi S., Neogi J. (2010) Method for Producing Nanocrystalline Diamond Coatings on Gemstones and Other Substrates. U.S. Patent Application 20100068503 A1, March 18.

Ogden J. (2008) A coat of many colours. *Gems & Jewellery*, Vol. 17, No. 1, pp. 9–11.

Patterson J.R., Catledge S.A., Vohra Y.K., Akella J., Weir S.T. (2000) Electrical and mechanical properties of C_{70} fullerene and graphite under high pressures studied using designer diamond anvils. *Physical Review Letters*, Vol. 85, No. 25, pp. 5364–5367, http://dx.doi.org/10.1103/PhysRevLett.85.5364.

Potocky S., Kromka A., Potmesil J., Remes Z., Polackova Z., Vanecek M. (2009) Growth of nanocrystalline diamond films deposited by microwave plasma CVD system at low substrate temperatures. *Physica Status Solidi (a)*, Vol. 203, No. 12, pp. 3011–3015.

Prawer S., Nemanich R.J. (2004) Raman spectroscopy of diamond and doped diamond. *Philosophical Transactions of the Royal Society A*, Vol. 362, No. 1824, pp. 2537–2565, http://dx.doi.org/10.1098/rsta.2004.1451.

Schmetzer K. (2008) Surface treatment of gemstones, especially topaz – An update of recent patent literature. *Journal of Gemmology*, Vol. 31, No. 1/2, pp. 7–13.

Shen A.H., Wang W., Hall M.S., Novak S., McClure S.F., Shigley J.E., Moses T.M. (2007) Serenity coated colored diamonds: Detection and durability. *G&G*, Vol. 43, No. 1, pp. 16–33, http://dx.doi.org/10.5741/GEMS.43.1.16.

Willis C. (1970) The complex refractive index of particles in a flame. *Journal of Physics D: Applied Physics*, Vol. 3, No. 12, pp. 1944–1948, http://dx.doi.org/10.1088/0022-3727/3/12/324.

Zaitsev A.M. (2001) *Optical Properties of Diamond: A Data Handbook*. Springer Verlag, Berlin, 502 pp.

The Dr. Edward J. Gübelin Most Valuable Article AWARD

Most Valuable Article

First Place

GIA's Symmetry Grading Boundaries for Round Brilliant Cut Diamonds

Ron H. Geurts, Ilene M. Reinitz, Troy Blodgett, and Al M. Gilbertson

Ron Geurts

Ron Geurts is research and development manager at GIA in Antwerp. For more than a decade, Mr. Geurts has helped develop GIA's diamond grading processes. **Ilene Reinitz**, a project manager at GIA, joined the New York lab in 1990. She holds a doctorate in geochemistry from Yale University and has written numerous articles for *G&G* and other publications. **Troy Blodgett** is a research scientist at GIA in Carlsbad. Dr. Blodgett holds a master's and doctorate in geology and remote sensing from Cornell University. **Al Gilbertson** is a research associate at GIA's Carlsbad laboratory. A former cutter and appraiser, Mr. Gilbertson is the author of *American Cut: The First 100 Years* (2007).

Second Place

Research on Gem Feldspar from the Shigatse Region of Tibet

Ahmadjan Abduriyim, Shane F. McClure, George R. Rossman, Thanong Leelawatanasuk, Richard W. Hughes, Brendan M. Laurs, Ren Lu, Flavie Isatelle, Kenneth Scarratt, Emily V. Dubinsky, Troy R. Douthit, and John L. Emmett

Ahmadjan Abduriyim

Ahmadjan Abduriyim is a GIA consultant and former chief research scientist at the Gemmological Association of All Japan Laboratory in Tokyo. He holds master's and doctorate degrees in mineralogy from Kyoto University. **Shane McClure** is director of identification services at GIA's Carlsbad laboratory. He is well known for his many articles and lectures on gem identification. **George Rossman** is profiled in the third-place entry. **Thanong Leelawatanasuk** is senior gemologist and chief of gem testing at the Gem and Jewelry Institute of Thailand, Bangkok. **Brendan Laurs** is editor and technical specialist of *G&G*, and holds a master's in geology from Oregon State University. **Ren Lu** is a research scientist at GIA's New York laboratory. He holds a master's in physics from Jilin University in China and a doctorate in mineral physics from the University of California, Davis. **Richard Hughes** is senior vice president at Hong Kong's Sino Resources Mining Corporation. Mr. Hughes has written numerous books and articles, and he received the 2010 Antonio C. Bonanno Award for Excellence in Gemology. **Flavie Isatelle** is a geologist and mining engineer with Vale Nouvelle-Calédonie. A graduate of the Ecole Nationale Supérieure de Géologie in Nancy, France, she has visited gem deposits around the world. **Ken Scarratt** is GIA's managing director for Southeast Asia and director of GIA Research. Mr. Scarratt headed the Gem Testing Laboratory of Great Britain, the AIGS Laboratory in Bangkok, and the AGTA Laboratory in New York before joining GIA in 2005. He is coauthor of *The Crown Jewels* and *The Pearl and the Dragon*. **Emily Dubinsky** is a research associate at GIA's New York laboratory. She holds a master's in geological and environmental sciences from Stanford University, and her current focus is the characterization of corundum. **Troy Douthit** put his Stanford University focus on materials science to use in a series of four Silicon Valley high-tech startups. He began developing thermochemical processes to improve Montana sapphire in 1989, and today he is a principal of Crystal Chemistry in Brush Prairie, Washington. **John Emmett**, a former associate director of the Lawrence Livermore National Laboratory, is also a principal of Crystal Chemistry. He holds a doctorate in physics from Stanford University.

Third Place

The Chinese Red Feldspar Controversy: Chronology of Research Through July 2009

George R. Rossman

George Rossman

George Rossman is professor of mineralogy at the California Institute of Technology in Pasadena. Dr. Rossman is a 2004 recipient of the Feynman Prize, Caltech's most prestigious teaching honor, and in 1998 a newly discovered species of tourmaline was named rossmanite in his honor.

We extend our thanks to all the readers who participated. And congratulations to **Andrea Blake** of Chevy Chase, Maryland, whose ballot was drawn from the many entries to win a one-year subscription to *G&G*, plus a flash drive containing the 2002–2011 back issues of the journal.

PRECISION MEASUREMENT OF INTER-FACET ANGLES ON FACETED GEMS USING A GONIOMETER

Andy H. Shen, William A. Bassett, Elise A. Skalwold, Nicole J. Fan, and Yong Tao

A classic two-circle reflecting goniometer was used to measure inter-facet angles on five faceted diamonds that included round brilliants and fancy shapes. The instrument provided significantly better precision (to within 2 minutes, or 0.034°) than the non-contact optical scanner that is customarily used at GIA for this purpose. With some procedural modifications, the goniometer could make measurements of all inter-facet angles, including the pavilion facets. The technique is potentially valuable for producing a well characterized set of reference stones for calibrating non-contact optical scanners.

In the modern gem trade, dimensions and facet angles on polished diamonds (figure 1) are usually measured with a computerized non-contact optical scanner (see Reinitz et al., 2005). Such devices are used by gem laboratories as part of the procedure for grading diamonds, and large manufacturers also employ them to determine the most profitable cuts. The scanner typically consists of a high-resolution digital camera, a rotating stage, a light source, and associated software. The camera takes hundreds of profile images as the diamond (usually placed table-down) rotates on the stage. The software then generates a 3D model of the polished diamond and calculates values for the dimensions, proportions, facet angles, and facet positions. The process may take as little as 10 seconds, depending on the number of pictures taken.

Makers of non-contact optical scanners usually claim a linear accuracy of ~10 µm and an angular accuracy of ~0.1°. But each manufacturer uses somewhat different algorithms in their proprietary software to generate the final 3D model, so the resulting values of the dimensions and angles can deviate from one maker to another. In fact, the results may vary from instrument to instrument. Therefore, users should establish a master set of standards, in the form of faceted gemstones with known dimensions and angles, so they can check the instrument to ensure accuracy and repeatability for daily operation. Unfortunately, these standard sets are not readily available. In addition, for calibration purposes the angles and dimensions of these "master stones" must be measured to even higher precision than non-contact optical instrumentation can provide. In this study, we examine the feasibility of using a well-established optical instrument—a classical two-circle reflecting goniometer—to measure the angles on faceted diamonds to very high precision, without relying on image analysis and computer algorithms.

BACKGROUND

For this investigation, we chose Cornell University's two-circle reflecting goniometer (figure 2). This type of goniometer was used extensively by mineralogists in the late 1800s and early 1900s to study the angles between faces on natural crystals (Burchard, 1998). Before the advent of X-ray diffraction techniques, these instruments played a major role in obtaining fundamental measurements that provided a deeper understanding of the geometry and structure of crystals.

While goniometers range in complexity and date back as early as the 1700s, the version used in this investigation is named for its inventor, Prof. V. M. Goldschmidt, the famous crystallographer and author of *Atlas der Krystalformen*. Made by Stoe & Rheinheimer of Heidelberg, with whom Goldschmidt worked closely, the Cornell instrument is a Model A, circa 1920 (O. Medenbach, pers. comm., 2011). According to Burchard (1998, p. 574), there are probably fewer than 800 reflecting goniometers predating World War II in existence, and only 10 of this particular model were manufactured in 1920. Interestingly, this goniometer was inspired by the need to measure a newly discovered gem. The pink spodumene crystals identified by George F. Kunz and now known as kunzite were so large that they could not fit in the pre-1905 Goldschmidt models

See end of article for About the Authors and Acknowledgments.
GEMS & GEMOLOGY, Vol. 48, No. 1, pp. 32–38,
http://dx.doi.org/10.5741.GEMS.48.1.32.
© 2012 Gemological Institute of America

Figure 1. These diamonds were used for the facet angle measurements in this investigation. From left to right, the stones weigh 0.20, 0.86, 0.62, 0.71, and 0.40 ct. Photo by Robert Weldon.

(Burchard, 1998). This design innovation suited our present needs in that it afforded adequate space for specialized mounting of the diamond. Modern reflecting goniometers (e.g., the Huber 302 model) employing the same principles as the Cornell instrument are typically used to orient crystals for X-ray diffraction. These high-precision instruments are capable of the same level of accuracy as the Cornell goniometer.

INSTRUMENTS AND METHODS

The two-circle reflecting goniometer consists of several key components, including two *wheels* (or *circles*), a

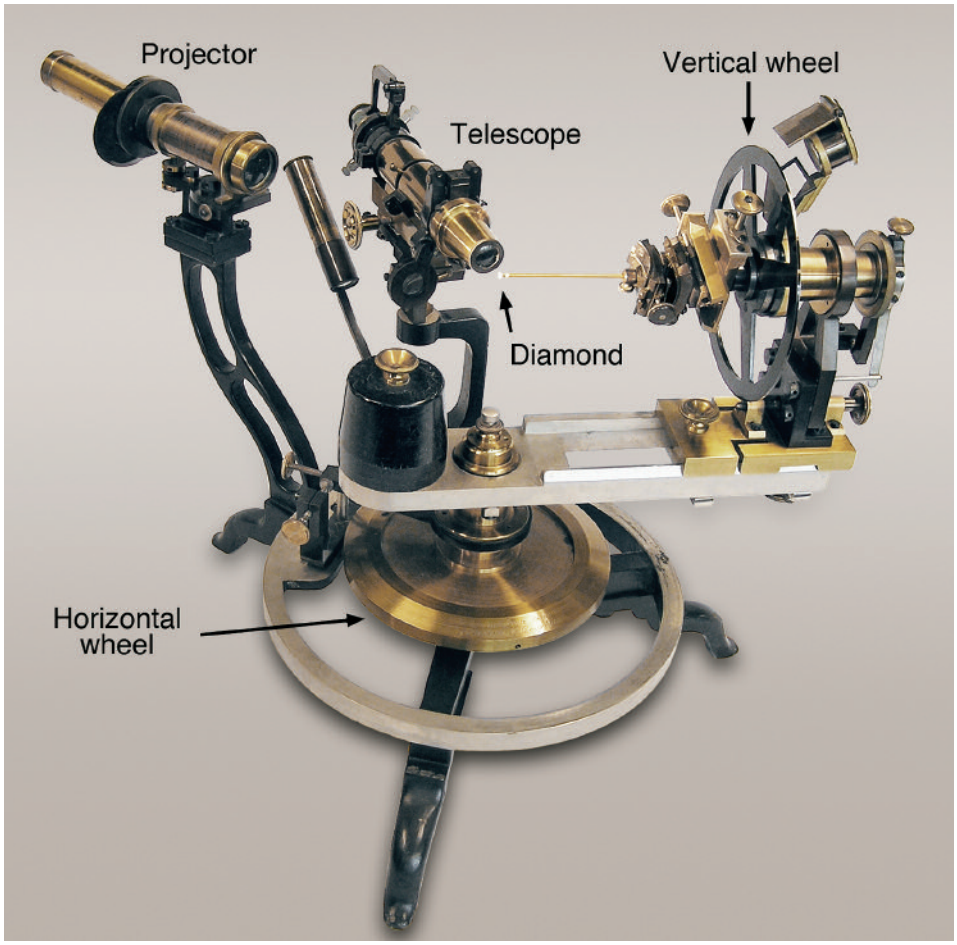

Figure 2. Cornell University's classic two-circle reflecting goniometer, built circa 1920, was used in this study. The instrument is approximately 42 cm tall. Photo by E. A. Skalwold.

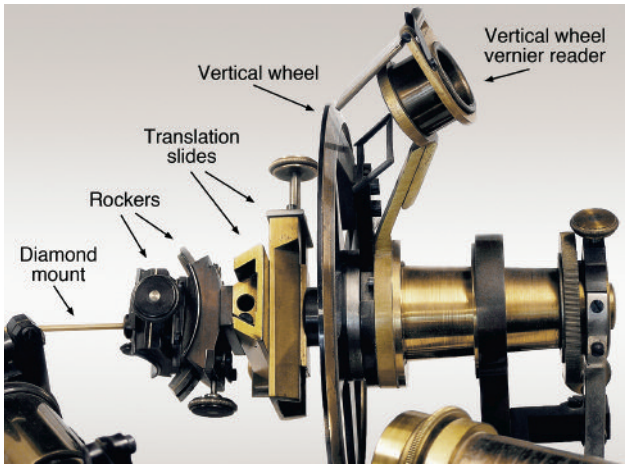

Figure 3. The goniometer head contains the rockers and translation slides needed to orient and position the specimen. After the gem was positioned at the end of the brass mounting tube, the rockers were used to make small corrections. Photo by E. A. Skalwold.

light source (*collimator* or *projector*), and a *telescope* (figures 3–5). The goniometer *head* features *slides* for centering the specimen at the point where the axes of the two wheels intersect so it can be precisely rotated to nearly any orientation. The goniometer head also has *rockers* for orienting the specimen. The telescope has an *auxiliary flip-up lens* to switch from focusing on the surface of the specimen to focusing on the target, a *Maltese cross* in the light source (see figure 4). Using the auxiliary lens, the operator can look directly at the specimen and observe flashes of light reflected from its facets, while rotating it through all possible orientations by turning the two wheels. Once a reflection has been spotted, the auxiliary lens is removed so the telescope is focused on the Maltese cross, using the specimen's reflecting face as a mirror. This causes the Maltese cross to appear in the telescope. Once the specimen has been oriented so that the Maltese cross image is centered on the crosshairs of the telescope, a unique orientation of the reflecting facet has been established. The operator can then record the angles on the scales of the two wheels, henceforth referred to as *angular coordinates* (box A), and then look for a new reflecting facet. When the image of the Maltese cross is exactly centered on the crosshairs, this new facet

In Brief

- Non-contact optical scanners are important components for grading diamonds in gem laboratories.
- Scanners are claimed to have a precision of ~0.1° for facet angle measurements, compared to a precision of 0.034° for the goniometer used in this study.
- Although time consuming, goniometer measurements of facet angles are useful for highly precise applications such as producing reference stones for calibrating optical scanners.

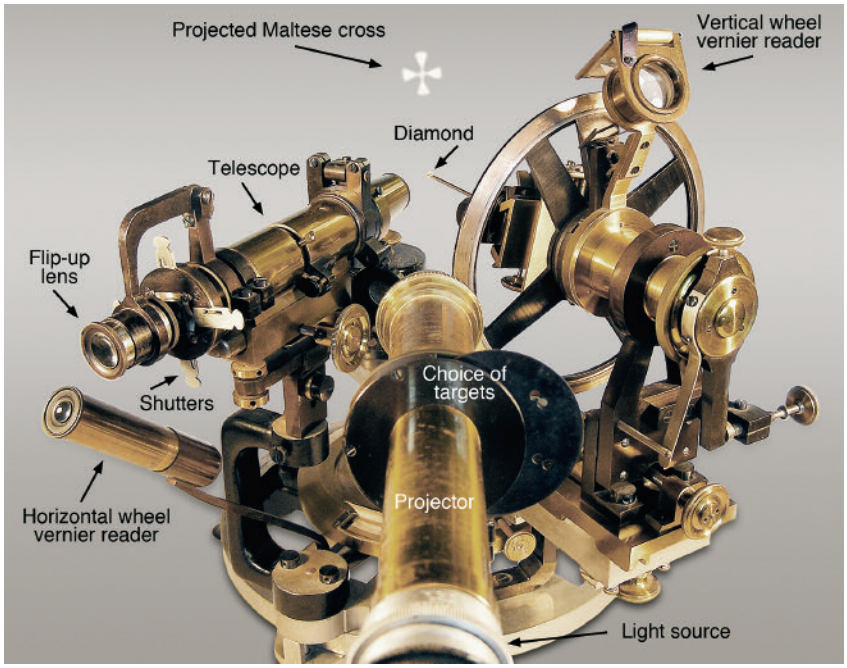

Figure 4. The Maltese cross projected onto the far surface is one of several target figures that can be chosen with the projector (collimator) of the goniometer. The position of the reflected target observed in the telescope is very sensitive to the orientation of the facet being observed. When the target image is perfectly centered on the telescope crosshairs, the angular coordinates of the facet can be measured very accurately. The angle between the projector and the telescope was reduced as far as possible without blocking the light path, enabling measurement of the pavilion facets. Photo by E. A. Skalwold.

BOX A: DERIVATION OF INTER-FACET ANGLES

The underlying principle of the technique used in this study is spherical geometry. If we place a round brilliant-cut diamond in the center of an imaginary sphere, the normals—that is, the imaginary lines perpendicular to the facets—will intersect the sphere at unique locations (designated by x in figure A-1). The *angular coordinates* of these locations provide all of the information needed to determine the stone's inter-facet angles.

The reflecting two-circle goniometer measures a pair of angular coordinates for each facet: ρ (the zenith angle, measured by the horizontal wheel) and ϕ (the azimuthal angle, measured by the vertical wheel). The angular coordinates of the table facet are determined first, as they provide the reference coordinates for all other measurements. The angular coordinates of a different facet (for instance, a crown or star facet) are obtained by subtracting the table facet's coordinates from the new readings. The angles between two facets can be calculated from the coordinates using the equation:

$$\alpha = \cos^{-1}(\sin\rho_1 \sin\phi_1 \sin\rho_2 \sin\phi_2 + \sin\rho_1 \cos\phi_1 \sin\rho_2 \cos\phi_2 + \cos\rho_1 \cos\rho_2)$$

where (ρ_1, ϕ_1) and (ρ_2, ϕ_2) are the angular coordinates of the normals to the two facets. This equation can be further reduced if one of the facets is the table facet, which has the angular coordinates of (0, 0). Setting (ρ_1, ϕ_1) to (0, 0), the equation is reduced to:

$$\alpha = \cos^{-1}(\cos 0 \cos\rho_2)$$

and because cos 0 = 1, the result is $\alpha = \rho_2$.

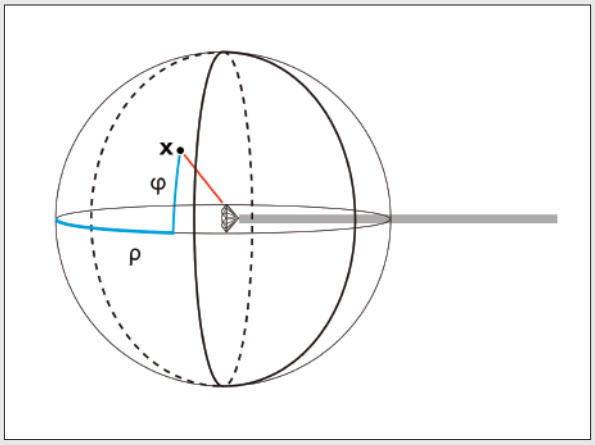

Figure A-1. A line perpendicular to a facet on a round brilliant intersects an imaginary sphere (point x) at angular coordinates ρ (zenith angle) and ϕ (azimuthal angle).

has the same orientation with respect to the telescope and light source. Reading the scales provides angular coordinates, from which the angles between observed facets can be calculated. The positions of the light source and the observation telescope must be kept fixed throughout all measurements of a particular stone.

In the process of finding reflections from a faceted stone, a constant challenge is created by multiple reflections produced by the many facets on the diamond. The *shutters* shown in figures 4 and 5 solve this problem by limiting the field of view to just that portion of the light reflected from the facet of interest. Once the selection is made, only the Maltese cross produced by that facet will appear.

The main challenge of using reflecting goniometers for measuring angles on faceted stones is accessing the pavilion facets on some fancy cuts such as oval and pear shapes. This is because the light source and telescope lie in the same plane as one of the circles used for making measurements, thus limiting the range of angles that can be measured with that wheel. Therefore, we mounted the diamond at the end of a long (76 mm) brass tube, which allowed us to move the vertical wheel and the goniometer head outward. This significantly reduced the angle between the light source and the telescope without obstructing the light path. The first step was to mount a round brilliant-cut diamond (~0.25 ct) so the table facet could be oriented perpendicular to the axis of the vertical wheel. A high-precision drill press was used to orient the table facet perpendicular to the axis of the brass tube. Once the stone was cemented in place, only minor adjustments using the rockers and slides were necessary. This arrangement made it possible to obtain reflections from all the facets on the stone without the need to remount it.

After positioning the table facet so it was clearly visible in the telescope, we oriented it to reflect light from the collimator into the telescope. By flipping up the auxiliary lens, we could use the Maltese cross to refine the orientation of the table facet by centering its reflected image on the crosshairs. Then the specimen was rotated about the axis of the horizontal wheel until

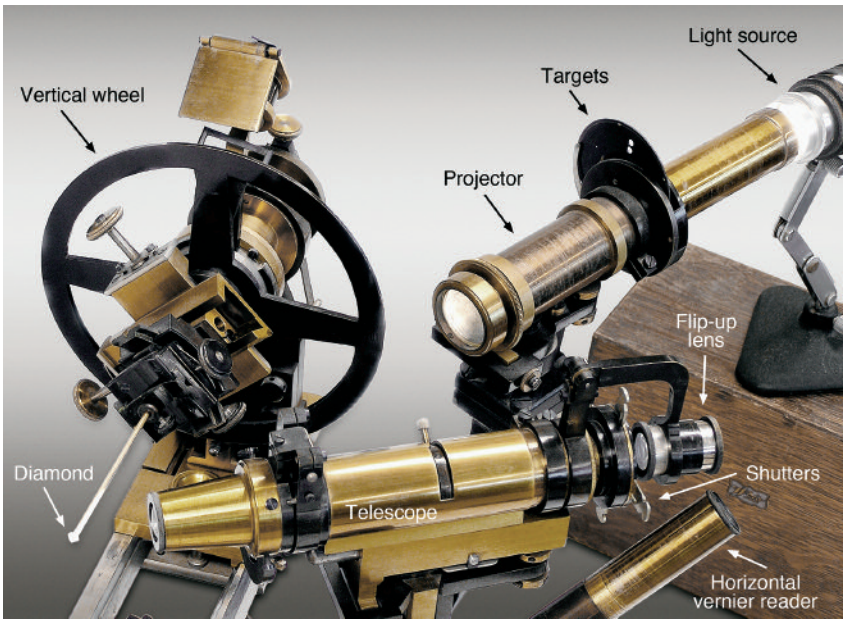

Figure 5. This view of the goniometer shows the positioning of the diamond, light source, and telescope for obtaining reflections from the pavilion facets. Photo by E. A. Skalwold.

the pavilion facets were in position to reflect light from the collimator/projector to the telescope (figures 4 and 5). We could then measure the angles between all the facets on a round brilliant. Oval- and pear-cut stones posed more of a challenge, in some cases requiring the operator to aim the light source between the spokes of the vertical wheel. Nevertheless, we were able to obtain measurements on these fancy cuts as well. In instances where the spokes blocked the light beam, we estimated the angle using an averaging method detailed in the Discussion section.

Five faceted diamonds (see table 1) were measured on the goniometer and the non-contact optical scanner: three round brilliants (nos. 1, 2, and 3), one oval brilliant (no. 92), and one pear brilliant (no. 93). With the goniometer, we focused on measuring the bezel facets and pavilion facets since the angles between these facets and the table have the most significant impact on the cut grade (Hemphill et al., 1998; Reinitz et al., 2001; Moses et al., 2004). We also measured the star facets on one of the round brilliants (no. 2), because these facets have the lowest angles from the table and are easily obscured when using a non-contact measuring device. Each diamond was inscribed on the girdle, and this inscription served as a standard position from which to begin recording the measurements. The same diamonds were also measured 10 times on a commercially available non-contact optical scanner, set for total of 400 scans and a scanning rate of 10 scans/second. The scanner is representative of those used in GIA's laboratory since 2010. According to the manufacturer, the precision of the angle measurement is 0.1°.

RESULTS AND DISCUSSION

The calculated inter-facet angles for each diamond are listed in table 2. At first glance, the results from the goniometer compare very favorably to those from the non-contact optical scanner. In more than 78.3% of the tests, the angles measured by each instrument were within 0.2° of one another. Only 40.8% of the measurements achieved less than 0.1° deviation, and six of the 83 measurements deviated significantly (greater than 0.4°, indicated by bold font). The largest deviation, which occurred from a star facet, was 1.28°. To determine the precision of the goniometer measurements, we first obtained readings of the bezel or pavilion facets on the two fancy-shaped diamonds, which, due to their larger size, required shifting the stone using the translation slides. We then returned to the table facet to see

TABLE 1. Diamonds examined in this study.

Sample no.	Shape	Weight (ct)	Dimensions (mm)
1	Round	0.20	3.77–3.80 x 2.30
2	Round	0.40	4.79–4.82 x 2.75
3	Round	0.62	5.66–5.70 x 3.37
92	Oval	0.86	7.43 x 5.19 x 3.24
93	Pear	0.71	7.75 x 4.92 x 3.19

TABLE 2. Comparison of angles (in degrees) relative to the table facet, measured by the goniometer and non-contact optical scanner.[a]

Sample no.	1 (Round)		2 (Round)		3 (Round)		92 (Oval)		93 (Pear)	
Facet	Goniometer	Scanner	Goniometer	Scanner	Goniometer	Scanner	Goniometer	Scanner	Goniometer	Scanner
Bezel 1	34.00	33.8	30.08	29.8	26.58	26.4	34.85	34.9	35.77	35.9
Bezel 2	34.00	33.9	30.10	29.9	26.67	26.5	36.92	36.8	38.23	38.3
Bezel 3	33.97	34.1	30.03	30.0	26.53	26.6	38.17	38.1	32.60	32.6
Bezel 4	33.98	34.2	29.93	30.1	26.63	26.6	35.77	35.7	31.22	31.2
Bezel 5	33.97	34.2	29.92	30.1	26.58	26.6	35.53	35.5	33.03	**32.5**
Bezel 6	34.02	34.0	29.92	29.9	26.65	26.6	37.33	37.4	34.83	34.7
Bezel 7	34.02	33.8	29.93	29.6	26.67	26.5	37.73	37.8	41.02	41.2
Bezel 8	34.05	33.8	30.07	29.7	26.58	26.4	35.80	36.0	–	–
Bezel 1[b]	–	–	–	–	–	–	34.87	34.9	35.77	35.9
Pavilion 1	40.52	40.6	40.40	40.6	41.88	42.0	36.87	36.5	38.53	38.4
Pavilion 2	40.40	**40.8**	40.38	40.6	41.92	41.9	36.32	36.6	41.52	41.4
Pavilion 3	40.57	**41.0**	40.43	40.5	42.03	41.9	36.23	**37.0**	41.37	41.4
Pavilion 4	40.92	41.0	40.67	40.5	42.03	41.9	36.67	36.7	36.90	36.7
Pavilion 5	41.08	40.9	40.72	40.5	42.05	42.0	–	–	36.93	36.9
Pavilion 6	41.02	40.7	40.67	40.5	41.97	42.1	–	–	40.83	40.7
Pavilion 7	40.83	40.6	40.47	40.5	41.68	**42.1**	–	–	–	–
Pavilion 8	40.45	40.6	40.42	40.5	42.05	42.1	–	–	–	–
Star 1	–	–	15.47	15.4	–	–	–	–	–	–
Star 2	–	–	15.50	15.5	–	–	–	–	–	–
Star 3	–	–	15.52	**16.8**	–	–	–	–	–	–
Star 4	–	–	15.40	15.6	–	–	–	–	–	–
Star 5	–	–	15.40	15.7	–	–	–	–	–	–
Star 6	–	–	15.38	15.5	–	–	–	–	–	–
Star 7	–	–	15.42	15.5	–	–	–	–	–	–

[a] *Bold font indicates a deviation of greater than 0.4° between measurements.*
[b] *This bezel 1 measurement was performed after a full 360° rotation of the vertical wheel for purpose of assessing the instrument's precision.*

if the readings of the table reference point had changed. The maximum deviation was 2 minutes (0.034°), which we established as representing the precision of the instrument. The finest division on the goniometer scale is 1 minute or 0.017°. According to the historical literature (e.g., Tutton, 1922), the two-circle reflecting goniometer was believed to be capable of a precision of 30 seconds (0.0083°). With careful estimation, one can easily estimate the angles between two divisions and improve the precision down to 30 seconds. But even at a precision of 2 minutes, we were achieving far better precision than the non-contact measuring device (for which 10 measurements of each stone showed a repeatability of within 0.1°).

The main source of uncertainty in goniometer measurements is human error in reading the scales. During this investigation, two observers read each measurement while a third independently checked their readings. The other source of error occurs when the Maltese cross image is blocked by part of the instrument, as described above. We encountered this situation only a couple of times in the course of our research, and obtained an average of two measurements to overcome this problem. The first measurement was taken at the nearest horizontal position where the full Maltese cross was visible, and the second was taken from a different position with approximately the same separation between the center of the crosshairs and the first Maltese cross position. The typical separation between these two positions was within 10 minutes (0.17°). This approach provided consistent results, and the error introduced should still be quite comparable to the direct measurement (i.e., <2 minutes, or 0.034°).

As described earlier, non-contact optical scanners rely on computer algorithms to construct a 3D model of the actual stone. These algorithms require a basic model of the stone—an ideal plot of a round brilliant cut, emerald step cut, and so forth—to achieve high precision. In most cases, this requires the operator to choose from a selection of models available in the

software. For the sake of argument, we will disregard the possibility of choosing the wrong model. More likely, the actual stone has an extra facet, or foreign material such as dirt or lint on its surface during measurement. Surface contamination is most problematic for determining the low angles of star facets on a brilliant cut, because the shadows can badly skew the image analysis. Indeed, the largest deviation we observed (1.28°) was from a star facet. Also challenging are some fancy-shape measurements, such as crown facets on an emerald cut that are at a low angle from the table facet.

Although the two-circle reflecting goniometer avoids the use of computer algorithms or pre-installed ideal models of faceted gems, its application in a modern gem lab will be limited because it is time consuming. Nevertheless, its use may be justified in certain circumstances. For example, its high precision make it an excellent technique to establish a master set of reference stones with very accurately determined inter-facet angles. Much like the master sets used for color-grading diamonds, these can be considered calibration standards for angle measurement. We believe the deviations shown in table 2 arise mostly from 3D model construction or some surface contamination. In the gem lab these discrepancies can potentially result in different cut grades, since the cut-grade software uses whatever pavilion and crown angles are obtained from the non-contact optical scanner. To ensure the accuracy and precision of these measurements, optical scanners need to be checked routinely with master stones.

Another possible use for the two-circle reflecting goniometer is evaluating facet quality. The small curvature shown by a poorly cut facet is easily observed via deformation or blurring of the reflected Maltese cross target. This effect was not observed in any of the facets we measured in this study.

CONCLUSIONS

The two-circle reflecting goniometer can be used to measure inter-facet angles on faceted gemstones with a very high degree of precision (to within 2 minutes, or 0.034°). The angular coordinates of any facet can be determined without remounting the sample. The instrument can provide a valuable means to independently calibrate the non-contact optical scanners widely used in gem labs, and can also be used to evaluate facet quality. Finally, the classic goniometer provides an excellent basis for the future design of a fully automated optical goniometer made specifically for faceted gemstones.

ABOUT THE AUTHORS

Dr. Shen (andy.shen@gia.edu) is a research scientist at GIA in Carlsbad. Dr. Bassett is a research scientist and professor emeritus of geology at Cornell University in Ithaca, New York. Ms. Skalwold is editor of Journal of Gemmology, *and an author and gemologist involved in research and curating at Cornell University. Ms. Fan is a metrologist at GIA in New York. Dr. Tao is a former metrologist at GIA in New York.*

ACKNOWLEDGMENTS

The authors are indebted to Dr. Olaf Medenbach (Institute of Geology, Mineralogy, and Geophysics at Ruhr University, Bochum, Germany) for insightful discussions on the historical and practical aspects of goniometers.

REFERENCES

Burchard U. (1998) History of the development of the crystallographic goniometer. *Mineralogical Record*, Vol. 29, No. 6, pp. 517–583.

Hemphill T.S., Reinitz I.M., Johnson M.L., Shigley J.E. (1998) Modeling the appearance of the round brilliant cut diamond: An analysis of brilliance. *G&G*, Vol. 34, No. 3, pp. 158–183, http://dx.doi.org/10.5741/GEMS.34.3.158.

Moses T.M., Johnson M.L., Green B.D., Blodgett T., Cino K., Geurts R.H., Gilbertson A.M., Hemphill T.S., King J.M., Kornylak L., Reinitz I.M., Shigley J.E. (2004) A foundation for grading the overall cut quality of round brilliant cut diamonds. *G&G*, Vol. 40, No. 3, pp. 202–228, http://dx.doi.org/10.5741/GEMS.40.3.202.

Reinitz I.M., Johnson M.L., Hemphill T.S., Gilbertson A.M., Geurts R.H., Green B.D., Shigley J.E. (2001) Modeling the appearance of the round brilliant cut diamond: An analysis of fire and more about brilliance. *G&G*, Vol. 37, No. 3, pp. 174–197, http://dx.doi.org/10.5741/GEMS.37.3.174.

Reinitz I.M, Yantzer K., Johnson M.L., Blodgett T., Geurts R.H., Gilbertson A.M. (2005) Measurement tolerances: Accuracy and precision in the gem industry. *Rapaport Diamond Report*, Vol. 28, April 1, pp. 183–185.

Tutton A.E.H. (1922) *Crystallography and Practical Crystal Measurements*, 2nd ed. Macmillan, London, 760 pp.

The Vallerano Diamond from Ancient Rome: A Scientific Study

Alessandro Bedini, Sylvana Ehrman, Stella Nunziante Cesaro, Maria Pasini, Ida Anna Rapinesi, and Diego Sali

Archaeological excavations during the 1990s at Vallerano, a municipality on Rome's southern periphery, uncovered a cemetery from the Roman empire. One tomb was that of a young woman, believed to be of Syrian origin. It contained a wealth of everyday objects and jewels, among them a gold and diamond ring. The diamond's gemological and spectroscopic properties were examined using portable instruments. Infrared spectroscopy indicated a type Ia diamond with evidence of B aggregates and probable A aggregates.

Excavations undertaken in 1993 in Vallerano, between the Via Pontina and Via Laurentina on Rome's southern outskirts, revealed a necropolis of 113 tombs (Bedini et al., 1995). One of these, Tomb 2, belonged to a young woman believed to be about 18 years old. Her marble sarcophagus contained a wealth of personal effects, an ivory doll, and finely crafted gold jewels set with gems (Bedini, 1995). The collection, whose richness is unusual among ancient Roman tombs, is on permanent exhibit at the National Roman Museum at Palazzo Massimo.

Of the artifacts, one is particularly noteworthy: a solid-band gold ring set with a rough octahedral diamond (figure 1). Its form corroborates Pliny the Elder's belief that the Romans valued diamonds above gold. The value of the Vallerano ring, the only known diamond-mounted ring in ancient Rome, is accentuated by its craftsmanship and simplicity of design.

One of the common objects discovered in the tomb was an oil lamp bearing the hallmark of Lucius Fabricius Masculus, active between 150 and 180 CE. This makes it possible to date the tomb to the reign of Marcus Aurelius. The richness of the Vallerano girl's tomb can be explained not so much by her family's wealth as by a particular ritual, most likely tied to religions of eastern origin. The material wealth and funeral rites of the Vallerano find, similar to those of other young Roman women such as Crepereia Tryphaena and the Grottarossa mummy (Bedini, 1995), can be linked to the Syrian community in ancient Rome. The Syrian enclave had its own religious, traditional, and commercial ties to Palmyra, a major caravan crossroad near the Euphrates River where luxury goods from the Persian Gulf and Arabia converged en route to Rome.

Among these were Indian diamonds that had been gathered on the Deccan altiplano, either from mines or in river gravels, as attested by both Pliny (Corso et al., 1988, Book 37) and Sanskrit literary sources (Chakraborti, 1966, pp. 244–245). These were objects of trade, along with other gems, spices, and luxury textiles. Pliny considered diamond the most precious of all stones, destined for kings and accordingly not meant for common use. Among the few archaeological specimens of diamond rings, this jewel is the only one whose chronological and social context is known (Marshall, 1968; Ogden, 1982).

In Brief

- Among the artifacts uncovered from ancient Roman tombs at Vallerano during the 1990s was a gold ring containing a rough diamond (approximately 0.15 ct).
- The ring can be linked to a young Syrian woman who died during the reign of Marcus Aurelius, making it the only Roman diamond jewel with a known background.
- Analyses conducted at the National Roman Museum point to a type Ia diamond with evidence of B aggregates and probable A aggregates.

See end of article for About the Authors and Acknowledgments.
Gems & Gemology, Vol. 48, No. 1, pp. 39–41,
http://dx.doi.org/10.5741.GEMS.48.1.39.
© 2012 Gemological Institute of America

Figure 1. This gold and diamond ring, believed to belong to a young woman of Syrian origin, was discovered at the Vallerano site. The side view shows that the rough diamond was simply inserted into a central enlargement in the gold band. Photos by M. Letizia.

MATERIALS AND METHODS

The analyses were conducted at the National Roman Museum, using portable instruments. The stone was not removed from its fragile mounting, and in fact the researchers preferred leaving the stone in its supportive setting. Gemological examination was performed with a GIA Portalab equipped with a fiber-optic light and a binocular polarized microscope. Fluorescence was observed with long- and short-wave UV lamps. The diamond's infrared spectrum was collected with a Bruker Optics Alpha-R portable spectrometer with an external reflectance head covering a circular area of about 5 mm of diameter. The investigated spectral range was 7500–375 cm^{-1}, with a resolution of 4 cm^{-1} and 120 scans per acquisition (about two minutes).

Figure 2. The rough diamond in the ancient gold ring is seen here through the bottom of the mounting. Photo by D. Sali.

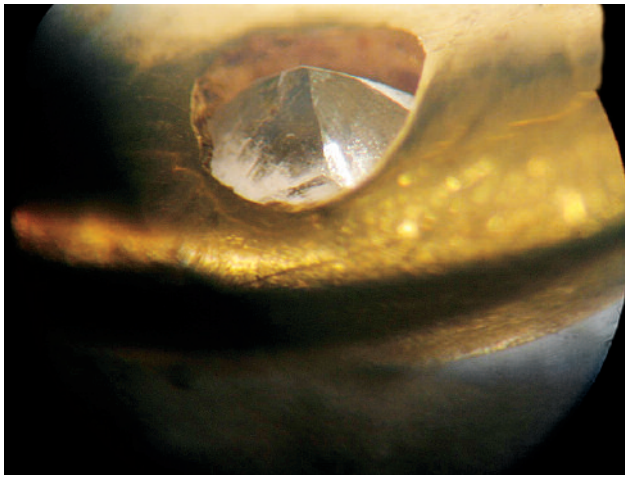

RESULTS AND DISCUSSION

The diamond measured 2.2 × 1.5 × 2.6 mm, corresponding to an estimated weight of 0.15 ct. The crystal had an adamantine surface luster and an octahedral form that was slightly rounded (figure 2). Trigons were not detected.

The diamond was inert to short-wave UV and fluoresced moderate blue to long-wave UV radiation. In neither case did the stone show phosphorescence. Magnification revealed a group of crystalline inclusions, the nature of which could not be determined due to the surface characteristics and the aforementioned precautions required in handling the ring.

Spectroscopic analyses of a number of points on the diamond provided reproducible spectra. Figure 3 shows the infrared spectrum in the 4000–375 cm^{-1} range, as no absorption occurred in the 7500–4000 cm^{-1} range. Absorptions were observed in the three-phonon spectral region (4000 to ~2800 cm^{-1}) at 3107 and 2786 cm^{-1}. The two absorptions had weak and very weak intensity, respectively, due to $C{=}CH_2$ group vibrations.

Moderate to weak absorptions at 2957, 2918, and 2851 cm^{-1} were attributed to CH_3 and CH_2 group stretching modes, likely due to grease contamination, as a thorough cleaning of the gem was avoided. The same molecular groups' bending mode was evident in a weak absorption at 1460 cm^{-1} (Iakoubovskii and Adriaenssens, 2002). Except for absorption due to atmospheric CO_2, no significant bands were observed in the two-phonon spectral region (Mendelssohn and Milledge, 1995).

The abundance of active absorptions in the one-photon spectral range at frequencies below the Raman threshold (1335 cm^{-1}) indicates the presence of nitrogen-impurity defects, leading to a classification of type Ia. Furthermore, the 1011 cm^{-1} absorption suggests the

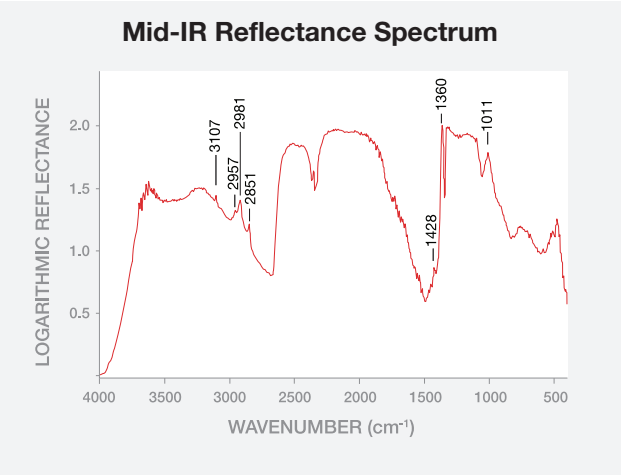

Figure 3. The Vallerano gem's FTIR spectrum classified it as a type Ia diamond.

presence of B aggregates (four atoms of nitrogen around a vacancy), and the intense narrow absorption at 1360 cm^{-1} shows the existence of platelet defects along (001) faces (Woods et al., 1993; Taran et al., 2006). A weak absorption at 1428 cm^{-1} could be attributed to N3 groups (Gaillou and Post, 2007).

Unfortunately, the spectrum was saturated in the interval indicative of A aggregates (pairs of nitrogen ions dispersed in a regular pattern in the structure) between approximately 1350 and 1100 cm^{-1}; Hainschwang et al., 2006), either because of an elevated concentration of nitrogen or, more likely, the difficulty of positioning the diamond while attempting to analyze it. As a consequence, the existence of a type IaA component can only be hypothesized.

CONCLUSIONS

The discovery of a diamond ring makes the rich collection of the young woman buried in Vallerano Tomb 2 a unique find. The ring's simplicity in no way detracts from the importance of the jewel, which presents a series of questions regarding the context of ritual practices in which this and analogous burials of young females uncovered in and around Rome must be placed.

The presence of nitrogen impurities led to the conclusive identification of the gem as a type Ia diamond, with evidence of B aggregates. The elevated nitrogen content, as well as limitations imposed in handling such a rare object, are probably responsible for the saturation of absorptions in the one-phonon spectral region, so that the presence of A centers can only be reasonably inferred. The presence of hydrogen inclusions was revealed by analysis of the three-phonon spectral range.

ABOUT THE AUTHORS

Dr. Bedini is a retired director of archaeology, and Dr. Rapinesi is an archaeological jewelry restorer, at the Special Superintendence for the Archaeological Heritage of Rome. Dr. Ehrman is president of Scientific Methodologies Applied to Cultural Heritage (SMATCH-USA) in Silver Spring, Maryland. Dr. Cesaro is a researcher at ISMN Institute of the National Council of Research (CNR) and president of SMATCH-ITALIA in Rome. Dr. Pasini is the lab director of Roma Credito su Pegno, UniCredit SpA. Dr. Sali is a research and development manager at Bruker Italia S.r.l. in Milan.

ACKNOWLEDGMENTS

The authors are indebted to Dr. Rita Paris, director of the National Roman Museum at Palazzo Massimo, for helpful discussions and for making this study possible. Thanks are also given to James Ehrman of SMATCH-USA for reviewing this manuscript.

REFERENCES

Bedini A. (1995) *Mistero di una fanciulla. Ori e gioielli della Roma di Marco Aurelio da una nuova scoperta archeologica*. Skira Publishing, Rome.

Bedini A., Testa C., Catalano P. (1995) Roma. Un sepolcreto di epoca imperiale a Vallerano. Quaderni di archeologia etrusco-italica 23. *Archeologia Laziale XII*, Vol. 1, pp. 319–331.

Chakraborti H. (1966) *Trade and Commerce of Ancient India (c. 200 B.C.–c. 650 A.D.)*. Academic Publishers, Calcutta.

Corso A., Mugellesi R., Rosati G. (1988) *Plinio, La Storia Naturale, Libri 33–37*. Giulio Einaudi, Turin.

Gaillou E., Post J. (2007) An examination of the Napoleon Diamond Necklace. *G&G*, Vol. 43, No. 4, pp. 352–357, http://dx.doi.org/10.5741/GEMS.43.4.352.

Hainschwang T., Notari F., Fritsch E., Massi L. (2006) Natural, untreated diamonds showing A, B and C infrared absorptions ("ABC diamonds") and H2 absorption. *Diamond and Related Materials*, Vol. 15, No. 10, pp. 1555–1564, http://dx.doi.org/10.1016/j.diamond.2005.12.029.

Iakoubovskii K., Adriaenssens G.J. (2002) Optical characterization of natural Argyle diamonds. *Diamond and Related Materials*, Vol. 11, No. 1, pp. 125–131, http://dx.doi.org/10.1016/S0925-9635(01)00533-7.

Marshall F.H. (1968) *Catalogue of the Finger Rings, Greek, Etruscan and Roman, in the Departments of Antiquities, British Museum*. British Museum Press, London, pp. 127–129.

Mendelssohn M.J., Milledge H.J. (1995) Geologically significant information from routine analysis of the mid-infrared spectra of diamonds. *International Geology Review*, Vol. 37, No. 2, pp. 95–110, http://dx.doi.org/10.1080/00206819509465395.

Ogden J. (1982) *Jewellery of the Ancient World*. Rizzoli International Publications Inc., New York.

Taran M.N., Kvasnytsya V.M., Langer K., Ilchenko K.O. (2006) Infrared spectroscopy study of nitrogen centers in microdiamonds from Ukrainian Neogene placers. *European Journal of Mineralogy*, Vol. 18, No.1, pp. 71–81, http://dx.doi.org/10.1127/0935-1221/2006/0018-0071.

Woods G.S., Kiflawi I., Luyten W., Van Tendeloo G. (1993) Infrared spectra of type IaB diamonds. *Philosophical Magazine Letters*, Vol. 67, No. 6, pp. 405–411, http://dx.doi.org/10.1080/09500839308240950.

RADIOACTIVE MORGANITE

Hiroshi Kitawaki, Yoichi Horikawa, Katsumi Shozugawa, and Norio Nogawa

Two strongly orangy pink morganites with residual radioactivity were studied. The dose rate of the samples, measured by a scintillation survey meter, ranged from 0.15 to 0.35 µSv/h. Although this radioactivity was likely not hazardous, it was above the recommended exposure limit set forth in 1990 by the International Commission on Radiological Protection. To identify the radionuclides, gamma rays from the samples were measured using a Ge(Li) semiconductor detector. The activation products ^{134}Cs, ^{54}Mn, and ^{65}Zn were detected, proving that the samples had been artificially irradiated with neutrons.

Figure 1. The morganite samples in this study weighed is 49.18 ct (left, sample 1) and 39.40 ct (right, sample 2). Photo by H. Kitawaki.

Some gem varieties (e.g., diamond, topaz, and quartz) are irradiated with gamma rays, electron beams, or neutrons to alter their original color (see, e.g., Ashbaugh, 1988). Disclosure of artificially colored gemstones is generally required at every level of the gem trade, and such material should only be sold as treated. These gems are typically not radioactive when they are commercially distributed. Exceptions include some radioactive green to black diamonds treated by compounds such as radium daughter-products and americium (Reinitz and Ashbaugh, 1993). In addition, radioactive cat's-eye chrysoberyl became a major issue in September 1997, and even drew mass media coverage. The chrysoberyl, originally from Orissa, India, had been irradiated with neutrons in an Asian country, and a portion of the activated material entered the gem market illegally (Johnson and Koivula, 1997). Several pieces of this material were identified in Japan, and one of the authors performed a detailed investigation that detected scandium-46 (^{46}Sc) and iron-59 (^{59}Fe), proving it had undergone artificial neutron irradiation (Kitawaki, 1998). Fortunately these radioactive cat's-eye chrysoberyls were not widely circulated in the gem trade.

Activated morganite appeared in the Japanese market in May 2010, and the Central Gem Laboratory has confirmed about 10 such specimens so far, including stones weighing >100 ct. The specimens typically show strongly orangy pink coloration (e.g., figure 1), and some are so orangy that they may fall outside the color range for morganite. Their radioactivity levels (measured with a NaI scintillation survey meter) ranged from 0.15 to 0.35 microsieverts per hour (µSv/h), or 5–10 times higher than the background radiation in Tokyo. While this is not believed to be a hazardous level, it is higher than the recommended exposure limit set by the International Commission on Radiological Protection in 1990 of 1 millisievert per year (or 0.114 µSv/h; about 3.8 times higher than the background radiation in Tokyo), except for exposure to natural and medical radiation.

Regulations set by the Japan Jewellery Association and the Association of Gemmological Laboratories Japan state that gems showing any possibility of artificial irradiation should be checked by a Geiger counter, and

See end of article for About the Authors and Acknowledgments.
GEMS & GEMOLOGY, Vol. 48, No. 1, pp. 42–44, http://dx.doi.org/10.5741.GEMS.48.1.42.
© 2012 Gemological Institute of America

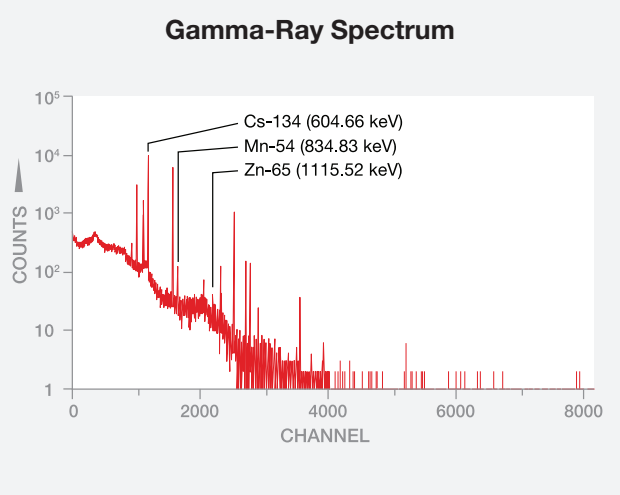

Figure 2. The gamma-ray spectrum of sample 1 shows peaks for ^{134}Cs, ^{54}Mn, and ^{65}Zn. The labeled peaks were used for quantification of the radioactivity in the samples.

those with residual radioactivity should not have gem identification reports issued. Yet there are natural gems containing radioactive impurities such as uranium (U) or thorium (Th) that emit very weak radioactivity. For this article, which was initiated in part by client demand, we identified the radionuclides in radioactive morganite to determine whether those stones had been artificially irradiated by a neutron source.

Materials and Methods. Radionuclide determination was performed on two morganites, weighing 49.18 and 39.40 ct (again, see figure 1). The samples were imported from Germany, according to our client, but when and where they may have been irradiated was unknown. Standard gemological properties were collected, and energy-dispersive X-ray fluorescence (EDXRF) analysis was performed with a JEOL JSX-3200 instrument. Gamma rays from the two samples were measured using a Princeton Gamma-Tec Ge(Li) semiconductor detector (see, e.g., Ashbaugh, 1992). The device, located in the Radioisotope Center at the University of Tokyo, has a relative efficiency of 34.4% at 1332 keV, and FWHM of 1.78 keV on the 1332 keV ^{60}Co γ-line and 743 eV on the 122 keV ^{57}Co γ-line. The measurement period had a live time of 7,200 seconds and a dead time of ~0.35%. The gamma-ray libraries used for nuclide identification were Spectrum Navigator (Seiko EG&G Co. Ltd.) and a nuclide library generation program (NucLib version 1.12), together with the IAEA Handbook of Nuclear Data for Safeguards. A nuclide was identified by two or more clear and independent peaks in the gamma-ray spectra that were more than 3σ above the baseline. The energy efficiency of the gamma rays was also corrected for, and an attenuation (decay) correction was set at the initiation of measurement.

Results and Discussion. Both morganites displayed a strong orangy pink color. Their RI measurements were 1.582–1.590 (birefringence 0.008), and their other gemological properties were consistent with morganite. EDXRF spectroscopy of both samples detected about 3.8 wt.% Cs_2O and traces of K_2O, FeO, and Rb_2O, as well as the major Al and Si expected for beryl.

Gamma-ray spectra obtained from the two samples are shown in figures 2 and 3. From the gamma-ray spectrum of sample 1, cesium-134 (^{134}Cs), manganese-54 (^{54}Mn), and zinc-65 (^{65}Zn) were detected; only ^{134}Cs and ^{54}Mn were identified in sample 2. All the detected radionuclides were activation products, clearly demonstrating that both samples had been neutron irradiated. The activities of each radionuclide are listed in table 1.

Both morganites contained more than 2,000 becquerels (Bq) of ^{134}Cs, suggesting that a high thermal neutron flux, such as a nuclear reactor or accelerator, was used for irradiation. Morganite generally contains a small amount of naturally occurring cesium (^{133}Cs), which becomes radioactive when irradiated with a neutron beam. The detected radionuclide with the shortest half-life was ^{65}Zn (244 days). Since the amount of time since the samples were irradiated is unknown, it is highly possible that some additional radionuclides had already decayed to below the detection limits when the samples were measured.

Figure 3. The gamma-ray spectrum of sample 2 shows peaks for ^{134}Cs and ^{54}Mn.

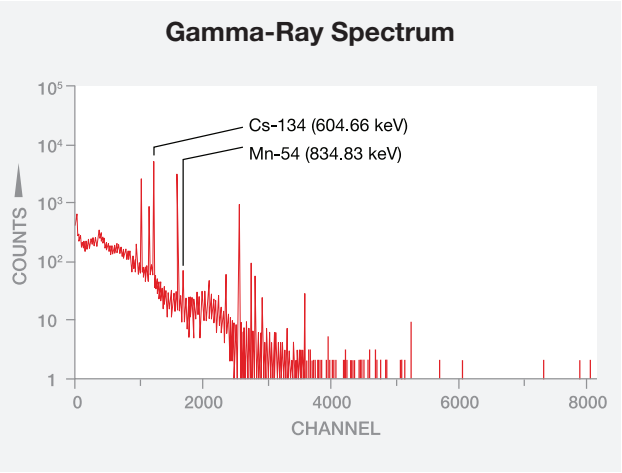

TABLE 1. Detected radionuclides and their estimated radioactivity.

Sample no.	Radionuclide	Half-life (days)	Radioactivity (Bq)	Error (Bq)	Detection limit
1	^{134}Cs	752.6	2612.4	±11.1	13.4
	^{54}Mn	312.2	36.7	±3.4	7.88
	^{65}Zn	244.0	22.1	±4.1	17.8
2	^{134}Cs	752.6	2019.0	±11.9	14.7
	^{54}Mn	312.2	32.5	±3.2	10.0

Conclusion. Two samples of morganite that registered significant dose rates using a scintillation survey meter were measured for gamma-ray emission to determine the radionuclides present. Radioactive isotopes including ^{134}Cs were detected in both samples, proving they had been artificially irradiated with neutrons. ^{134}Cs has a half-life of about two years, so the radioactivity of such morganites should decay to a safe level after a period of several years from when they were irradiated.

Additional radioactive morganites entering the Japanese market since 2010 also appear to have been artificially irradiated with neutrons. Although it is common to use gamma rays to deepen the hue of morganite, it is unknown why these samples were irradiated with neutrons. Proper identification of such radioactive stones by gemological laboratories, and full disclosure by exporting countries, are strongly urged.

ABOUT THE AUTHORS

Dr. Kitawaki (kitawaki@cgl.co.jp) is a researcher, and Mr. Horikawa is manager of the technical department, at the Central Gem Laboratory in Tokyo. Dr. Shozugawa is assistant professor in the Graduate School of Art and Science, and Dr. Nogawa is assistant professor of the Radioisotope Center, at the University of Tokyo.

ACKNOWLEDGMENTS

The authors thank Dr. Hiroyuki Kagi from the Geochemical Research Center at the University of Tokyo's Graduate School of Science for helpful discussions.

REFERENCES

Ashbaugh C.E. (1988) Gemstone irradiation and radioactivity. *G&G*, Vol. 24, No. 4, pp. 196–213.

Ashbaugh C.E. (1992) Gamma-ray spectroscopy to measure radioactivity in gemstones. *G&G*, Vol. 28, No. 4, pp. 104–111, http://dx.doi.org/10.5741/GEMS.28.2.104.

Johnson M.L., Koivula J.I., Eds. (1997) Gem News: Lab Alert: Radioactive cat's-eye chrysoberyls. *G&G*, Vol. 33, No. 3, pp. 221–222.

Kitawaki H. (1998) Radioactive cat's eye. *Gemmology*, Vol. 29, No. 349, pp. 276–277 [in Japanese].

Reinitz I., Ashbaugh C.E. (1993) Lab Notes: Treated green diamond. *G&G*, Vol. 29, No. 2, pp. 124–125.

For online access to all issues of GEMS & GEMOLOGY from 1981 to the present, visit:

store.gia.edu

TAKE THE 2012 GEMS & GEMOLOGY CHALLENGE

The following 25 questions are from the Spring, Summer, Fall, and Winter 2011 issues of *Gems & Gemology*. Refer to the feature articles, Notes and New Techniques, and Rapid Communications in those issues to find the **single best answer** for each question.

Mark your choice on the response card provided in this issue or visit gia.edu/gandg to take the Challenge online. Entries must be **received no later than Wednesday, August 1, 2012**. All entries will be acknowledged with an email, so please remember to include your name and email address (and write clearly).

Score 75% or better, and you will receive a GIA Continuing Education Certificate (PDF file). If you are a member of the GIA Alumni Association, you will earn 10 Carat Points. (Be sure to include your GIA Alumni membership number on your answer card and submit your Carat card for credit.) Earn a perfect score, and your name also will be listed in the Fall 2012 issue of *Gems & Gemology*.

1. Diffusion experiments conducted in 2008 found that copper easily enters plagioclase feldspar at temperatures
   A. as low as 750°C.
   B. above 1200°C.
   C. above 1500°C.
   D. above 1800°C.

2. A 1980 German postage stamp pays tribute to _____, who was one of the first scientists to document the hardness of diamond.
   A. Max Von Laue
   B. Albertus Magnus
   C. Friedrich Mohs
   D. Max Planck

3. The SG vs. magnetic susceptibility plot for pyrope and grossular shows that these properties _____ for these garnets.
   A. overlap
   B. were not obtainable
   C. are almost identical
   D. are easily distinguishable

4. Cathodoluminescence analysis of CVD-grown synthetic diamonds confirmed that boron is present at the interrupted interface, while photoluminescence showed the presence of _____-related defects.
   A. silicon
   B. carbon
   C. vacancy
   D. germanium

5. The liquid and gas phases found in multiphase inclusions in aquamarine from Thanh Hoa Province, Vietnam, were identified as
   A. K and Na_2O.
   B. CaO and CO_2.
   C. H_2O and CO_2.
   D. H_2O and Na_2O.

6. In general, rubies and sapphires from Vietnam's Tan Huong–Truc Lau area are
   A. facet grade.
   B. industrial grade.
   C. of carving quality.
   D. of cabochon quality.

7. Some cabochons of odontolite display a distinct pattern of curved intersection banding characteristic of
   A. elk and cow horn.
   B. nuts from ivory palm.
   C. walrus and narwhale ivory.
   D. elephant, mammoth, and mastodon ivory.

8. The chemical composition of aquamarine from Thuong Xuan in Vietnam is characterized by relatively high concentrations of
   A. Ca.
   B. Fe.
   C. K.
   D. Na.

9. Ten symmetry parameters are used by GIA's laboratory to determine the symmetry grade of round brilliant cut diamonds. These

include out-of-round, table off-center, and
A. bezel facet variations.
B. crown height variations.
C. girdle polishing variations.
D. upper and lower girdle facet variations.

10. Infrared absorption spectroscopy in the region of X-OH stretching vibrations (i.e., 3800–3000 cm^{-1}) has long been considered a useful means for distinguishing
A. treated vs. untreated feldspar.
B. natural vs. synthetic diamond.
C. natural vs. synthetic amethyst.
D. treated vs. untreated aquamarine.

11. Typical internal features in andradite from Antetezambato, Madagascar, are fluid inclusions and
A. clouds of hematite platelets.
B. crystalline aggregates of diopside.
C. three-phase inclusions containing calcite and albite.
D. voids with halos of decrepitated melt inclusions.

12. Of 32 elements studied, six were diagnostic for separating pallasitic and terrestrial peridot. They were Li, V, Mn, Co,
A. Si, and Zn.
B. Ni, and Fe.
C. Mg, and Fe.
D. Ni, and Zn.

13. Silicate garnets have the general formula $X_3^{2+}Y_2^{3+}Si_3O_{12}$, where X is commonly Ca^{2+}, Mn^{2+}, Fe^{2+}, and/or
A. Mg^{2+}.
B. Ti^{2+}.
C. Cu^{2+}.
D. Cr^{2+}.

14. The cause of the 405 nm band in UV-Vis-NIR reflectance spectra of cultured pearls from *Pinctada margaritifera* is attributed to
A. coproporphyrin.
B. protoporphyrin.
C. uroporphyrin.
D. melanin.

15. Heating odontolite to about 600°C under oxidizing conditions transforms octahedrally coordinated Mn^{2+} into _____, which substitutes for phosphorous in the fluorapatite.
A. cubically coordinated Ca^{3+}
B. trigonally coordinated Mn^{5+}
C. tetrahedrally coordinated Fe^{5+}
D. tetrahedrally coordinated Mn^{5+}

16. Irregular, tubular inclusions with a cellular structure seen in some Ethiopian opals are probably
A. rutile.
B. pyrite.
C. chabazite.
D. fossilized plant matter.

17. In separating natural from synthetic amethyst using FTIR spectroscopy, the existence of a 3595 cm^{-1} band with a width of 3.3 ± 0.6 cm^{-1} indicates that the stone is
A. natural.
B. synthetic.
C. not identifiable.
D. a heat-treated synthetic.

18. Based on GIA's laboratory standards for grading round brilliant cut diamonds, if nine of the symmetry parameters are within the Excellent range but the table is off-center by 0.7%, the best possible symmetry grade is
A. Superior.
B. Excellent.
C. Very Good.
D. Good.

19. Zircon crystals from Muling, China, showed a combination of tetragonal prismatic and
A. sphenoid faces.
B. pyramidal faces.
C. basal pinacoid faces.
D. hexagonal prismatic faces.

20. Most topaz from China should be expected to take _____ to decay below the exemption level after it is turned blue by neutron irradiation.
A. three to four weeks
B. two to three months
C. two to three years
D. five to six years

21. In general, both rubies and sapphires from Tan Huong–Truc Lau had relatively high _____ contents.
A. Fe
B. Zn
C. Na
D. Ca

22. The color zoning exhibited by some andradite crystals from Madagascar is caused by
A. staining in surface fractures.
B. exposure to natural radiation.
C. inhomogeneities in the distribution of trace elements.
D. light interference caused by multiple layers of inclusions.

23. Reports published in 2008 revealed evidence that copper was being diffused into _____ in Chinese and Thai facilities by a multi-step heating process.
A. albite
B. andesine
C. oligoclase
D. labradorite

24. Small black octahedral crystals sometimes seen in Ethiopian opals from Wollo Province are most likely
A. pyrite.
B. spinel.
C. chromite.
D. magnetite.

25. The color change of experimentally heat-treated red zircon from Muling, China, appears to be mainly related to the
A. original hue.
B. size of the sample.
C. amount of inclusions in the sample.
D. location where the sample was found.

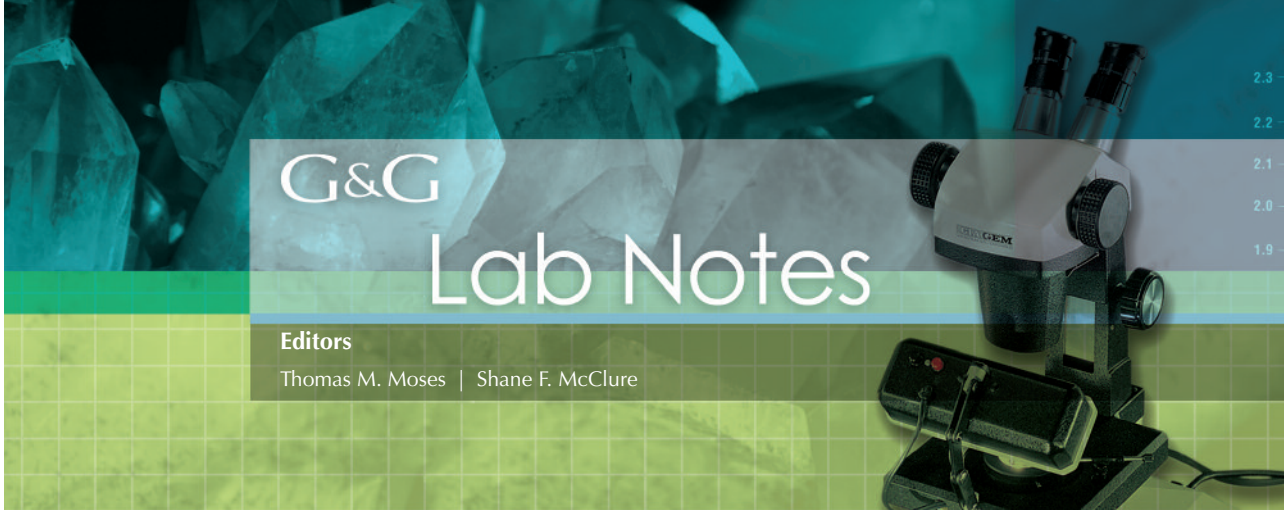

DIAMOND

Artificially Irradiated Type IIb

Saturated blue color is rare in natural diamond, and various treatment methods have been developed to introduce or enhance this effect. The more common techniques include the annealing of type IIb diamonds under high-pressure/high-temperature (HPHT) conditions and the high-energy beam irradiation of light-colored type Ia/IIa diamonds. In the New York laboratory, we recently examined a very rare case of a type IIb diamond artificially irradiated to enhance its blue color.

This modified step-cut shield (13.70 × 10.75 × 5.09 mm) weighed 4.13 ct and was color graded Fancy Deep green-blue (figure 1). It displayed a clear color concentration in the culet, an important visual indication of artificial irradiation. Infrared absorption spectroscopy revealed a typical spectrum for a type IIb diamond, with an intense 2800 cm^{-1} peak corresponding to an optically active boron concentration of ~40 ppb. A type IIb diamond with this size and boron concentration usually has a clear blue color (with a grayish or brownish component, depending on the intensity of plastic deformation) but not enough saturation for a Fancy Deep grade. The absorption spectrum in the UV-Vis region at liquid-nitrogen temperature showed strong GR1 absorption and a weak 666.7 nm peak, resulting in a transmission window in the green–light blue region. From these observations, we confirmed that this diamond had been artificially irradiated to improve its color. Strong plastic deformation indicated by high strain suggested that the diamond had a significant brown component before the treatment. This also explains the strong green coloration observed after irradiation.

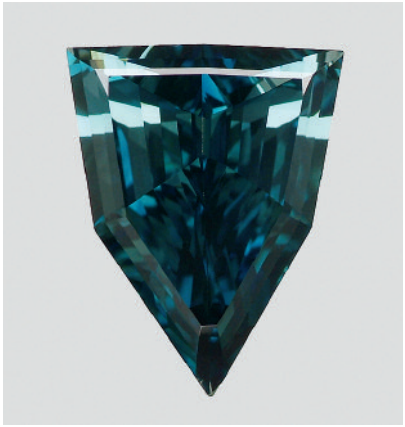

Figure 1. The Fancy Deep green-blue color of this 4.13 ct type IIb diamond is due to artificial irradiation.

Type IIb diamonds are rarely irradiated to improve their color. This unusual sample allowed us the opportunity to examine the interaction of a vacancy defect (GR1) with other defects in a type IIb diamond.

Wuyi Wang and Paul Johnson

Type IIb Green, Natural and Synthetic

Type IIb diamonds are typically blue, resulting from boron defects, and it is very unusual to see a distinct green color in such diamonds. The New York laboratory recently examined two type IIb green brilliants, a 5.84 ct pear shape and a 0.30 ct round, that were color graded as Fancy Dark gray-yellowish green and Fancy Light yellow-green, respectively (figure 2).

Both were very clean microscopically. In cross-polarized light, the pear showed the tatami strain typical of a natural diamond. The round brilliant did not exhibit any strain, but did show subtle color zoning (figure 3). DiamondView imaging of the pear shape revealed blue luminescence with dislocations (straight lines), indicating a natural diamond, while the round brilliant displayed a typical HPHT-synthetic growth pattern (figure 4). Spectroscopic analysis confirmed a natural color origin for the pear and an as-grown color for the round brilliant. Both were verified as type IIb by the boron bands in their mid-infrared spectra at ~2927 and ~2801 cm^{-1}.

Dislocations in a natural diamond occur during plastic deformation, which usually creates a brown color. In type IIb diamonds, the same process adds a gray component to the blue color. In this pear-shaped stone, however, plastic deformation also contributed a yellow component. The resulting combination of yellow and blue produced the 5.84 ct diamond's yellowish green bodycolor.

Interestingly, the light yellow-green synthetic diamond had a different cause of color. In addition to boron bands, a small amount of single substitutional nitrogen was detected at 1344 cm^{-1} in the mid-infrared spectrum. An earlier study reported mixed type IIb + Ib synthetic diamonds with blue and yellow growth sectors (J. E. Shigley et al., "Lab-grown colored diamonds from Chatham Created Gems," Summer 2004

Editors' note: All items were written by staff members of GIA laboratories.

GEMS & GEMOLOGY, *Vol. 48, No. 1, pp. 47–52, http://dx.doi.org/10.5741/GEMS.48.1.47.*

© 2012 Gemological Institute of America

Figure 2. These type IIb samples consist of a Fancy Dark gray-yellowish green natural diamond (5.84 ct, left) and a Fancy Light yellow-green synthetic diamond (0.30 ct, right).

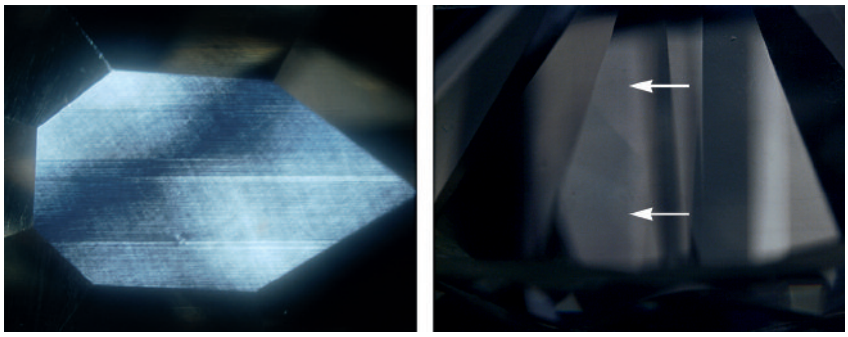

Figure 3. In cross-polarized light, the pear shape showed the tatami strain found in natural diamond (left, magnified 30×), while the synthetic round brilliant did not feature any strain but did show subtle color zoning (right, magnified 55×).

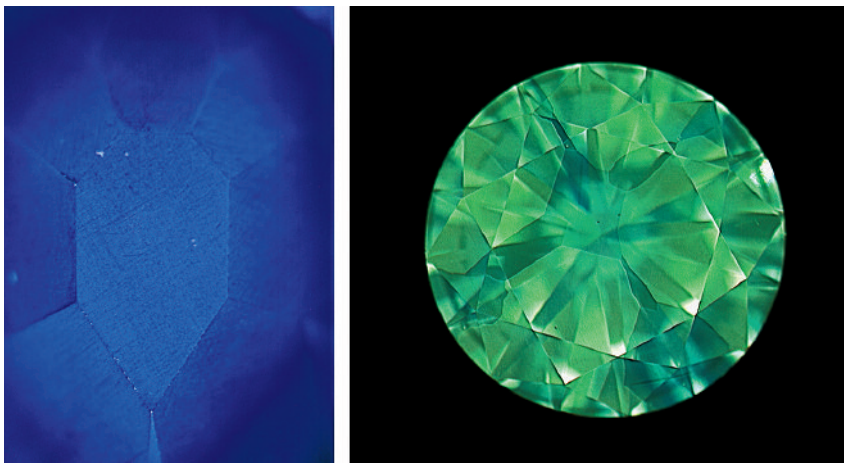

Figure 4. DiamondView imaging of the pear shape revealed blue luminescence and dislocations corresponding to a natural origin (left), while the round brilliant showed growth zoning indicative of an HPHT-grown synthetic diamond (right).

G&G, pp. 128–145). The article proposed that the combination of these growth sectors produced a green or grayish green color in faceted samples. In the 0.30 ct synthetic diamond reported here, the same coloring mechanism—the combined effect of a boron-dominated sector and an isolated-nitrogen sector—caused the yellow-green bodycolor. In both samples, the cutting orientation was critical to the proper mixing of the blue and yellow components. Therefore, other natural and synthetic diamonds containing blue and yellow color components may not show a green bodycolor.

These type IIb specimens demonstrate that plastic deformation or a combination of boron and nitrogen defects can result in unexpected green coloration at the hand of a skilled diamond cutter.

Kyaw Soe Moe

With Unusual Color Zoning

An optical center with a broad absorption band at ~480 nm is occasionally observed in some natural yellow-orange diamonds, as well as in "chameleon" diamonds. Yet little is known about this feature's atomic structure or its mechanism of formation in natural diamonds. In the New York laboratory, we recently encountered a particularly interesting manifestation of this optical center.

A 0.50 ct rectangular diamond (4.43 × 4.29 × 2.80 mm) was color graded Fancy Intense orange-yellow. Its absorption spectrum in the mid-infrared region showed moderate concentration of A-form nitrogen and some unassigned peaks. A strong absorption band at ~480 nm, detected in the UV-Vis spectrum at liquid-nitrogen temperature, appeared to be the cause of the intense orange-yellow color.

An outstanding feature of this diamond, visible during microscopic examination, was its distinct color zoning. The orange-yellow color was concentrated in parallel zones separated by near-colorless areas (figure 5). This banded color distribution was matched by the diamond's fluorescence reaction to long-wave UV radiation. The orange-yellow color zones showed very strong yellow-orange fluorescence, while the

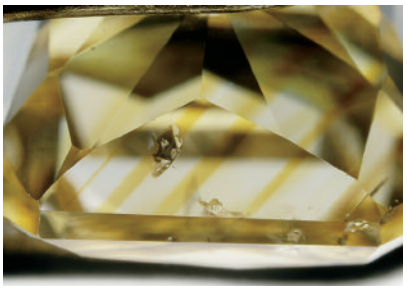

Figure 5. The orange-yellow color in this 0.50 ct diamond is concentrated in parallel zones separated by near-colorless bands.

near-colorless zones displayed strong blue fluorescence (figure 6). Microscopic observation with crossed polarizers showed little internal strain, and there was no observable strain variation between the different color zones. From these observations and the well-known fact that the 480 nm center luminesces yellow-orange to UV radiation, it became clear that the 480 nm center was distributed with a zoned structure. It was also obvious that this banded structure was not associated with plastic deformation, a very common cause of color zoning in natural diamonds.

While the origin of the unusual distribution of the 480 nm center in this diamond is unknown, the skillful orientation of the color banding by the cutter produced a face-up appearance that received a Fancy Intense color grade.

Marzena Nazz

Large EMERALD with *Gota de Aceite* Structure

Gota de aceite (Spanish for "drop of oil") is a transparent angular or hexagonal growth structure rarely seen in emerald (R. Ringsrud, "*Gota de aceite*: Nomenclature for the finest Colombian emeralds," Fall 2008 *G&G*, pp. 242–245). The New York laboratory had the opportunity to examine a 24.25 ct emerald showing this phenomenon (figure 7).

Microscopic observation revealed transparent growth structures with an oily appearance throughout the stone (figure 8, left). The effect could even be seen with the unaided eye. Some of the structures displayed six well-defined arms intercalated with six growth sectors, forming a 12-sided outline (figure 8, right); others showed an angular outline without arms. These structures occurred as individuals or in elongated groups. The c-axis of each growth structure was parallel to the optic axis of the host emerald. Such columnar growth zoning may have been developed by the parallel growth of numerous sub-crystals, which were overgrown by the host emerald (E. J. Gübelin and J. I. Koivula, *Photoatlas of Inclusions in Gemstones*, Vol. 3, Opinio Publishers, Basel, Switzerland, 2008, pp. 433–434).

The sample's jagged two- and three-phase inclusions and spectroscopic features confirmed it was a Colombian emerald. Individual and compact groups of colorless, transparent prismatic inclusions were identified by Raman spectroscopy as quartz (see photo in the *G&G* Data Depository at gia.edu/gandg), a well-known inclusion in Colombian emerald but not previously reported in *gota de aceite* specimens. The stone also contained strong planar color zoning, as well as partially healed fissures and fractures that showed evidence of clarity enhancement.

Figure 7. This 24.25 ct Colombian emerald showed the rare gota de aceite *growth structure.*

Viewed in diffused light, the emerald's green color was clearly concentrated within the growth structures described

Figure 6. When the diamond was exposed to long-wave UV radiation, the orange-yellow color zones fluoresced very strong yellow-orange, while the near-colorless zones showed strong blue fluorescence.

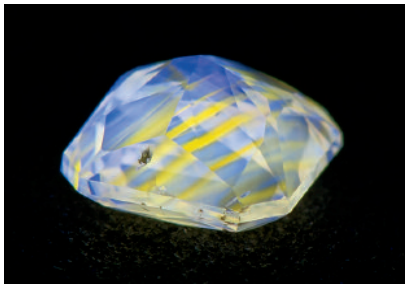

Figure 8. Fiber-optic illumination of the emerald clearly shows growth structures formed individually or in groups (left, magnified 25×). Some of the growth structures consist of six well-defined, intersecting arms intercalated between six growth sectors, creating a 12-sided outline (right, magnified 55×).

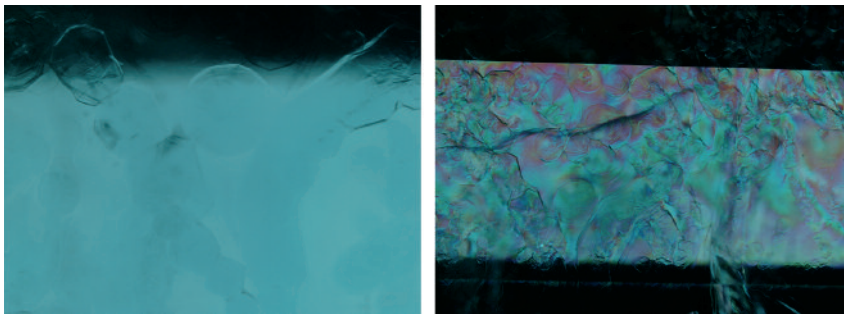

Figure 9. In diffused light, the emerald's green color was strongly concentrated in the growth structures (left, magnified 30×). The growth structures also showed high-order interference color in cross-polarized light (right, magnified 15×).

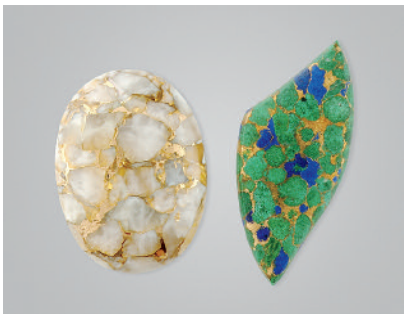

Figure 10. These 76.63 ct oval and 34.53 ct freeform cabochons proved to be manufactured composites that contain artificial metallic veining.

above, which also showed high-order interference colors when viewed down the optic axis in cross-polarized light (figure 9). A high-resolution UV-Vis-NIR absorption spectrum (available in the *G&G* Data Depository) showed broad bands at ~425 and ~613 nm, and a doublet at 680 and 683 nm; all these features are due to Cr^{3+}. Interestingly, we also detected a very weak broad band at ~830 nm, caused by Fe^{2+}. The presence of this band, not previously reported in Colombian emeralds, may be due to the high resolution of the spectrum.

So far, the *gota de aceite* structure has only been reported in Colombian emeralds, and thus it provides a useful tool to identify geographic origin, along with the multiphase inclusions and spectroscopic features shown by these emeralds.

Kyaw Soe Moe and Wai L. Win

Update on Artificial Metallic Veining in MANUFACTURED GEM MATERIALS

A Winter 2010 Lab Note (pp. 303–304) on artificial metallic veining in composite turquoise speculated that this type of veining could appear in other gem materials. Such was the case with an interesting pair of cabochons (figure 10) that were recently examined in the Carlsbad laboratory.

The first cabochon was a 76.63 ct oval composed of white angular fragments suspended in a yellow metallic matrix. Magnification revealed cleavages in the white fragments and foliated metal flakes suspended in colorless plastic (figure 11) that was easily indented by a needle and produced an acrid odor when tested with a thermal probe. Gemological testing gave spot RI readings up to 1.65 that showed a birefringence blink. The sample was inert to long- and short-wave UV radiation. Raman analysis identified the white fragments as calcite, which is consistent with the observed gemological properties. EDXRF spectroscopy revealed Cu and Zn as the dominant elements in the veins. This alloy produced an effective "gold" imitation. It is clear from the cabochon's appearance that it is intended to imitate gold-veined quartz, an attractive and rather expensive ornamental gem material.

Figure 11. The imitation gold-in-quartz cabochon was composed of calcite veined by colorless plastic containing very fine metallic flakes consisting of copper and zinc. The foliated texture is distinctive of manufactured origin. Magnified 30×.

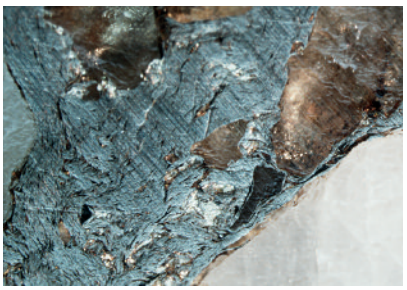

The second sample was a 34.53 ct green and blue freeform cabochon with copper-colored metallic veining. Magnification and Raman analysis revealed it was composed of sand-sized quartz grains suspended in a matrix of malachite, azurite, metallic flakes, and colorless plastic that also produced an acrid odor when tested with a thermal probe (figure 12). A spot RI of 1.54 was consistent with the high percentage of quartz grains present in the piece. The sample was inert to long- and short-wave UV radiation. EDXRF analysis showed that the metallic flakes were composed primarily of Cu with a small amount of Zn. A copper-colored matrix was appropriate for this imitation, considering that azurite and malachite are both copper minerals.

Figure 12. Magnification of the other cabochon shows small rounded grains of quartz suspended in a colored matrix of malachite and azurite with metallic veining. Magnified 15×.

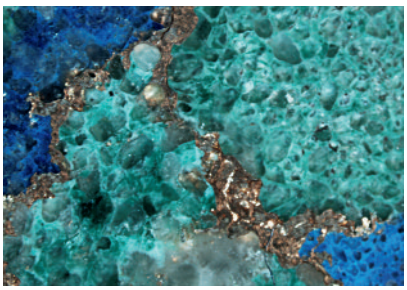

This is the first time we have seen this manufacturing technique applied to these particular materials, and it is reasonable to assume that additional composites with artificial metallic veining could appear in a wide variety of combinations. Nevertheless, the foliated appearance of the metallic veining is quite diagnostic of manufactured origin, regardless of the component material.

Nathan Renfro and Amy Cooper

Shell-Nucleated Freshwater Cultured PEARLS

In November 2011, the New York laboratory received three large flat baroque pearls for identification: one white, one orange-pink (figure 13, left), and one multicolored. They ranged from 25.57 × 16.16 × 8.04 mm to 19.54 × 16.44 × 6.34 mm. Their shapes were similar to ones we have seen in the past that were nucleated with coin- or lentil-shaped beads, first mentioned in *G&G* nearly 30 years ago (Summer 1984 Lab Notes, pp. 109–110). Both types of beads are often used for nucleation in freshwater mollusks to produce flattened cultured pearls in various shapes.

Standard gemological testing showed that all three were freshwater pearls, but X-ray images revealed an unusual internal structure (e.g., figure 13, center). All three contained what appeared to be a solid "nucleus" with distinct edges, but the outlines were not symmetrical, or even remotely uniform. The shapes of the nuclei were clearly not natural but could not be readily identified as beads, either, due to their irregular and varied morphology.

With the client's permission we cut open the orange-pink pearl, as its X-ray images revealed the most pronounced atypical structure, featuring one very straight edge. We sliced down the center lengthwise and found what appeared to be a roughly cut piece of shell, evidently used as the nucleus (figure 13, right). The shell nucleus had an irregular shape with some visible lustrous nacreous areas. The cross-section of the cultured pearl showed a nacre thickness ranging from ~1 to 2 mm. EDXRF spectroscopy of the shell nucleus and the surrounding nacre indicated that both were of freshwater origin, as did the strong luminescent reactions when exposed to X-rays.

While it has become more common to nucleate freshwater cultured pearls with beads, this typically involves using symmetrical pieces of shell, either round (such as those commonly used in saltwater cultured pearls) or "fancy"-shaped (as found in "coin pearls"). This is the first time we have examined freshwater cultured pearls nucleated with roughly cut shell. Using these relatively large shell nuclei produces a bigger cultured pearl in a shorter time, and the irregular shape results in a more natural baroque appearance.

Akira Hyatt

Lazurite Inclusions in RUBY

The Carlsbad laboratory recently examined a large 5.09 ct unheated ruby with a noteworthy inclusion suite. Standard gemological testing gave refractive indices of 1.762–1.770 and a strong red reaction to long-wave UV radiation. Examination with a desk-model spectroscope revealed fine lines at 460, 470, and 694 nm, along with a broad absorption band centered at 560 nm, which confirmed the stone was a ruby. Microscopic examination showed dense clouds of fine iridescent rutile, unaltered protogenetic carbonates, polysynthetic twinning, and several "fingerprints." The overall inclusion suite, combined with the strong fluorescence, suggested a low-iron, marble-hosted ruby, most likely of Burmese origin.

One particularly unusual type of inclusion stood out, however. Numerous crystallographically aligned negative crystals (see Fall 2009 Lab Notes, p. 212) were in-filled with a vibrant blue mineral that was identified by Raman analysis as lazurite (figure 14). Lapis lazuli is known to occur in Myanmar, and this geologic overlap could provide an explanation for lazurite inclusions in a corundum host.

One of these contributors (VP) saw similar blue inclusions in rubies he collected from Namya (or Nanyaseik), Myanmar, in December 2002. Analysis of a sample purchased during that trip confirmed that the inclusions (figure 15) were lazurite.

Figure 13. The orange-pink baroque cultured pearl on the left (25.57 × 16.16 × 8.04 mm) showed an asymmetrical "nucleus" in X-ray images taken from two different orientations (center; arrows show outline of nucleus). It was sliced down its center lengthwise to reveal a roughly cut piece of shell that was apparently used as the nucleus (right).

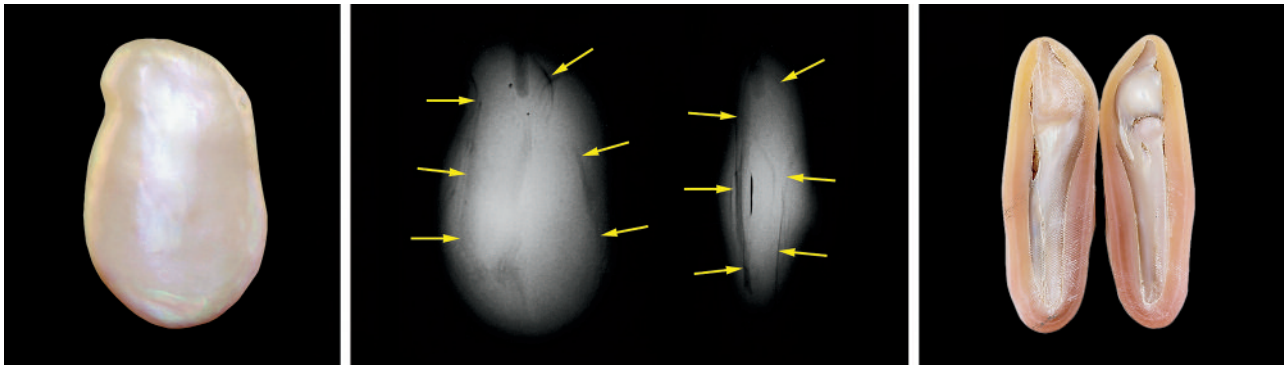

Figure 14. A 5.09 ct ruby was host to numerous lazurite-filled negative crystals. Magnified 25×.

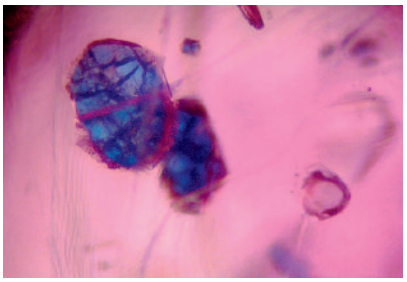

Figure 15. These blue inclusions in a 1.40 ct ruby, collected a decade ago in Namya, Myanmar, consist of lazurite-filled negative crystals similar to those in figure 14. Magnified 40×.

Blue inclusions in ruby are extremely rare, and the presence of lazurite in the 5.09 ct sample strongly supports a Burmese origin. This finding is reinforced by the other inclusions present in the stone and a low-iron composition consistent with Burmese rubies. To our knowledge, this is the first documented occurrence of inclusions of lazurite in ruby.

Nathan Renfro and Vincent Pardieu

A Coated SHELL Assemblage

Whole shells are rarely submitted to GIA for identification, so the Bangkok laboratory was interested to see such a specimen recently. The specimen (figure 16) weighed 240.5 g and measured 132 × 69 × 56 mm. The client wanted a report identifying it as a natural seashell. Such right-handed conch shells are rare compared to left-handed varieties, and they are coveted by religious devotees who consider them to be natural representations of Hindu deities.

The object did appear to be a shell, though the surface texture felt rather smooth and the piece seemed somewhat hefty for its size. Closer examination with a loupe and a gemological microscope indicated that the surface was not shell but a resinous-looking substance that contained small gas bubbles. Nor were there any obvious shell-related characteristics such as flame structure or evidence of parasite holes or channels within the shell. When exposed to long-wave UV radiation, the sample fluoresced a weak-to-moderate chalky uneven yellow rather than the more commonly encountered blue reaction, further adding to our doubts about the nature of the specimen. Raman analysis did not reveal the characteristic aragonite peaks at 1085 and 705/701 cm^{-1} (doublet) that would be expected for most shells. EDXRF chemical analysis indicated minimal levels of calcium (the major component of any natural shell), and traces of strontium (also a common constituent of shells). Both elements should have been more prominent if the sample was a true shell.

Natural coiled gastropod shells show characteristic spiral structures when viewed in cross section or examined by microradiography. Our microradiographic examination of this object (figure 17) clearly showed the presence of natural shell with another component—most likely a filler material used to add heft. An artificial layer of material was then used to coat the assemblage and give it a realistic appearance.

This coated shell assemblage shows that even these simple religious icons may be manufactured with the intent to deceive an unsuspecting buyer.

Nick Sturman and Hpone-Phyo Kan-Nyunt

PHOTO CREDITS
Jian Xin (Jae) Liao—1, 2 (left), 5, 6, 7, and 13; Sood Oil (Judy) Chia—2 (right); Kyaw Soe Moe—3, 4, 8, and 9; Robison McMurtry—10; Nathan Renfro—11, 12, and 14; Vincent Pardieu—15; Nuttapol Kitdee—16; Artitaya Homkrajae—17.

Figure 16. This specimen (13.2 cm long) proved to consist of a natural shell that contained a filler material and was covered by an unidentified artificial coating.

Figure 17. A microradiograph of the thicker end of the specimen (left image) shows the spiral shell structure and some of the filler material (whiter area on far right side). The microradiograph on the right shows part of the chamber area of the shell (A) and some of the filler used within the item (B).

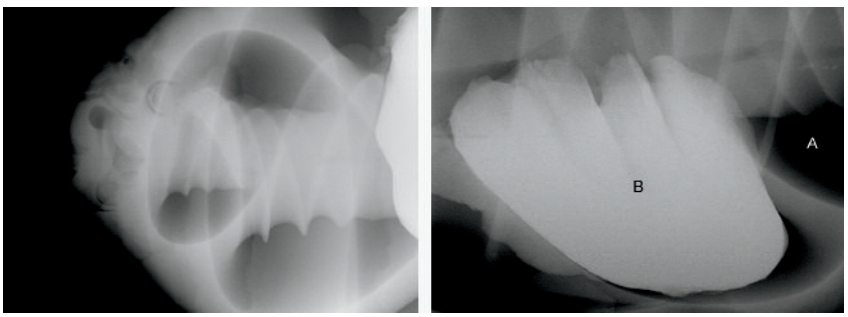

What's *missing* from your collection?

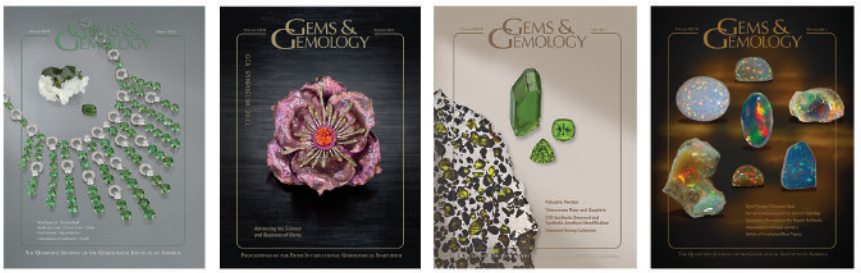

Spring–Winter 2011

Spring 2008
Copper-Bearing (Paraíba-type) Tourmaline from Mozambique
A History of Diamond Treatments
Natural-Color Purple Diamonds from Siberia

Summer 2008
Emeralds from Byrud (Eidsvoll), Norway
Creating a Model of the Koh-i-Noor Diamond
Coated Tanzanite
Coloring of Topaz by Coating and Diffusion Processes

Fall 2008
Identification of Melee-Size Synthetic Yellow Diamonds
Aquamarine, Maxixe-Type Beryl, and Hydrothermal Synthetic Blue Beryl
A New Type of Synthetic Fire Opal: Mexifire
The Color Durability of "Chocolate Pearls"

Winter 2008
Color Grading "D-to-Z" Diamonds at the GIA Laboratory
Rubies and Sapphires from Winza, Tanzania
The Wittelsbach Blue

Spring 2009
The French Blue and the Hope: New Data from the Discovery of a Historical Lead Cast
Gray-Blue-Violet Hydrogen-Rich Diamonds from the Argyle Mine
Hackmanite/Sodalite from Myanmar and Afghanistan
Pink Color Surrounding Growth Tubes and Cracks in Tourmalines from Mozambique
Identification of the Endangered Pink-to-Red *Stylaster* Corals by Raman Spectroscopy

Summer 2009
Celebrating 75 Years of *Gems & Gemology*
The "Type" Classification System of Diamonds
Spectral Differentiation Between Copper and Iron Colorants in Gem Tourmalines
Andalusite from Brazil
Peridot from Sardinia, Italy

Fall 2009
Characterization of "Green Amber"
Crystallographic Analysis of the Tavernier Blue
"Fluorescence Cage": Visual Identification of HPHT-Treated Type I Diamonds
Ammolite Update
Polymer-Filled Aquamarine
Yellow-Green Haüyne from Tanzania
Aquamarine from Masino-Bregaglia Massif, Italy

Winter 2009 (PDF only)
Ruby and Sapphire Production and Distribution: A Quarter Century of Change
Cutting Diffraction Gratings to Improve Dispersion ("Fire") in Diamonds
Chrysoprase and Prase Opal from Haneti, Central Tanzania
Demantoid from Val Malenco, Italy

Spring 2010
Strongly Colored Pink CVD Lab-Grown Diamonds
Color Alterations in CVD Synthetic Diamond with Heat and UV Exposure
Possible "Sister" Stones of the Hope Diamond
Confocal Micro-Raman Spectroscopy
Bastnäsite-(Ce) and Parisite-(Ce) from Malawi

Summer 2010
The Wittelsbach-Graff and Hope Diamonds: Not Cut from the Same Rough
Play-of-Color Opal from Ethiopia
A New Type of Composite Turquoise
Fire Opal from Madagascar
X-ray Computed Microtomography Applied to Pearls
Hibonite: A New Gem Mineral

Fall 2010
An Era of Sweeping Change in Diamond and Colored Stone Production and Markets
Gem Localities of the 2000s
Gemstone Enhancement and Its Detection in the 2000s
Developments in Gemstone Analysis Techniques and Instrumentation During the 2000s

Winter 2010
Synthetic Gem Materials in the 2000s
Yellow Scapolite from Madagascar
Pietersite from Namibia and China
Update on Mexifire Synthetic Fire Opal
Gems in a Ciborium from Einsiedeln Abbey

Spring 2011
Demantoid and Topazolite from Antetezambato, Northern Madagascar
The Chinese Red Feldspar Controversy: Chronology Through July 2009
UV-Vis-NIR Reflectance Spectroscopy of Natural-Color Saltwater Cultured Pearls from *Pinctada Margaritifera*
Brownish Red Zircon from Muling, China
Aquamarine from the Thuong Xuan District, Vietnam

Summer 2011
Proceedings of the 5th International Gemological Symposium
Research on Gem Feldspar from the Shigatse Region of Tibet

Fall 2011
Ruby and Sapphire from the Tan Huong–Truc Lau Area, Vietnam
Infrared Spectroscopy of Natural vs. Synthetic Amethyst: An Update
The Origin and Nature of Luminescent Regions in CVD Synthetic Diamond
Identification of Extraterrestrial Peridot by Trace Elements
A History of Diamonds through Philately: The Frank Friedman Collection

Winter 2011
Dyed Purple Hydrophane Opal
Determining Garnet Composition from Magnetic Susceptibility
GIA's Symmetry Grading Boundaries for Round Brilliant Cut Diamonds
A Historic Turquoise Jewelry Set Containing Fossilized Dentine (Odontolite) and Glass
The Radioactive Decay Pattern of Blue Topaz Treated by Neutron Irradiation

For a complete list of articles from 1981 forward, visit gia.edu/gandg

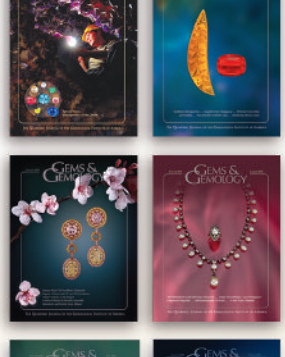

GEMS & GEMOLOGY®

The Quarterly Journal That Lasts A Lifetime

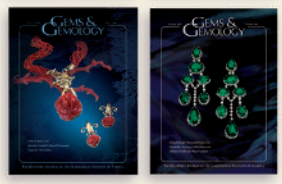

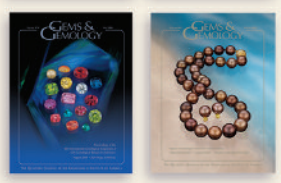

1981–2011 Back Issues

Order Your Issues at
store.gia.edu
Call toll free 800-421-7250 ext. 7306
or 760-603-4000 ext. 7306
Fax 760-603-4595

E-mail gandg@gia.edu
or write to
Gems & Gemology
PO Box 9022, Carlsbad, CA
92018-9022, USA

Complete volumes of 1992–2011 print back issues (except 2009) are available, as are limited issues from 1985–1991.

10% discount for GIA Alumni and active GIA students.

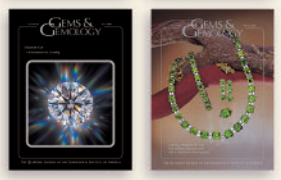

Order Your
BACK ISSUES
CHARTS & BOOKS
Today!

G&G
Gem News International

Editor
Brendan M. Laurs (blaurs@gia.edu)

Contributing Editors
Emmanuel Fritsch, *CNRS, Team 6502, Institut des Matériaux Jean Rouxel (IMN), University of Nantes, France* (fritsch@cnrs-imn.fr)
Michael S. Krzemnicki, *Swiss Gemmological Institute SSEF, Basel, Switzerland* (gemlab@ssef.ch)
Franck Notari, *GGTL GemLab–GemTechLab, Geneva, Switzerland* (franck.notari@gemtechlab.ch)
Kenneth Scarratt, *GIA, Bangkok, Thailand* (ken.scarratt@gia.edu)

TUCSON 2012

This year's Tucson gem and mineral shows saw brisk sales of high-end untreated colored stones (and mineral specimens) as well as some low-end goods, but sluggish movement of mid-range items. In addition to the more common colored stones, many rarities such as pallasitic peridot (figure 1) and hibonite (figure 2) were seen at the shows. Cultured pearls continued to have a strong presence, and particularly impressive were the relatively new round beaded Chinese freshwater products showing bright metallic luster and a variety of natural colors (figure 3). An unusual historic item seen in Tucson is the benitoite necklace suite shown in figure 4. Several additional notable items present at the shows are described in the following pages and will also be documented in future issues of *G&G*.

The theme of this year's Tucson Gem and Mineral Society show was "Minerals of Arizona" in honor of Arizona's Centennial, and next year's theme will be "Fluorite: Colors of the Rainbow."

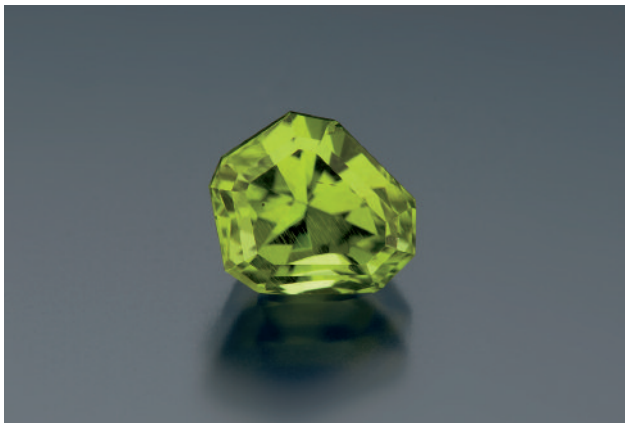

Figure 1. Pallasitic peridot had a strong presence at the 2012 Tucson gem shows. This unusually large and fine example weighs 2.26 ct and is courtesy of Scott Davies, American-Thai Trading, Bangkok. Photo by Robert Weldon.

Editor's note: Interested contributors should send information and illustrations to Brendan Laurs at blaurs@gia.edu or GIA, The Robert Mouawad Campus, 5345 Armada Drive, Carlsbad, CA 92008. Original photos will be returned after consideration or publication.

Gems & Gemology, Vol. 48, No. 1, pp. 54–72,
http://dx.doi.org/10.5471.GEMS.48.1.54.
© 2012 Gemological Institute of America

Figure 2. This exceedingly rare faceted hibonite from Myanmar weighs 0.96 ct and was recently cut from a crystal weighing 0.47 g, which also yielded a 0.26 ct stone. Courtesy of Mark Smith (Thai Lanka Trading, Bangkok); now in the Herbert Obodda collection. Photo by Robert Weldon.

Figure 3. Beaded Chinese freshwater cultured pearls showing a metallic luster and a variety of natural colors were popular in Tucson this year. Also known as "Edison pearls," the examples shown here are 12.5–13.5 mm in diameter. Courtesy of Jack Lynch (Sea Hunt Pearls, San Francisco); photo by Robert Weldon.

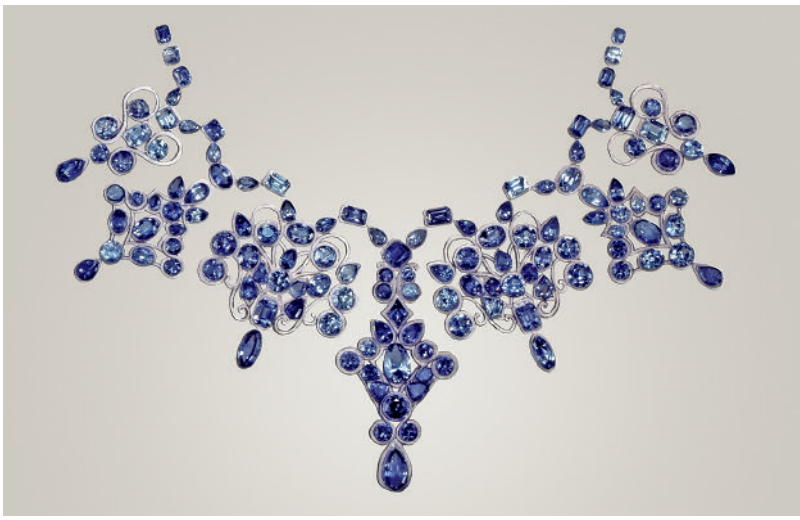

Figure 4. This historic set of 133 benitoites (0.16–3.50 ct) with a total weight of 130.89 carats was faceted from rough material collected by Edward Swoboda and Peter Bancroft in the 1920s and 1930s. The stones are shown on a drawing of a necklace that was designed specifically for this suite. The collection was offered for sale for the first time by Rob Lavinsky (The Arkenstone, Garland, Texas). Courtesy of Bryan Swoboda.

G&G appreciates the assistance of the many friends who shared material and information with us this year, and also thanks the American Gem Trade Association for providing space to photograph these items during the AGTA show.

COLORED STONES AND ORGANIC MATERIALS

Aquamarine from Mavuco, Mozambique. Alluvial deposits at Mavuco in the Alto Ligonha pegmatite district in northern Mozambique are well-known as a source of copper-bearing tourmaline (B. M. Laurs et al., "Copper-bearing [Paraíba-type] tourmaline from Mozambique," Spring 2008 *G&G*, pp. 4–30). During this author's 2008 fieldwork at Mozambique Gems' claim, quartz-rich granitic pegmatites were seen adjacent to the tourmaline mines that were reportedly mined sporadically for aquamarine in the 1980s and 1990s. In November 2011, Mozambique Gems worked this pegmatite area for a two-week period, producing additional aquamarine. This material (e.g., figure 5) was exhibited at the Gem & Jewelry Exchange (GJX) show by mine partner Saint-Clair Fonseca Junior (Mozambique Gems, Nampula, Mozambique, and BC Gemas do Brasil, Governador Valadares, Brazil). He indicated that dynamite was used to blast the hard rock in search of aquamarine, which is frozen in the host quartz rather than being found in gem pockets. They recovered ~300 kg of aquamarine, of which 10 kg contained gem-quality areas. Approximately 500 carats have been faceted in calibrated sizes measuring up to 9 × 7 mm. These untreated gems show a rather saturated pure blue color for their size.

Mr. Fonseca also had several necklace sets composed of faceted and tumbled Cu-bearing tourmaline that was produced from his claim during the past year. Most of this material was unheated, and it displayed a broad range of color similar to the tourmaline documented in the Spring 2008 *G&G* article referenced above.

Brendan M. Laurs

Figure 5. These aquamarines are from Mavuco, Mozambique. The oval center stone weighs 0.94 ct and the others are ~0.4 ct each. Photo by Robert Weldon.

Azurite in granitic rock from Pakistan. At the 2011 and 2012 Tucson gem shows, Warren Boyd (R. T. Boyd Ltd., Ontario, Canada) showed *G&G* an interesting new gem material from the Skardu area in northern Pakistan. This area is famous for producing well-crystallized specimens of tourmaline, aquamarine, topaz, and garnet. In 2010, local prospectors discovered the new gem material in a remote valley. Now marketed as Raindrop Azurite, this unusual rock contains distinctive blue spots that make for attractive specimens, cabochons, and *objets d'art* (e.g., figure 6).

Mr. Boyd reported that the material is mined using simple hand tools, and the pieces are transported on foot or using pack animals to the closest road. So far ~4,000 kg of rough has been stockpiled, and nearly 600 pieces have been cut and polished in Shenzhen and Bangkok. He reported that the material is not treated in any way.

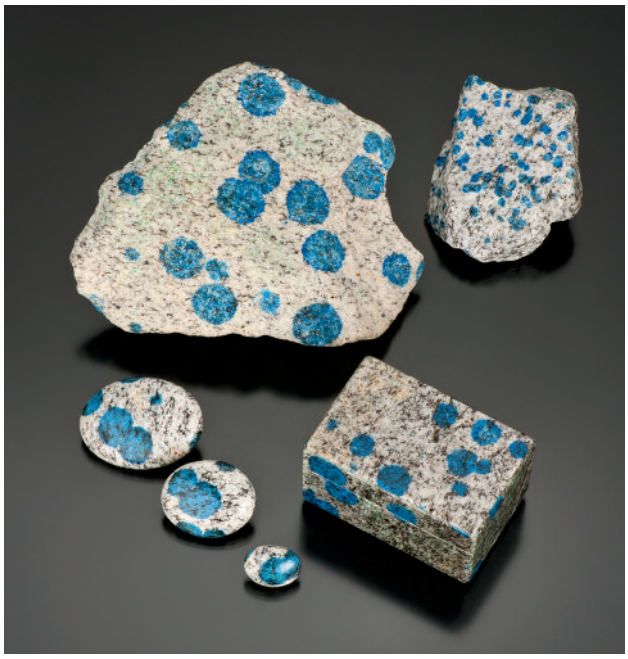

Figure 6. Raindrop Azurite is an azurite-bearing granitic rock from northern Pakistan. Shown here are two pieces of rough (404 and 87 g), cabochons (8.80–61.55 ct), and a box (6 × 4 × 3 cm) made by Silverhorn of Santa Barbara, California. Photo by Robert Weldon.

Raman analysis by Garry Du Toit at GIA in Bangkok confirmed that the blue spots consist of azurite, which occur in a matrix of sodic plagioclase, quartz, and muscovite.

Jan Iverson (jan.iverson@gia.edu)
GIA, Carlsbad

Cat's-eye emerald from the Belmont mine, Brazil. Chatoyant emerald has been known for decades (e.g., Fall 1982 Lab Notes, p. 169) but remains rather uncommon. During the 1990s, several stones were produced from the Santa Terezinha de Goiás emerald mines in Brazil (Gem News, Spring 1992, p. 60, and Spring 1995, pp. 60–61). Now small amounts of cat's-eye emeralds are coming from another source in Brazil, the Belmont mine.

At the GJX show, Marcelo Ribeiro Fernandes (Belmont, Itabira, Brazil) showed this contributor several attractive cat's-eye emeralds (e.g., figure 7) that were cut from material recovered since January 2010. Mr. Ribeiro indicated that rough material from his mine is now being examined by a specialist to identify the chatoyant material. He estimated that 100 g annually are separated out for cutting ~100 cat's-eye emeralds per year. Although cabochons ranging from 1 to 30 ct can be cut, Mr. Ribeiro indicated that 5 ct stones are most popular.

This is the first time that chatoyant emeralds have been specifically being targeted at Belmont during the rough sorting process, and the initiative is expected to increase the availability of this rare material in the future.

Brendan M. Laurs

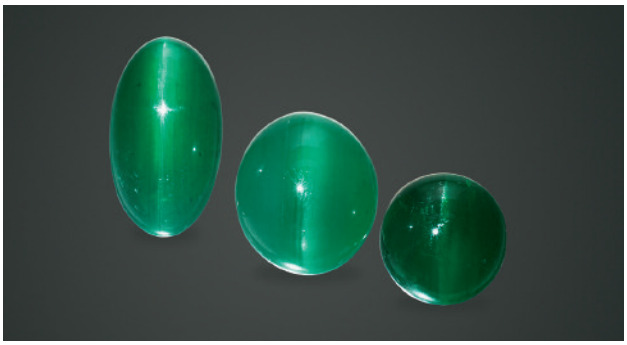

Figure 7. Cat's-eye emeralds such as these (16.75–29.14 ct) are now being cut from rough material that is carefully screened for chatoyancy at the Belmont mine in Brazil. Photo by Robert Weldon.

New production of purple common opal from Mexico. During the Tucson gem shows, Tom Elliot of Opal Royale (Bozeman, Montana) showed this author some purple Mexican opal colored by fluorite inclusions. While this material has been known for some time (E. Fritsch et al., "Mexican gem opals—Nano and micro structure, origin of colour, and comparison with other common opals of gemological significance," *Australian Gemmologist*, Vol. 21, No. 6, 2002, pp. 230–233), recent mining has made significant quantities of rough available to the market. The material was sold under the trade name "Opal Royale" and comes from central Mexico. Similar Mexican purple opal was also being sold in Tucson under the trade name "Morado Opal" and more generically as "Mexican purple opal."

According to Mr. Elliot, there are two basic varieties. A mottled purple and white to light gray variety typically occurs in veins, while a more uniformly colored darker purple version is generally found in nodules, with a chalcedony skin. Samples of both varieties (figure 8) were subsequently studied at GIA's Carlsbad laboratory. One cabochon of each type was examined

Figure 8. These samples of purple common opal are colored by fluorite inclusions. The rough pieces, which weigh 116 and 130 g, are shown with 13.98 and 15.24 ct cabochons. Photo by C. D. Mengason.

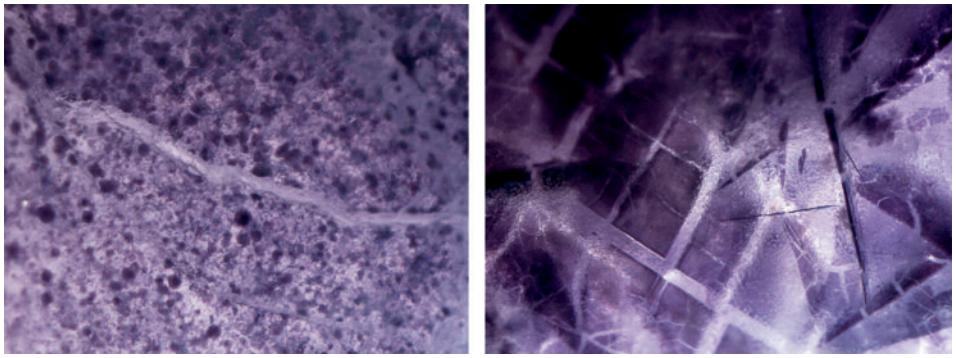

Figure 9. Microscopic examination reveals small rounded masses of purple fluorite in the Mexican opal, along with veins of chalcedony (left, magnified 60×). Brecciated planes of purple fluorite were also seen (right, magnified 40×). Photomicrographs by N. Renfro.

using standard gemological testing methods. Both gave a spot RI measurement of 1.44 and a hydrostatic SG of 2.18. The samples showed a very weak green reaction to long-wave UV exposure and a very strong green reaction to short-wave UV radiation, indications that they likely contained traces of uranium. Microscopic examination revealed small, dense irregular crystals and brecciated planes of purple material (figure 9) that was confirmed as fluorite by Raman analysis. The fluorite inclusions were much more clearly defined in the darker sample. Quartz was also detected in both cabochons.

Buyers should not confuse this non-phenomenal or common opal naturally colored purple by fluorite inclusions with dyed purple hydrophane opal exhibiting play-of-color (N. Renfro and S. F. McClure, "Dyed purple hydrophane opal," Winter 2011 *G&G*, pp. 260–270).

Nathan Renfro (nrenfro@gia.edu)
GIA, Carlsbad

Rare stones used in jewelry: smithsonite, cobaltite, pyrrhotite, nickeline, and Nuummite. Rare gems have long enjoyed popularity with collectors, but this year's Tucson shows saw several of these materials being purchased specifically for jewelry use (figure 10). At the GJX show, Mauro Pantò (The Beauty in the Rocks, Perugia, Italy) reported selling several varieties to jewelry manufacturers.

Yellow **smithsonite** ($ZnCO_3$), once mined in Sardinia, is no longer available since the closing of the Masua and Monteponi mines more than 40 years ago. The best-quality material is translucent and shows an even deep yellow color. Mr. Pantò has cut ~1,000 carats in standard and fancy shapes that mostly weighed 1–10 ct. He said it is difficult to obtain good-quality material; his entire inventory has come from old collections.

Cobaltite (CoAsS) from the Canadian town of Cobalt, Ontario, is an ore of cobalt with an appealing silver metallic luster. A few hundred carats were available in fancy shapes, with typical weights of 8–15 ct.

Although not particularly rare in nature, **pyrrhotite** (an iron sulfide) is seldom faceted, perhaps because of its low hardness (Mohs 3½–4½). Mr. Pantò had a few hundred carats of pyrrhotite from Mexico ranging from 3 to 10 ct.

The **nickeline** (NiAs) that Mr. Pantò obtained is from Cobalt, Canada. He said it must be mounted with great care, so only a few stones have been used in jewelry so far. Also known as niccolite in Europe, it was initially called *Kupfernickel*, or copper nickel, because the German miners who first saw the copper-red metallic mineral were convinced it was a rich ore of copper.

Nuummite (iridescent orthoamphibole) is normally seen in the market as tumbled stones or cabochons. This was the first time Mr. Pantò had offered faceted Nuummite, which came from the classic Greenland deposits (e.g., P. W. Uitterdijk Appel and A. Jensen, "A new gem material from Greenland: Iridescent orthoamphibole," Spring 1987 *G&G*, pp. 36–42). Similar faceted Nuummite is also known from Mauritania (see Fall 2011 Gem News International [GNI], pp. 242–243). Mr. Pantò had cut a few hundred carats in the 3–6 ct range.

Jan Iverson

Rosalinda: A new ornamental scapolite rock from Peru. White ornamental rock with red spots is known in two varieties: "chicken-blood stone" from China, and "myrickite" from northern California and elsewhere. The former material is a

Figure 10. Rare stones purchased by jewelry manufacturers in Tucson included, from left to right: yellow smithsonite (8.55 ct), cobaltite (13.36 ct), pyrrhotite (9.43 ct), nickeline (18.87 ct), and Nuummite (5.93 ct). Photo by Robert Weldon.

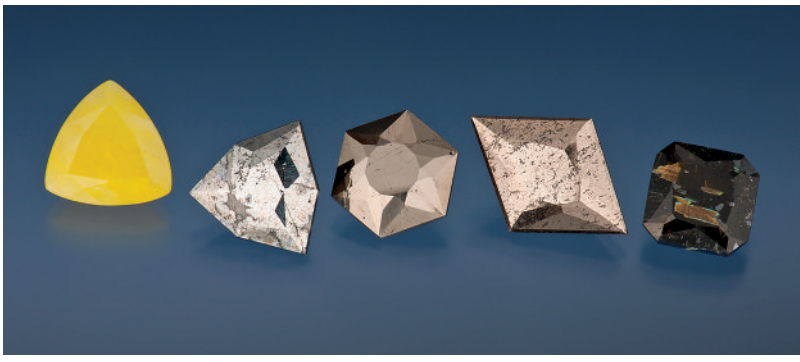

mixture of clay and quartz that is colored by cinnabar (e.g., W. Fuquan and G. Jingfeng, "Chicken-blood stone from China," Fall 1989 *G&G*, pp. 168–170), while the latter consists of silicified cinnabar-bearing rock. A new ornamental rock from Peru, known as Rosalinda, has a similar appearance but quite a different composition.

The first specimens were produced in September 2011 from an unnamed mountain (figure 11) close to the archaeological site of Tambo Colorado, an Inca fortification situated about 40 km east of Pisco, along the main road from the coast to Ayacucho. The outcrop covers an area of about 20 × 10 m, with substantial reserves; boulders approaching 50 cm wide have been recovered. The rock is white, with irregularly shaped pink to red spots that are usually several millimeters wide, though in rare cases they can measure several centimeters across.

XRD analysis of the white matrix mineral identified it as marialite, an Na- and Cl-rich member of the scapolite group. The scapolite is typically fine grained, occasionally forming long needles dispersed in white calcite. The red spots, also identified by XRD, are a member of the epidote-piemontite series, most likely Mn-rich epidote. Viewed with a loupe, some specimens also showed small (up to 1 mm) yellow grains of grossular.

Gemological examination of seven cabochons revealed the following properties: RI of the scapolite—1.54, SG of the rock—2.50–2.59, and Mohs hardness—6. The UV fluorescence shown by the scapolite is distinctive, and is quite useful for separating the material from similar-appearing rocks: It fluoresces orange to red (short-wave) or white (long-wave). Pure red Mn-rich epidote from the same locality showed: RI— >1.78, SG—3.15–3.20, Mohs hardness—5–6, and no reaction to UV radiation.

By the end of 2011, more than 20 tonnes of the rock had been prepared for export. The material can be used for cabochons, beads, and especially carvings (figure 12), some of which are quite large. At the 2012 Tucson shows it was marketed at the Hotel Tucson City Center as Rosalinda by Ramos Minerals, a Lima-based trading company. They had several hundred cabochons in various calibrated sizes; additional material is being polished in Lima.

Figure 11. A mountainside near Tambo Colorado, Peru, is the source of the new ornamental stone known as Rosalinda. Photo by J. Hyršl.

Jaroslav Hyršl (hyrsl@hotmail.com)
Prague, Czech Republic

Figure 12. The samples of Rosalinda on the left include cabochons up to 4 cm long and beads up to 8 mm in diameter. The Rosalinda elephant carving on the right measures 20 cm across. Courtesy of Ramos Minerals; photos by J. Hyršl.

Figure 13. These rare vlasovites (0.42 and 0.53 ct) are from Sheffield Lake in southwestern Quebec. Photo by Robert Weldon.

Vlasovite from Quebec. At the GJX show, Bradley Wilson (Coast to Coast Rare Stones International, Kingston, Ontario) exhibited nearly three dozen faceted samples of the rare mineral vlasovite ($Na_2ZrSi_4O_{11}$; figure 13). The brownish yellow gem material was mined in September 2008 at Sheffield Lake, near Témiscaming in Quebec, Canada, where it occurred with the more abundant mineral eudialyte. The rough had a uniform color and was transparent in small pieces. More than half of the cut samples he displayed were between 0.10 and 0.30 ct, and the largest stone was 0.53 ct. Although faceted vlasovite has occasionally been available to rare stone collectors, Mr. Wilson's stock at this year's Tucson show was significantly larger than has been seen in the past.

Discovered in 1961 in northern Russia, vlasovite has been found periodically at the Sheffield Lake locality. A 0.27 ct sample from the nearby Kipawa River in southwestern Quebec was reported in the Winter 1993 Gem News section (pp. 287–288).

Stuart D. Overlin (soverlin@gia.edu)
GIA, Carlsbad

SYNTHETICS AND SIMULANTS

"Sterling Opal" debuts. At the Pueblo Gem & Mineral Show, Sterling Foutz (Sterling Opal, Tempe, Arizona) had a wide selection of a new impregnated synthetic opal. The material was developed by James E. Zachery, an electrical engineer who also created the process for Zachery-treated turquoise (see Spring 1999 *G&G*, pp. 4–16). The gem-quality synthetic opal was developed by accident, during the course of 22 years of research on producing nanoparticles for medical applications. The process yields opalescent layers that are then stabilized by impregnation with a specially developed resin that has the same RI as the synthetic opal. Marketed as "Sterling Opal," the material was introduced in nine varieties showing various play-of-color patterns and in bodycolors ranging from white to medium blue (e.g., figure 14).

Mr. Foutz said the product has a hardness similar to that of Zachery-treated turquoise (Mohs 4–5), and he currently manufactures about 18 kg per week. The rough material is fabricated in 2 × 2 in. (5 × 5 cm) tiles that weigh approximately 20–30 g each. The tiles are sliced in half along their thinnest direction, and the sawn surface of each half is polished in a variety of shapes. These tiles were offered in Tucson, along with about 3,000 cabochons cut from 2–3 kg of the rough material. Most of the cabochons ranged from 7 × 5 mm to 25 × 18 mm (ovals) and 10–25 mm (squares). Also available were a few doublets with black backings to accentuate the play-of-color, as well as cabochons of "Picasso opal" featuring a mosaic of tiny synthetic opal pieces set in an epoxy "matrix." Some of these mosaic cabochons had been heated to give the "matrix" a dark color.

Preliminary gem testing of a polished slab and a cabochon of "Sterling Opal" (not doublets or the Picasso variety) at GIA gave RI readings of 1.465 and 1.467, and hydrostatic SG values of 1.72 and 1.74, respectively. These values are within the range of those expected for impregnated opal—natural or synthetic—so care must be taken to correctly identify this material. More information will be reported in a future *G&G* article.

Brendan M. Laurs
Shane F. McClure
GIA, Carlsbad

Bicolored tourmaline imitation. As the popularity of bicolored tourmaline has grown over the last few years, its price has risen accordingly. It is hardly surprising, then, that someone would develop an inexpensive imitation of this material.

Figure 14. "Sterling Opal" features various play-of-color patterns, with a white to medium blue bodycolor. The cabochons shown here range from 1.95 to 17.55 ct, and the rough piece (upper right) weighs 22.1 g. Photo by Jeff Scovil.

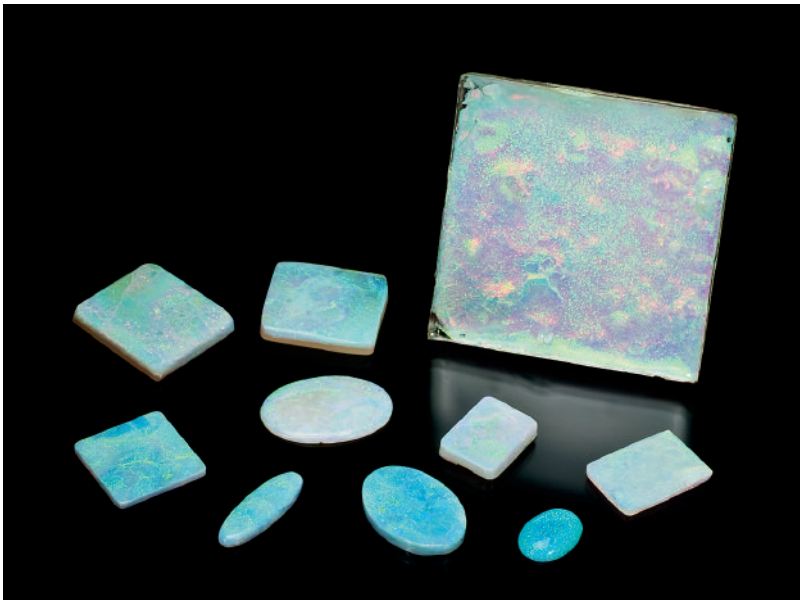

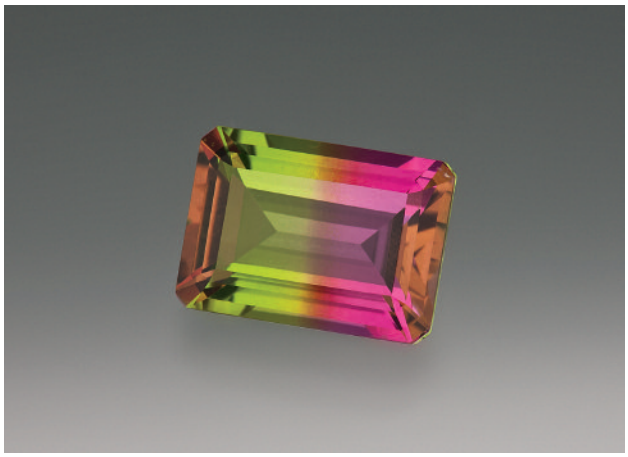

Figure 15. This triplet (6.97 ct) consists of crown and pavilion layers made of colorless quartz that are joined together with a red and green cement layer. Photo by Robert Weldon.

Rajneesh Bhandari (Rhea Industries, Jaipur, India) showed this contributor a new bicolored tourmaline simulant (figure 15). The imitations were offered for sale at the GJX show by RMC of Bangkok and Hong Kong. By the end of the show, they had sold out of all their merchandise on hand.

Mr. Bhandari indicated that the triplets consisted of colorless quartz crown and pavilion layers that were joined together with a red and green cement layer.

One sample was obtained by this contributor for examination. The emerald cut displayed a low-saturation brownish pink color at its extreme ends, likely caused by reflections combining the pink and green colors but somewhat imitative of pleochroism. Immersion in water showed colorless crown and pavilion sections, which both had the RI values and optic character of quartz. No inclusions were seen in the quartz with up to 63× magnification. The cement layer was clearly visible along the girdle (though not as obvious as in many synthetic spinel triplets). The cement layer was thinner than most, and with the microscope it appeared cloudy and contained several gas bubbles. The demarcation zone between the red and green areas was nearly centered and showed a smooth but sharp transition, as commonly seen high-quality bicolored tourmalines.

Viewed face-up with the unaided eye, these new triplets make a surprisingly convincing imitation of bicolored tourmaline.

Andy Lucas (alucas@gia.edu)
GIA, Carlsbad

CONFERENCE REPORTS

U.S. Faceters Guild seminars. The U.S. Faceters Guild seminars were held February 3 at the Old Pueblo Lapidary Club in Tucson. In "Heat Treating Your Gems," **Lisa Elser** (Lisa Elser Custom Cut Gems, Vancouver, Canada) discussed heating gems such as aquamarine, amethyst, zircon, topaz, tourmaline, and tanzanite using a small programmable burnout oven or butane torch. She suggested sawing off a small piece of rough or choosing a poor-quality stone for experimentation. In an oven, the test stone is covered with investment powder (used in lost wax casting) and then slowly heated no more than 100ºC/hour, with incremental adjustments of 25ºC or less. The gem remains at the desired temperature for 60–90 minutes and is then allowed to cool to room temperature before removal. Because heating carries the risk of damage, Ms. Elser emphasized that she only attempts this treatment when a stone is unsalable and there is a good chance for substantial improvement. By keeping careful notes on stones from different lots, she found that material from the same lot often can be treated identically to yield similar color improvements, while similar material from different lots (and possibly different locations or digs) may require slight temperature adjustments. Her tests demonstrate that small dealers do not need expensive ovens to improve the color of certain gems (e.g., figure 16).

In a session titled "Training in Afghanistan," **Jim Rentfrow** (Green Gem Foundation, Berkeley, California) described efforts by the USAID-funded Afghanistan Small and Medium Enterprise Development program to foster private-sector

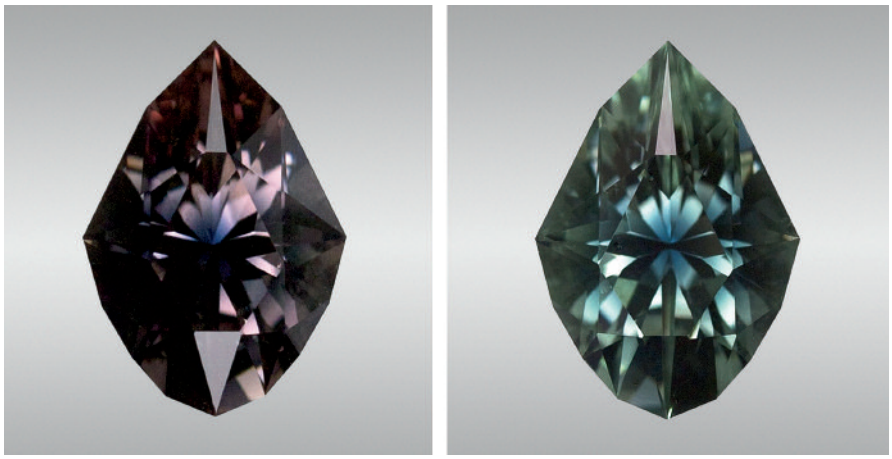

Figure 16. A 3.65 ct Nigerian tourmaline is shown before and after heat treatment. Photo by C. Tom Schlegel.

Figure 17. An Afghan woman in Kabul facets with a modern Ultra Tec machine. Photo by Jim Rentfrow.

growth. Over the past two years in Kabul, he worked with cutters on Chicken Street to increase their capacity. When he first arrived, only one local cutter used modern techniques and earned $25 per stone. The rest used primitive methods and lower standards, earning $4–$8 per stone. Mr. Rentfrow showed the cutters how to use modern machines (figure 17) and implement proper polishing techniques to remove windows from stones, improve meet points, and read modern facet diagrams. He also taught them accounting principles, provided basic business coaching, and helped them network with local business owners.

Al Gilbertson (agilbert@gia.edu)
GIA, Carlsbad

MISCELLANEOUS

Meteorite watches. At the GJX show, Robert and Patricia Van Wagoner (Beija-flor Wholesale, Haiku, Hawaii) exhibited an interesting selection of watches by Larimar Conlight of Denzlingen, Germany. The dials were made from a Swedish meteorite known as Muonionalusta (figure 18). It was discovered in 1906 in the Norrbotten region, north of the Arctic Circle (67°48′N, 23°07′E). Legend has it that two children were tending cattle and kicking stones when one of them struck a heavy rusty object, which they took to their village. In 1910 it was identified as an iron meteorite by Prof. A. G. Högbom, who named it after the municipality of Muonio.

Muonionalusta is composed of a nickel-iron alloy and classified as an octahedrite. After acid etching, slices of the meteorite display a spectacular crystalline texture (Widmanstätten pattern). Inclusions of troilite (FeS) are present in some of the watch dials, and Mr. Van Wagoner indicated that they are sealed under vacuum to prevent the troilite inclusions from oxidizing.

Mr. Van Wagoner also had watches with dials made from the Seymchan meteorite (also an octahedrite) that was found in the Magadan region of Russia in 1967.

Jan Iverson

Figure 18. The dials in these watches are fashioned from the Muonionalusta meteorite. Inclusions of troilite are visible at the 10 and 12 o'clock positions of the men's stainless steel watch on the left, and at the nine and 12 o'clock positions of the women's titanium watch on the right. Photo by Robert Weldon.

GNI REGULAR FEATURES

DIAMONDS

Diamond mining to resume at Birim River, Ghana. For decades Ghana's Birim River (figure 19) has been a significant world diamond source since its discovery in 1924. The deposits have yielded as much as 3 million carats yearly, though more than 80% of the output is industrial quality or weighs <0.20 ct (figure 20). During the 1980s, however, production went into steep decline. After intermittent activity, Ghana Consolidated Diamonds discontinued operations in 2007, after running at a loss for a number of years. Now a Ghanaian consortium is working to revive the Birim River deposits.

Figure 19. Workers wash gravel in search of diamonds along the Birim River in Ghana. Photo by R. Shor.

Figure 20. Independent miners sell their Birim River diamonds in the nearby town of Akwatia. Photo by R. Shor.

The new consortium, Great Consolidated Diamonds of Ghana (GCD), has begun rehabilitating old mining equipment and plans to resume operations by September 2012.

Production will initially focus on 20 million cubic meters of tailings spread over 17,100 hectares. A sampling program has indicated an average grade of 0.20 carats per cubic meter, with trace amounts of gold. The company has two other concessions in the area totaling 75,000 hectares. A 1985 survey estimated reserves in the two concessions at 14 million carats. The company estimates that production could reach 1 million carats yearly. Company officials offered no timeline because they are still assessing the extent of rehabilitation necessary to resume activity. Several of the processing plants built in the 1920s are in serious disrepair, and most of the mechanized equipment was sold off in 2007 when mining ceased.

Some areas within the concessions are being dug by hand. The miners sell their goods to local dealers in the nearby town of Akwatia (figure 21). According to Kimberley Process statistics, Ghana exported 333,827 carats of diamonds in 2010, valued at $11.9 million. The vast majority of these were from Birim River diggings. In 2007, the last year of formal mining, Ghana exported 643,289 carats of rough, valued at $16.5 million.

GCD has promised to protect the livelihoods of the artisanal miners who have moved into the area, many of them former employees of the previous operator. The company has also pledged to reclaim mined-out areas to allow small-scale farming.

Russell Shor (rshor@gia.edu)
GIA, Carlsbad

COLORED STONES AND ORGANIC MATERIALS

Iris agate from Montana. At the 2012 gem and mineral shows in Quartzsite, Arizona, Brad Payne (The Gem Trader, Cave Creek, Arizona) encountered a large stock of iris agate from eastern Montana. Iris agate from Montana has been known for decades (e.g., F. T. Jones, "Iris agate," *American Mineralogist*, Vol. 37, 1952, pp. 578–587), but is only rarely seen on the market. The approximately 500 slices ranged from ~1 to 18

Figure 21. Diamonds from the Birim River deposits are typically small (<0.20 ct). Photo by R. Shor.

cm long, and most of them were slightly domed for cabochon use. Mr. Payne was told the material is collected seasonally along the banks and sandbars of the Yellowstone River, and that this selection represented a single production lot—at least a decade's worth of collecting, which took four years to slice and polish.

The thin slices mostly had a banded light orangy brown bodycolor, and showed an attractive rainbow effect when illuminated with oblique transmitted light (figure 22). However, the iridescence will not be seen if the piece is too thick or not cut in the proper orientation relative to the bands. Many of the larger pieces were cut so thin that they had broken at some point and been repaired with epoxy. In addition to size considerations, iris agate's quality is judged by the amount of iridescence displayed, which Mr. Payne reported was quite variable across the specimens.

Stuart D. Overlin

Figure 22. This 2.65 ct (16.31 × 12.60 × 1.21 mm) iris agate from eastern Montana is shown in reflected light (left) and oblique transmitted light (right). Photos by Brad Payne.

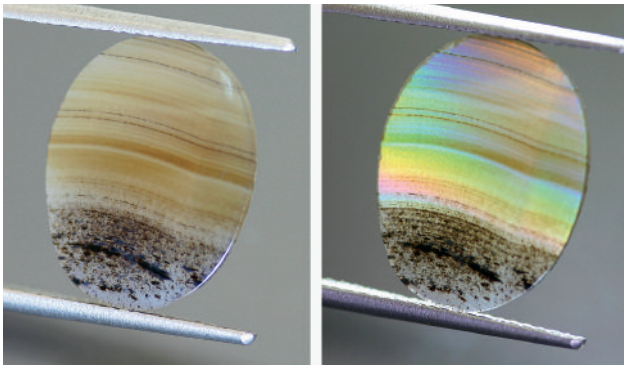

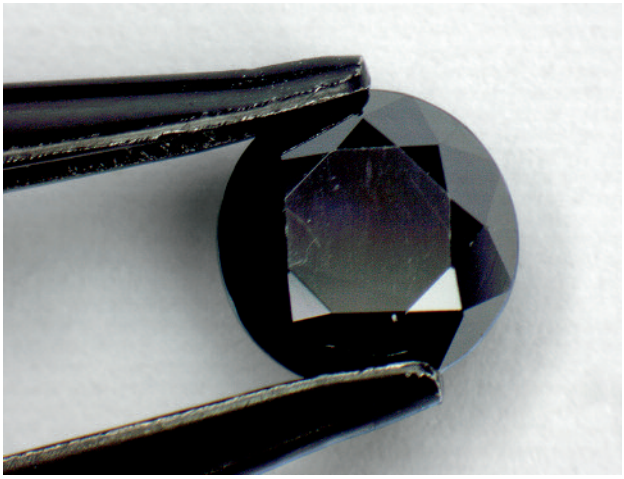

Figure 23. This 2.03 ct semitranslucent black stone is a cassiterite. Photo by I. Gaievskyi.

Black cassiterite. Black gemstones tend to be rarely encountered and are often somewhat difficult to identify. The State Gemological Centre of Ukraine recently examined a black 2.03 ct round brilliant (figure 23). The semitranslucent stone had an adamantine luster, and with strong fiber-optic illumination the stone appeared yellowish brown. It had a very high SG of 7, refractive indices that were above the limit of a standard refractometer, and was inert to both long- and short-wave UV radiation. The sample's observed pleochroism was weak, and its anisotropic optic character was evident from the doubling of facets when viewed through an immersion microscope with a polariscope. Unusual flow lines were also seen with the microscope (figure 24).

Most of these properties are consistent with cassiterite (M. O'Donoghue, Ed., *Gems*, 6th ed., Butterworth-Heinemann, Oxford, UK, 2006, p. 395). Energy-dispersive X-ray fluorescence (EDXRF) analysis detected major amounts of Sn as well as traces of Fe and Cu, confirming the cassiterite identification.

Figure 24. The cassiterite exhibited unusual flow lines. Photomicrograph by I. Iemelianov; magnified 22×.

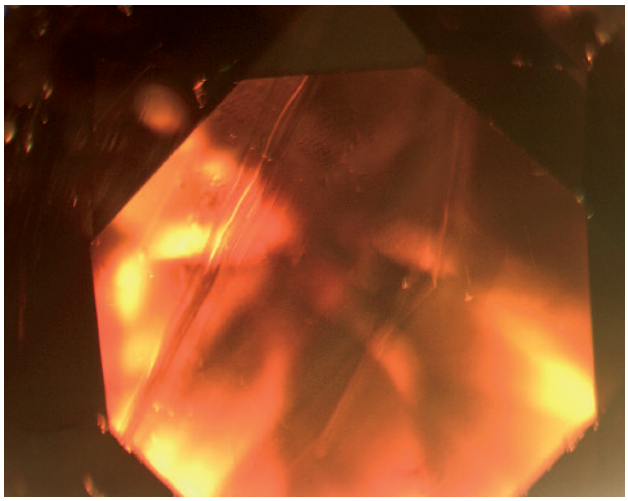

Cassiterite is rarely encountered as a gemstone. Faceted light brownish yellow material from Bolivia was described in the Summer 2002 GNI section (pp. 175–176), but this is the first time that we are aware of black cassiterite being faceted. A very dark brown (nearly black) cassiterite cabochon with imitation asterism was described by S. F. McClure and J. I. Koivula ("A new method for imitating asterism," Summer 2001 *G&G*, pp. 124–128).

Iurii Gaievskyi (gaevsky@hotmail.com) and Igor Iemelianov
State Gemological Centre of Ukraine, Kiev

Diopside from Kenya. While gem-quality diopside is not uncommon, it is usually seen as a transparent green or opaque black star gem. Given that, it was surprising when a parcel of transparent colorless to yellow gems submitted for examination by Dudley Blauwet (Dudley Blauwet Gems, Louisville, Colorado) proved to be diopside. He reported that the rough material came from Kajiado, Kenya, which is located 63 km south of Nairobi. He obtained 71 grams of rough in June 2009, from which he has cut 146 clean stones weighing 49.36 carats.

Gemological properties of the stones Mr. Blauwet submitted to the GIA (figure 25) were within the expected range for diopside, with average RIs of 1.666–1.696 and biaxial optic figures. The SG of the samples, measured hydrostatically,

Figure 25. This colorless to light yellow diopside (0.58–1.12 ct faceted, 0.50–0.73 g rough) is from Kajiado, Kenya. Photo by Robert Weldon.

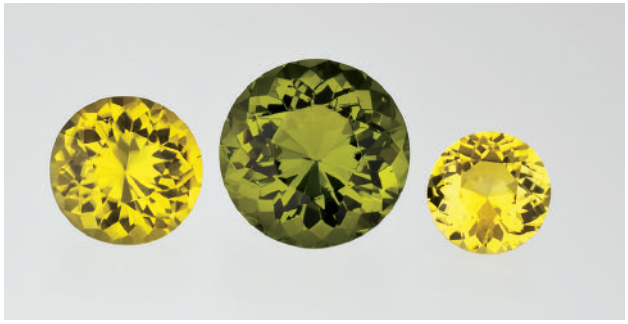

Figure 26. Dark yellow and yellowish green diopside (here, 0.83–2.94 ct) is also known from the Kajiado locality. Photo by Robert Weldon.

was between 3.27 and 3.46. Interestingly, the colorless material fell to the low side of this range, and SG values increased proportionally with the saturation of yellow color. Raman analysis provided confirmation that the stones were diopside.

Microscopic examination revealed numerous small needles and low-relief birefringent crystals (too small and deep in the stones for Raman analysis) but the material appeared fairly clean to the unaided eye. Notably, the colorless samples fluoresced a strong chalky greenish yellow to short-wave UV radiation and were inert to long-wave UV, while the most intensely yellow-colored diopside was inert to both long- and short-wave UV. Therefore, the fluorescence strength of the samples was inversely proportional to their color saturation.

To determine the cause of color, we performed visible spectroscopy and chemical analysis. A yellow sample showed a prominent 450 nm feature along with a weak sideband at 430 nm. The spectrum of a colorless sample was nearly featureless except for a very weak 450 nm feature.

Figure 27. Emeralds are being mined at Mingora, Pakistan, from tunnels such as this one. Photo by A. Lucas.

Chemical analysis revealed significantly more iron in the most saturated yellow diopside (≥2300 ppmw) than in the colorless sample (~600 ppmw). Minor traces of known chromophores Cr (~20 ppmw) and V (~2 ppmw) were also detected in both the colorless and yellow samples, but absorption features associated with them could not be clearly resolved, indicating that these two elements had little impact on the coloration. Instead, Fe^{3+} appears to be responsible for the color (R. G. Burns, *Mineralogical Applications of Crystal Field Theory*, 2nd ed., Cambridge University Press, 1993, p. 225). The difference in chemical composition may explain the diminished short-wave UV fluorescence of the relatively high-iron yellow samples, as iron is well known to quench fluorescence.

At the 2011 and 2012 Tucson gem shows, Jim Walker (Bridges Tsavorite, Tucson, Arizona) also had yellow to yellowish green samples of diopside from the same locality (figure 26). He reported that the material was a byproduct from a blue marble mine that also produces vesuvianite, grossular, and low-quality blue and black spinel. Diopside from this area has been known since 2010 ("Diopside finds niche in gem world," *Jewellery News Asia*, No. 314, October, pp. 38, 40).

Nathan Renfro and Andy H. Shen
GIA, Carlsbad

Emerald mining in Mingora, Pakistan. Rarely does a producing gem mine occur within a city, much less in a location where you can almost drive up to the entrance from a city street. That is the case in Mingora, the main municipality in the Swat Valley of Pakistan's Khyber Pakhtunkhwa Province. The Mingora emerald mine, visited by this contributor in October 2011, lies on a hill overlooking the city and the Swat River.

Emerald has been mined at this site since 1958 (see, e.g., E. J. Gübelin, "Gemstones of Pakistan: Emerald, ruby, and spinel," Fall 1982 *G&G*, pp. 123–139). The property covers nearly 74 hectares, 23 of which are believed to be emerald bearing. Mineralization is hosted by talc-carbonate schist, and the miners follow veins of quartz or calcite to find the emeralds. The finer-color material is reportedly associated with calcite veins.

Three operations were being worked concurrently; two of them were ramp-style tunnels (e.g., figure 27), while the third was a 6-m-deep shaft that branched out into underground galleries (figure 28). Personnel entered and exited the shaft on a wooden ladder, and the galleries were supported by timbers. The miners used only pneumatic jackhammers, picks, and shovels, as there were no explosives or mechanized equipment. Generally, one miner in each tunnel would use a jackhammer while the others helped break up the schist with hand tools. The schist was removed from the tunnels by either a windlass or a wheelbarrow, and then taken to a processing area. There, the schist was placed in piles, one for each tunnel. One worker would load the material on a wire screen while another sprayed it with water and a third sifted for emerald rough. The emeralds were placed in a locked box monitored by a guard.

The Mingora mine reportedly produced 2 kg of emerald rough in 2010. In October 2011, however, the mine was producing ~400 g of rough per month (e.g., figure 29). According to the management, the value of the material ranges from 500 to 10,000 Pakistani rupees (US$5.50 to $110) per carat. Approximately 35% of the production is facet-quality, in pieces weighing 0.2–0.6 g. Most of the production is sold to local dealers. Miners currently receive about 10,000 rupees per month, and the payroll also includes a number of security personnel armed with AK-47 rifles.

This contributor also visited several gem and mineral dealers in Mingora. Many of them also sold antiques, jewelry, carpets, handicrafts, and textiles. Although their gem inventory was limited, a wide range of material could be found, including synthetics (ruby and sapphire), imitations (glass and triplets), and treated stones (glass-filled rubies); all were straightforward to identify with a loupe. Emerald rough was available only in lower-quality parcels. As is often the case in mining areas, the asking prices were high.

The people of Swat, including those in the gem trade, were exceedingly friendly and glad to see a foreigner interested in their land and their culture. Many suffered greatly under Taliban rule and during the resulting conflict. They are eager for outsiders to visit this beautiful land, which has been called the "Switzerland of Central Asia."

Andy Lucas

Figure 28. The mine manager at the Mingora emerald deposit climbs down the shaft to inspect production. The hand-powered windlass behind him is used for moving equipment and mined material in and out of the shaft. A pneumatic jackhammer is used to break up the emerald-bearing schist (see inset). Photos by A. Lucas.

Dark yellowish green enstatite from Kenya. Enstatite ($MgSiO_3$) is a normally colorless end member of the pyroxene solid-solution (enstatite-ferrosilite) series. It displays color when additional elements, such as Fe and Cr, substitute for Mg. Gem-quality green specimens are rare, and have been reported from Arizona, East Africa, and Pakistan (G. R. Crowningshield, "Enstenite!" [*sic*], Fall 1965 *G&G*, pp. 334–335; C. M. Stockton and D. V. Manson, "Peridot from Tanzania," Summer 1983 *G&G*, pp. 103–107; Fall 2009 GNI, p. 219). In September 2011, GIA received some dark green gem material, represented as enstatite from Kenya, from gem dealer Dudley Blauwet. He obtained 62 grams of rough from his regular East African supplier, and has cut 66 stones totaling 55 carats. His supplier indicated that the material was mined in late 2010 from Maktau, in the Taita Hills of southern Kenya, near Tsavo National Park. Mr. Blauwet noted that the etched appearance of the crystals was typical of (brown) enstatite from East Africa.

Mr. Blauwet supplied six faceted (0.54–6.75 ct; figure 30) and 14 rough pieces to GIA for examination. They were dark

Figure 29. Emeralds from Mingora typically consist of hexagonal prisms (0.2–0.6 g) that show good color saturation. Photo by A. Lucas.

Figure 30. These enstatites, reportedly from Kenya, range from 0.54 to 6.75 ct. Photo by Robert Weldon.

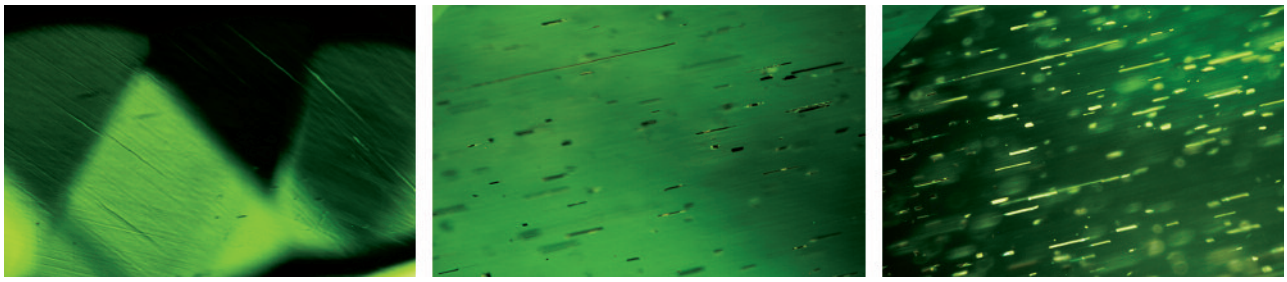

Figure 31. Colorless growth tubes were common in the enstatite (left, magnified 50×). Same samples had growth tubes that were filled with brown needles (center, magnified 105×) that appeared highly reflective in certain directions (right, magnified 85×). Photomicrographs by K. S. Moe.

yellowish green, and showed moderate to strong pleochroism in light to dark yellowish green. The refractive indices were 1.663–1.671 and the SG, determined hydrostatically, was 3.26. Both of these properties are within the range expected for enstatite, and Raman spectroscopy confirmed this identification. All of the samples were inert to both long- and short-wave UV radiation. Microscopic examination revealed numerous parallel, transparent growth tubes (figure 31, left). A few two-phase (solid-gas) and three-phase (solid-liquid-gas) inclusions were found among the growth tubes. Interestingly, many samples had needles trapped inside the growth tubes. The needles were dark brown and appeared highly reflective when viewed in certain directions (figure 31, center and right). Planar color banding (possibly related to polysynthetic twinning) was observed in a few samples (figure 32). One hazy-looking stone did not contain any internal features except for a roiled structure.

Qualitative EDXRF analysis detected Fe, Ca, Cr, Zn, Al, Ni, and Ga, in addition to the main components Mg and Si. A high-resolution visible-NIR spectrum showed a broad transmission window at ~550 nm that was responsible for the samples' yellowish green color. Small broad bands at 506 and 680 were caused by Fe^{2+} and Cr^{3+}, respectively. Infrared spectroscopy showed OH-stretching bands (i.e. hydrous defects) in the 3600–3000 cm^{-1} range.

Figure 32. Planar color banding, possibly related to polysynthetic twinning, was observed in a few enstatite samples. Photomicrograph by K. S. Moe; magnified 72×.

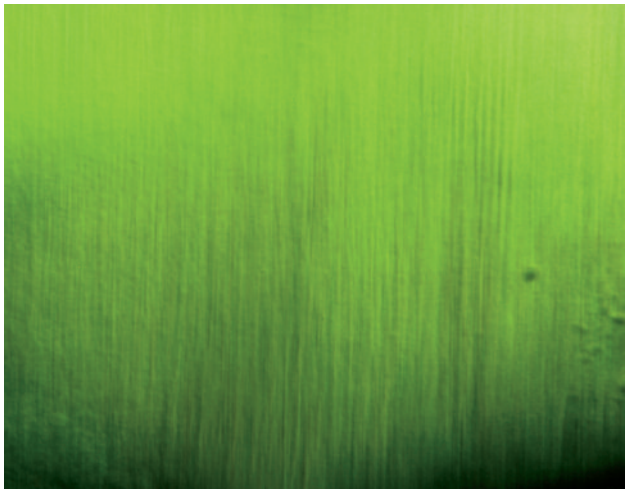

Enstatite has Raman doublet bands at 685–663 cm^{-1} (Si-O-Si stretching) and 1033–1014 cm^{-1} (Si-O stretching) that reflect the proportions of Mg^{2+}, Fe^{2+}, and Ca^{2+} (A. Wang et al., "Characterization and comparison of structural and compositional features of planetary quadrilateral pyroxenes by Raman spectroscopy," *American Mineralogist*, Vol. 86, 2001, pp. 760–806). The samples' relatively high Raman shifts (>660 cm^{-1} for the first doublet) suggested a higher proportion of Mg^{2+} than both Fe^{2+} and Ca^{2+}. Analysis of the Raman spectra—marked by the presence of a 236 cm^{-1} band (slightly shifted to 238 cm^{-1}) and the absence of 431 and 369 cm^{-1} bands—suggests that these samples are the polymorph orthoenstatite (P. Ulmer and R. Stalder, "The Mg(Fe)SiO_3 orthoenstatite-clinoenstatite transitions at high pressures and temperatures determined by Raman-spectroscopy on quenched samples," *American Mineralogist*, Vol. 86, 2001, pp. 1267–1274). Spectra and additional photomicrographs are available in the *G&G* Data Depository at gia.edu/gandg.

Kyaw Soe Moe (kmoe@gia.edu) and Nathan Renfro
GIA, New York and Carlsbad

New gem discoveries in Ethiopia. Ethiopia is well known for its opals, particularly those discovered in early 2008 in Wollo Province (see, e.g., B. Rondeau et al., "Play-of-color opal from Wegel Tena, Wollo Province, Ethiopia," Summer 2010 *G&G*, pp. 90–105). Other gems reported from Ethiopia include peridot (Spring 1993 Gem News, p. 59), fluorite (Summer 2007 GNI, pp. 168–169), and pyrope-almandine (Summer 2005 GNI, p. 177).

From late 2010 to early 2012, gem dealer Farooq Hashmi (Intimate Gems, Glen Cove, New York) documented several additional gems during buying trips to this little-explored country. In addition to sapphire and zircon (Fall 2011 GNI, pp. 247–248), he encountered emerald, aquamarine, morganite, tourmaline, apatite, pyrope, and phenakite (figure 33). Emerald and morganite from Ethiopia will be described in future reports, and notes on the other gems are provided here.

The **aquamarine** reportedly is mined from a remote area ~30 km from Shakiso in southern Ethiopia. Granitic pegmatites in this area have been worked by hand tools near the surface,

Figure 33. Several gems have recently been produced from Ethiopia. From top to bottom, these include aquamarine (6.50 and 7.85 ct), tourmaline (3.36 ct), apatite (4.98 ct), pyrope (2.01 ct), and phenakite (0.61 ct). All stones were cut by Hassan Z. Hamza (Noble Gems Enterprises, Dar es Salaam, Tanzania) for this report. Photo by Robert Weldon.

and have also yielded rock crystal, tourmaline, and beryl of various colors besides aquamarine. On Mr. Hashmi's first trip to Ethiopia, several hundred kilograms of blue-to-green aquamarine were available in the capital city of Addis Ababa, although only 5–10 kg were of gem quality. More good-quality rough appeared at the October 2011 Munich mineral show, and Mr. Hashmi learned on his latest trip that nearly 1,000 kg of semi-gem aquamarine had recently been produced. He indicated that multiple mining areas are active; one deposit that he visited consisted of an eroded mountainside with a large exposed pegmatite.

Tourmaline is also apparently being mined from multiple deposits in Ethiopia. Dark blue-to-green material is produced from the pegmatites in the Shakiso area, and Mr. Hashmi also obtained a single piece of lighter bluish green tourmaline (represented to him as sapphire) from an unspecified alluvial deposit. Several kilograms of the Shakiso crystals were available during his initial buying trip in relatively small sizes (<2 g). By 2012, tourmaline output had increased considerably, with new mining areas producing larger clean sizes (up to 10 g) in pink and blue-green colors. Electron microprobe analyses by two of the authors (WBS and AUF) of a 0.91 ct faceted dark blue tourmaline from Mr. Hashmi showed it to be elbaite with 2.30 wt.% MnO and 0.52 wt.% FeO. It had an unusual trace-element composition, containing 0.29 wt.% PbO, 0.07 wt.% ZnO, 0.04 wt.% V_2O_3, and 0.02 wt.% Cr_2O_3.

Greenish yellow **apatite** was available in transparent pieces as large as 20 g during Mr. Hashmi's 2010 trip, and the next year he saw rough parcels totaling several kilograms. According to Seid Abdella (RV Gems, Addis Ababa), the material comes from two localities near Aroresa in the Siddama area of southern Ethiopia.

Orangy red **pyrope** comes from the Borana area of southern Ethiopia. Since late 2010, Mr. Hashmi has encountered ~20 kg of material weighing up to 5–6 g apiece. Similar pyrope-almandine was described in the Summer 2005 GNI entry mentioned above from Hagare Mariam in the southern part of the country.

The source of **phenakite** in Ethiopia was not disclosed by Mr. Hashmi's supplier, who at the time thought the rough material was diamond. The supplier offered several hundred grams of colorless broken fragments ranging up to several grams apiece.

The recent discovery of so many gem materials in Ethiopia suggests interesting possibilities for future finds.

Brendan M. Laurs

William B. ("Skip") Simmons and Alexander U. Falster
University of New Orleans, Louisiana

Burmese spessartine. In March 2010, Hussain Rezayee (Rare Gems & Minerals, Beverly Hills, California) informed GIA about a new find of spessartine in Myanmar (Burma). He indicated that small quantities have been inconsistently produced from a gold mining area since early 2010, in clean pieces weighing up to 4 g. The color ranges from bright orange to dark brownish red, and attractive faceted stones weighing 20+ ct have been cut.

Mr. Rezayee loaned a 6.66 ct reddish orange gem for examination (figure 34). The gemological properties of this cushion mixed cut were: RI—over the limits of the standard refractometer; hydrostatic SG—4.22; fluorescence—inert to both long- and short-wave UV radiation; and absorption features consisting of a 440 nm cutoff (due to Mn^{2+}), a weak 520 nm line (Fe^{2+}), and weak bands at 570, 615, and 690 nm (Fe^{2+}) seen

Figure 34. This 6.66 ct reddish orange spessartine is reportedly from Myanmar. Photo by Robert Weldon.

Figure 35. Microscopic observation of the spessartine revealed whitish irregularly shaped corroded inclusions. Photomicrograph by HyeJin Jang-Green; field of view 3.0 mm.

with the desk-model spectroscope. Visible-NIR absorption spectra collected with an Ocean Optics e-scope showed the same features, as well as a very weak absorption at 495 nm (Mn^{2+}). Microscopic examination revealed small fluid "fingerprints," numerous whitish irregularly shaped corroded inclusions (figure 35), and pronounced straight and angular growth zoning.

EDXRF spectroscopy showed major Mn, moderate Fe, and traces of Ca. Based on its absorption spectrum and chemical composition, this reddish orange garnet is spessartine with a significant almandine component.

Editor's note: Consistent with its mission, GIA has a vital role in conducting research, characterizing gems, and gaining knowledge that leads to the determination of gemstone origins. The sample studied in this report is not subject to the Tom Lantos Block Burmese JADE Act of 2008, and its import was in accordance with U.S. law.

HyeJin Jang-Green (hjanggre@gia.edu)
GIA, New York

SYNTHETICS AND SIMULANTS

Enameled jewels in the Chinese market. With the jewelry market booming in China, a variety of new materials are being used in jewelry, including enamels, ceramics, plastics, and composites. Enamels consist mainly of mixtures of quartz, feldspar, borax, and fluorite. Traditional enameled copper jewelry, called *jingtailan* (cloisonné), dates back hundreds of years. These relatively inexpensive ornaments are popular for their beautiful color and luster.

TABLE 1. Chemical composition of the Chinese enamels.[a]

Sample no.	Color	Elements
1	Green	Si, K, **Cr,** Cu, **Pb**, Sb
2	Blue	Si, K, Ti, Mn, Cu, **Pb**
3	Black	Si, K, Mn, Fe, Cu, **Pb**

[a] *Potentially hazardous elements are shown in bold font.*

Figure 36. These pieces of enameled silver (1.7 cm in diameter) contained potentially hazardous traces of Pb (as well as Cr in the green sample). Photo by Y. Zhang.

In December 2011, the National Gemstone Testing Center (NGTC) lab received a donation for research of three pieces of enameled silver (figure 36) that were reportedly representative of new material for use in fashion jewelry. The pieces measured 1.7 cm in diameter and weighed 2.02–2.18 g. The enamels were blue, green, and black, and had spot RIs ranging from 1.57 to 1.58. Microscopic examination revealed numerous air bubbles in the enamel portions (e.g., figure 37). The bubbles were typically round and ranged from a few microns to ~200 microns in diameter.

To investigate the internal structure of the enamels, one of them (black sample) was broken apart. The piece was found to consist of three parts (figure 38): a top enamel layer (0.5–1 mm), the central silver layer (0.3–1 mm), and a bottom enamel layer (0.05–0.1 mm).

EDXRF chemical analysis of the enamels (table 1) showed major amounts of Si and K in all three samples. The minor elements varied depending on the enamel's color. It should be noted that the toxic element Pb was detected in all three

Figure 37. Magnification of the enamels revealed an abundance of air bubbles. Photomicrograph by Y. Zhang.

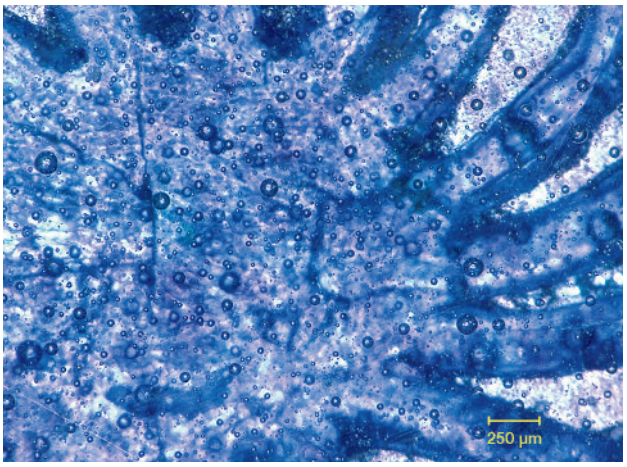

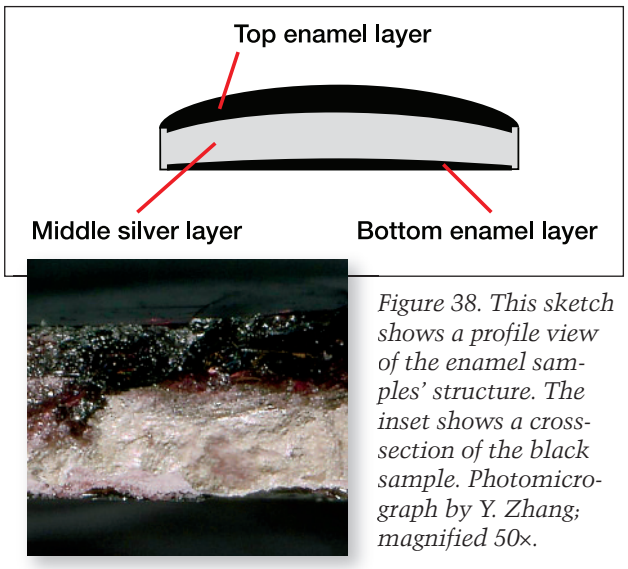

Figure 38. This sketch shows a profile view of the enamel samples' structure. The inset shows a cross-section of the black sample. Photomicrograph by Y. Zhang; magnified 50×.

samples, and the green piece also contained Cr. Both elements were present in amounts that exceeded their allowed concentrations of 0.1% defined by the Chinese national standard (Jewellery - Fineness of Precious Metal Alloys and Designation, GB 11887-2008, November 1, 2009, 12 pp.). The presence of Pb and Cr in this jewelry could be hazardous to the wearer's health, so testing the safety of such enamels is paramount.

As the Chinese jewelry market grows and new materials are used in jewelry, NGTC will continue to monitor these developments and protect consumers.

Yong Zhang (zyongbj@126.com), Taijin Lu, Hua Chen, and Yan Lan

National Gems & Jewelry Technology Administrative Center, Beijing

Geikielite from Sri Lanka with fake star effect. While on a buying trip to Ratnapura, Sri Lanka, in October 2010, one of these contributors (TP) purchased what was represented as a rutile cabochon with an artificial 11-ray star (figure 39). The process of engraving or scratching cabochons to produce asterism has already been well documented (S. F. McClure and J. I. Koivula, "A new method for imitating asterism," Summer 2001 *G&G*, pp. 124–128; K. Schmetzer and M. P. Steinbach, "Fake asterism—two examples," *Journal of Gemmology*, Vol. 28, No. 1, 2002, pp. 41–42). However this stone appeared fully opaque under strong fiber-optic light, which is unusual for rutile. Also, its specific gravity (4.12) and strong attraction to a neodymium magnet were not consistent with rutile, so we decided to investigate further.

Chemical analysis by energy-dispersive spectroscopy on a JEOL 5800LV scanning electron microscope gave the following composition (in element %): Ti = 18.97, Mg = 15.09, Fe = 6.46, and O = 59.49. This composition is consistent with ferroan geikielite, the Mg-rich member of the ilmenite group, with 70% geikielite and 30% ilmenite *sensu stricto*. Geikielite was first discovered in the Ratnapura area in 1892, so it is no wonder that this interesting piece was sold in Sri Lanka, with the added curiosity of a fake star. To the best of our knowledge, this is the first occurrence of geikielite as a gem.

Thierry Pradat (tpradat@gems-plus.com)
G-Plus, Lyon, France

Benjamin Rondeau
Laboratoire de Planétologie et Géodynamique
CNRS 6112, University of Nantes, France

Jean-Pierre Gauthier
Centre de Recherches Gemmologiques, Nantes, France

TREATMENTS

A dyed blue opal with play-of-color. Since the discovery of opal from Ethiopia's Wollo Province in 2008, large quantities of this material have entered the marketplace, at a much lower price than the Australian counterpart. Until September 2011, most were white or light yellow, with strong play-of-color. Due to the abundance of this material, gem laboratories have expected to see treated versions in a variety of colors.

The Gem Testing Laboratory of Jaipur, India, recently received an unusual blue opal for identification (figure 40). The sample weighed 0.45 ct and measured 7.00 × 5.08 × 1.84 mm. It appeared to be opal, but its unusual color and striking play-of-color raised doubt regarding its authenticity. Microscopic observation with fiber-optic lighting revealed a cellular play-of-color (or "digit pattern") with grayish cloudy interstitial areas, features indicative of Wollo opal (see B. Rondeau et al., "Play-of-color opal from Wegel Tena, Wollo Province, Ethiopia," Summer 2010 *G&G*, pp. 90–105).

Although the cellular structure identified this as natural (not synthetic) opal, we doubted that the blue bodycolor was

Figure 39. This 2.21 ct cabochon, represented as rutile with an imitation 11-ray star, proved to be geikielite. Photo by J.-P. Gauthier.

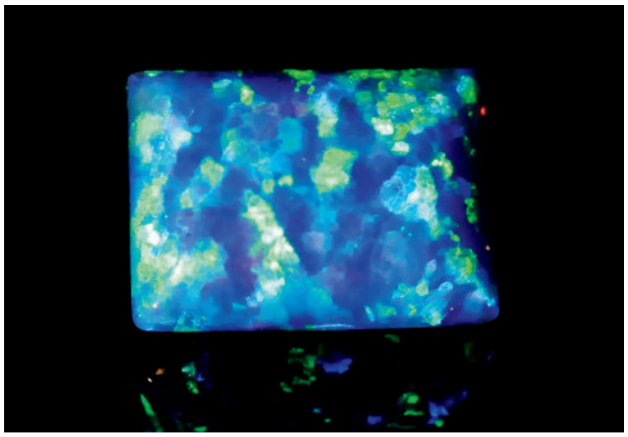

Figure 40. This 0.45 ct blue opal with striking play-of-color proved to be dyed. Besides its color, the sample's gemological properties were consistent with opal from Wollo, Ethiopia. Photo by G. Choudhary.

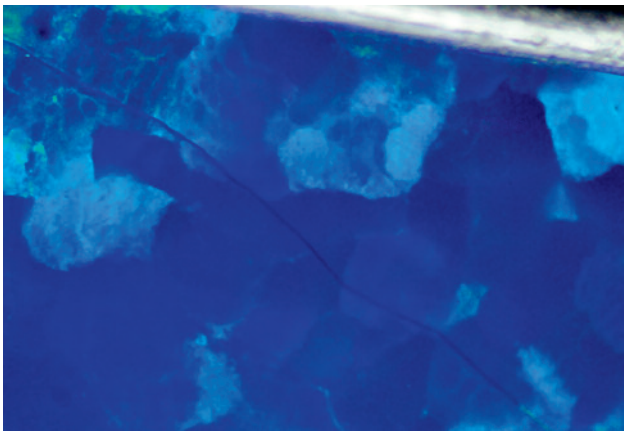

Figure 41. The opal in figure 40 displayed blue color concentrations along a surface break, indicating dye treatment. Photomicrograph by G. Choudhary; magnified 64×.

also natural. Careful gemological testing proved useful in determining the cause of color. The sample had a spot RI of approximately 1.45 and a hydrostatic SG of 1.76; no signs of porosity were seen while taking the SG reading. It displayed strong red UV fluorescence (both long- and short-wave). With the desk-model spectroscope, three distinct bands were seen at ~540, 580, and 650 nm. This absorption pattern, associated with cobalt, is often seen in dyed blue materials. The opal displayed a strong red reaction to the Chelsea filter, confirming the presence of a blue dye.

The opal was once again observed with the microscope to locate any signs of color concentrations. This time, we noted a surface break with blue color concentrations along its length (figure 41). On the basis of microscopic observations and gemological properties, the sample was identified as a dyed opal.

A dyed green-blue opal showing play-of-color was recently documented along with dyed purple material that originated from Wollo Province (N. Renfro and S. F. McClure, "Dyed purple hydrophane opal," Winter 2011 *G&G*, pp. 260–270), and treated black Wollo opals also have been reported (see C. Williams and B. Williams, "Smoke treatment in Wollo opal," www.stonegrouplabs.com/SmokeTreatmentinWolloOpal.pdf). We can expect to see other treated colors of Ethiopian opals in the future.

Gagan Choudhary (gagan@gjepcindia.com)
Gem Testing Laboratory, Jaipur, India

CONFERENCE REPORTS

Mines to Market conference. On November 2–3, 2011, the Gem and Jewelry Export Promotion Council of India hosted the first-ever International Colored Gemstone Mines to Market Conference in Jaipur. **Yianni Melas** (Limassol, Cyprus), who brought together the international group of speakers, served as master of ceremonies. The presentations covered a wide range of topics in the colored stone industry, from the miner to the retail point of sale, and brief summaries of some of them are provided here.

The keynote speaker was **Alberto Milani** (Buccellati, New York), who indicated that the perception among many wealthy consumers in the U.S. and Europe is that the quality of luxury products is declining. He pointed out that the luxury market is rapidly splitting into two tiers, high-end and entry-level. To expand their market, luxury companies must emphasize quality to keep their brand positioned, provide excellent customer service, and keep their message direct and simple.

Ian Harebottle (Gemfields, London) demonstrated how larger gem producers can make significant contributions toward social responsibility and improving the image of the industry. He also stressed that if the supply chain rested solely on artisanal mining, it would be difficult to create a constant supply of colored stones to fuel future growth. **Robert Weldon** (GIA, Carlsbad) gave a multimedia presentation that followed the production of ametrine from the mine to the jewelry marketplace. The methodology developed by mine owner Ramiro Rivero can serve as a sustainability model for small-to-medium scale miners and manufacturers, and includes environmentally friendly mining practices and a working environment that promotes innovation in cutting design and jewelry manufacturing.

Richard Hughes (Sino Resources Mining Corp., Hong Kong) gave a multimedia presentation on ruby and sapphire deposits. He emphasized the romance of the colored stone industry, the exotic sources of these rare gems, and the effort and passion involved in bringing them to the market. **Dr. Federico Pezzotta** (Natural History Museum of Milan, Italy) relayed the importance of Madagascar in supplying the trade with blue sapphires and rubies when other sources had limited production, as well as the nation's abundant potential for producing a wide variety of gem materials in coming decades. **Edward Boehm** (RareSource, Chattanooga, Tennessee) discussed how ruby sources have evolved over the last decade with the depletion of the Mong Hsu deposit and discovery of new localities in Tanzania and Mozambique.

Federico Bärlocher (Yangon, Myanmar) spoke on the past and future of Myanmar's gem deposits, including Mogok ruby, and presented a short video called "Myanmar the Ruby Land." He noted that there are half a million people living in Mogok, "involved only in looking for ruby, sapphire, and spinel, and everyone living only for gems."

Glenn Lehrer (Lehrer Designs, Larkspur, California) described how gem carving takes several times longer than faceting and that the main time consuming factor is the final polish of carved areas, especially channels and other tight areas. **Shaltiel Cohen** (Zamrot, Jerusalem) presented a video of an Israeli cutting system that incorporates the speed of jam-peg cutting with the precision of a vertical mast faceting machine.

Nirupa Bhatt (GIA India, Mumbai) spoke on the importance of education and how the future of the gem industry depends on the training of today. GIA India is working with the Indian industry to develop new education models that cooperate with the industry to reach students and provide the skills they will need to succeed. **This contributor** focused on the disclosure—or in many cases the lack thereof—of major treatments. He advocated that full disclosure be given to the consumer including a clear description of the treatment, how it affects the appearance and durability of the stone, and any special care and cleaning considerations, rather than using simplified trade-oriented terminology.

Steve Bennett (GemsTV, Worcestershire, U.K.) stressed how focus groups and surveys regarding gem-buying preferences often show more about how consumers feel about themselves and their desire to be perceived, rather than how they actually make decisions. **Dr. Chuck Lein** (Stuller, Lafayette, Louisiana), who spoke on being "jeweler to the jewelers," revealed that the average turnover of stock for independent retail jewelers in the U.S. was only 0.7 times annually.

At the close of the conference, GJEPC chairman **Rajiv Jain** made some astute observations on issues the colored stone industry needs to address to grow and prosper. These included developing a mine-to-market strategy similar to that of the diamond trade, securing production of rough material and improving cutting techniques, and increasing colored stones' share in the luxury market.

Andy Lucas

Gem-A Conference 2011. The annual Gem-A Conference took place November 6 in London. Highlights of some of the presentations offering new information are given here.

Brian Jackson (National Museums Scotland, Edinburgh) reviewed optical phenomena in gems. He described how heat—even the low heat from your hand—can cause some fluorites to emit light.

Willy Bieri (GemResearch Swisslab, Bangkok) spoke on distinguishing untreated Tibetan copper-bearing andesine from its diffusion-treated counterpart using advanced analytical methods. Scanning electron microscopy (SEM-EDX) can be used to detect up to 40 different elements and compounds in andesine, including native copper, copper oxides, naturally melted glass, silver, and gold. He also described how isotope testing and laser ablation–inductively coupled plasma–mass spectrometry (LA-ICP-MS) can be used to prove whether the color is natural, diffusion-treated, or of undeterminable origin. Due to expense and potential for damage, Mr. Bieri noted, advanced testing is only practical on random samples from a parcel.

Steve Bennett (Gems TV, Worcestershire, U.K.) pointed out that his company's television shopping network, which offers 90 gems in 540 varieties from 60 countries, far outsells their online retail division. Mr. Bennett affirmed his belief in selling the dream rather than the product, avoiding information overload, and upholding the mystique and folklore of gems and jewelry.

Branko Deljanin (Canadian Gemological Laboratory, Vancouver) overviewed the screening and identification of enhanced and synthetic diamonds in the market today. He discussed advanced testing equipment but added that some additional characteristics should be considered: the morphology of the rough, the detection of diamond type using crossed polarizers, and the fluorescence colors commonly displayed by natural diamonds (blue), HPHT synthetics (green to yellow), and CVD synthetics (brownish orange).

Alan Hart (Natural History Museum, London) spoke on evaluating and recreating the original Koh-i-Noor (Persian for "Mountain of Light") diamond. The motive to recut the diamond can be traced to the poor reception it received at the Great Exhibition in 1851. The gem was described as resembling a dull piece of glass, prompting *Punch* magazine to dub it the "Mountain of Darkness."

Douglas Kennedy (dkennedy@gia.edu)
GIA, Carlsbad

MISCELLANEOUS

Gem news from Myanmar. In mid- to late 2011, this contributor's lab in Taunggyi, Myanmar, received some interesting items for identification. Among these were smooth egg-shaped samples with a waterworn appearance that measured 7–8 cm long. They were typically green (also yellow and red) and contained large gas bubbles, making them easy to identify as glass.

A new deposit of blue kyanite has been found near Zayatkwin village in Thabeikkyin township (Mandalay division). Stones weighing 2–4 ct have been faceted, and they typically contain hollow tube inclusions. Some of the stones have been set into reasonably priced jewelry.

Cabochons of dark blue sapphire weighing 1–2 ct (e.g., figure 42) appeared in the market in 2011 from near Bawma village (north of Kyatpyin in the Mogok area), which recently became known for producing orangy red to purplish red spinel (e.g., Summer 2010 GNI, p. 154). The sapphires contain abundant partially healed fractures, groups of elongate solid crystals, irregular black crystals, twin planes (sometimes with associated white spike-like inclusions), thin films, small rutile needles in a single plane, unidirectional fluid inclusions, and uneven patches of greenish blue color zoning.

Figure 42. These sapphires are from a new find near Bawma village in the Mogok area of Myanmar. The cabochons weigh ~1–2 ct. Photo by U T. Hlaing.

In early 2012 this contributor learned of a new gem mining area in Karen State—in the headwaters of the Bilin River—that is the source of pink to red spinel, dark blue sapphire, and dark brownish red garnet. The rough gems show various amounts of rounding due to alluvial transport, and most pieces weigh ~0.4 g.

The mid-year session of the 2011 Myanma Jade, Gems & Pearl Emporium took place December 24, 2011–January 3, 2012 in Naypyidaw. More than 5,400 merchants attended the government-run sale, nearly a third of them foreigners. The emporium sold 8,290 of the 11,821 jade lots offered, as well as 39 of the 230 gem lots and 212 of the 270 cultured pearl lots. An official who spoke to the *Myanmar Times* quoted total sales of US$903 million, much lower than the $2.9 billion recorded a year ago. Traders attributed the decline to China's 35% tax on gem imports from Myanmar, up from 10% last year, and its raising the minimum deposit on bids from 10,000 euros to 50,000 euros.

U Tin Hlaing
Dept. of Geology (retired)
Panglong University, Myanmar

ERRATUM

Figure 10 of the Winter 2011 phosphorescent diamond Lab Note (pp. 310–311) was redrafted incorrectly by *G&G*. A corrected version is shown below, which also includes error bars showing the standard deviation for each average value.

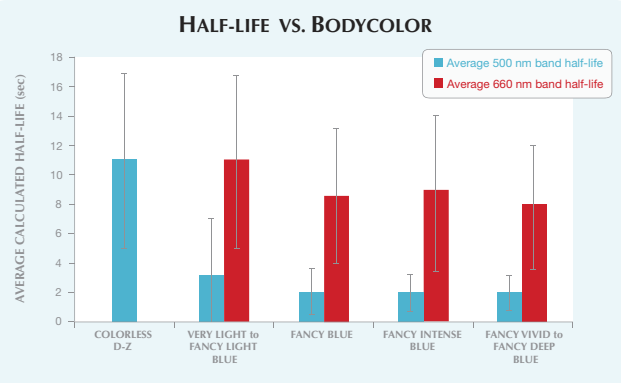

GEMS & GEMOLOGY®

HAS TURNED A NEW PAGE

Your trusted resource for the most reliable research on diamonds and colored stones is now available for iPad.

- Peer-reviewed research
- Groundbreaking discoveries
- Latest gem news
- Superb photography
- Interviews with industry experts, videos, slideshows, and much more...

GIA®

World Headquarters
The Robert Mouawad Campus
5345 Armada Drive
Carlsbad, CA 92008
www.gia.edu

Free iPad App Available Now!
LEARN MORE at gia.edu/gandg/ipad

Figure 1. Open-pit mining at Belmont is conducted on a large scale. Trucks are constantly being filled with ore to be taken to the processing plant. Photo by A. Lucas.

Brazil's Emerald Industry

Andy Lucas

Since the 1970s, Brazil has been a consistent source of emerald. This is especially true today, with steady production from the Itabira/Nova Era belt in the gem-rich state of Minas Gerais.

Along with successes there have been challenges for the Brazilian emerald industry. Increasingly strict environmental regulations and higher labor costs have made production more expensive. Mining companies have had disagreements with land owners, and there have been legal issues with the independent miners known as *garimpeiros*. Another challenging issue facing the mining, cutting, and trading sectors is the rapid rise of the Brazilian real against the U.S. dollar.

While Brazilian emeralds were not traditionally known for their quality, this perception has been changing. Stones from the Itabira/Nova Era belt reportedly sell for up to $30,000 per carat. Nova Era tends to produce clean faceted stones, which are highly popular with jewelry manufacturers. The emeralds' fine color and good transparency make this material highly sought after in the marketplace.

Belmont, Minas Gerais

The Belmont property was originally a cattle ranch and remains one today. But since 1978, Belmont has also operated a well-known emerald mine. It is managed by Marcelo Ribeiro, whose grandfather discovered emeralds on the ranch by accident. It began as an open-pit operation (figure 1). Bulldozers remove the weathered emerald-bearing material and transport it to a processing area for washing and sorting.

After two decades of open-pit mining, Belmont added underground operations in 1998. Miners were lowered into a 75 m vertical shaft, from which they dug side tunnels by hand or using explosives, removing the schist and bringing it back up the shaft.

An elevator carried five personnel as well as mined material in and out of the underground mine. During this contributor's visit to Belmont in 2004, the company estimated another 10–15 years of production remained in the open-pit mine. Now they believe the open-pit area may have a much longer life span.

Since 2004, Belmont has expanded the underground operation into a ramp-style underground mine where trucks drive directly into the workings. The emerald-bearing schist is broken up by explosives, and front loaders empty it onto trucks to be taken to the processing plant.

Optical sorting has replaced hand picking of the emeralds. These devices are faster and have a higher recovery rate, while eliminating the possibility of theft. The optical sorting instrument used by Belmont can be customized to identify a variety of minerals. A charge-coupled device (CCD) camera recognizes the emeralds in the schist by color, triggering an air blast that moves them to a conveyor belt (figure 2).

Belmont has processed 70,000 tonnes of ore annually for the last three years, recovering 250,000 grams of rough emerald per year. That works out to 1 g of emerald per 0.28 tonnes of processed ore. But to obtain the 70,000 tonnes of emerald-bearing ore, Belmont must first remove 350,000 tonnes of overburden. While the average production of emerald-bearing schist is 6,000 tonnes per month, the output is higher during the dry season and lower during the rainy season that runs from September through February. Eighty percent of the production is from open-pit mining, 20% from the underground operation. This is because Belmont's processing plant is designed primarily for the weathered material from the open-pit operation. The processing plant is being expanded to better handle the harder emerald-bearing schist. By the end of 2012, Belmont expects underground mining to account for half of the output.

On average, 1 g of rough emerald produces 1ct of faceted emerald, or 250,000 carats per year. The typical size range of the rough is 2–20 mm or 0.2–20 g. Belmont is known for high-quality rough that allows cutters to consistently produce calibrated 1–5 mm rounds, as well as 1–10 ct center stones for jewelry manufacturers.

The rough sorting facility is located in the nearby town of Itabira. Belmont sorts the rough for its manufacturing customers into 15 qualities and five different size ranges, for a total of 75 rough categories. About 80% of the rough sold by Belmont is cut in India.

The mine is currently undergoing expansion and will be adding another highly efficient optical sorter. The company is also expanding mining operations through a joint venture with former owners of the Rocha emerald mine, which borders Belmont to the north. Rocha opened in 2005 but closed after only a few years. The new joint venture is a 50/50 split between Belmont and the Rocha group, and Rocha has been renamed the Canaan mine, its original name. Discussions are ongoing between the mining partners

Figure 2. A conveyer belt brings ore into the optical sorter at Belmont for the CCD cameras to scan. Photo by Eric Welch.

Figure 3. Much of the production at Capoeirana is done by independent miners. The processing of the ore is accomplished by simple hand washing. Photo by A. Lucas.

and the land owner, who prefers the operation be an underground mine. Under Brazilian law a percentage of the production goes to the land owner, even when another company owns the mining rights. Belmont has opened a tunnel entrance into the Canaan mine that is currently 120 m long. Once it is 400 m long and 50 m deep, the drive-in tunnel will reach the mineralized zone, where core samples showed emerald-bearing rock. Belmont estimates that by July 2012 it will be removing the first trucks of emerald-bearing ore from Canaan for processing. Mr. Ribeiro expects a production rate comparable to that of the underground operation at Belmont, which is 3.5 to 4 g of emerald per tonne of ore. He believes the emeralds will be larger but have a lighter color due to lower chromium content.

Belmont's water reclamation system incorporates a five-pond system that uses filtering and gravity to remove particles introduced by mining and processing. With plans to increase underground mining, there will be less fine particle overburden to remove by washing, resulting in less need for water. The company expects its water reclamation to be even more efficient and less expensive at that point, minimizing the impact on the environment.

Belmont estimates the life of the mine according to the market price for emerald. If the price goes up 30%, the mine's life expectancy doubles. If the price drops 30%, the life of the mine is cut in half. At current prices, Mr. Ribeiro expects 20–30 more years of profitable operation unless the production rate increases significantly. Also contributing to the mine's life span is the fact that Belmont cuts some of its own rough, thus moving up the value chain and recording higher profits per tonne of ore mined. By earning more revenue per tonne, Belmont can afford to mine deeper underground.

They currently cut 25% of the production by value (10% by volume). All of their cutting is done close to the mine.

Capoeirana, Minas Gerais

Emeralds were discovered in the Capoeirana area of Nova Era in 1988. Here the extraction is done primarily by independent miners and smaller-scale operations. The emeralds can be of very good color and quality, surpassing those previously produced from Santa Terezinha de Goiás.

In 2004, this contributor saw considerable activity by independent miners in pits, tunnels, and shafts. The work was very labor intensive. The miners used some explosives but mostly hammers, picks, and shovels. They would load the ore in wheelbarrows, take it to a washing area, and dump a barrel of water over it. The miners would then use hammers to break up some of the larger pieces of schist, shovel the ore onto a washing screen, and continue breaking the pieces with a hammer. They would then sort through the screen by hand to look for any schist that contained emerald crystals (figure 3).

One operation was somewhat mechanized: The miner was strapped to a cable and lowered by a winch into the mine and then brought back up with bags full of ore to be processed.

Figure 4. At Montebello, miners drill into the hard schist to prepare it for blasting. Photo by A. Lucas.

A 2009 visit to the Capoeirana area revealed that things had changed considerably since 2004. This time there were far fewer miners working, and the village itself seemed noticeably quieter—there were no dealers in the street, and nobody offered emerald crystals for sale. One reason given for the downturn was that the area's mines were becoming too deep for independent miners. Some of the shafts were reaching depths of 100 m, where it was difficult to work the hard rock using ladders and hand tools. Also, some of the underground workings were becoming very close to each other, and the thin walls between them increased the risk of cave-ins. The global economic recession also took its toll on the Capoeirana emerald miners, as it has on the entire Brazilian gem industry. Because emeralds are traded in the U.S. dollar and the Brazilian real has gained so dramatically against the dollar, it has become very difficult for these independent miners to make a living. Many have moved on to other areas where the deposits might be easier to work, while others have returned to agriculture. Companies such as Belmont were looking to purchase some of these properties so they could bring in a more sophisticated and profitable operation.

Mining at Capoeirana is done by a cooperative in which individual miners hold rights to sections of the deposit. The miners must be part of the cooperative, and they can only buy mining rights from individuals who have purchased theirs from the cooperative.

The Montebello mine, under the management of Sergio Martins (Stone World, São Paulo), is a small but fairly mechanized operation, especially for Capoeirana, where most of the mining is done by *garimpeiros*. Montebello is an underground mine where the miners drill into the mica schist (figure 4) and load the holes with explosives. Using various hand tools and shovels, they load carts with ore. The carts are pulled along tracks to take the ore to the elevator, where it is hauled up to the surface for processing. The mineralized zone is approximately 100 m wide and 300 m deep.

Processing at the Montebello mine is also more sophisticated than elsewhere in the Capoeirana area. After washing the ore through sluices, the workers put it on a sorting table and carefully look for emerald crystals in the schist.

In recent months, since the beginning of the more sophisticated small-scale operations such as Montebello, Capoeirana has turned out fine-quality material and faceted stones from 10 to 20 ct. Overall production figures are hard to estimate due to the degree of small-scale mining, but a low estimate for the last two years is 20 to 30 kg per month of facet-grade material, with fine-quality material accounting for at least 1 to 2 kg of the total. Emeralds from this area tend to be larger, and it is rare to find rough less than 1 g (e.g., figure 5). However, most of the crystals break during removal from the schist. Even the broken pieces can weigh 20–50 g, and rough fragments as large as 1 kg have been recovered. The higher-quality material is typically kept in Brazil for cutting, with the rest exported primarily to India.

Bahia

The state of Bahia produces approximately 500 to 1,000 kg of emerald each month, but the quality is usually lower than that of Itabira/Nova Era. While there are

Figure 5. Emerald crystals recovered from the schist at Capoeirana can be large. Photo by A. Lucas.

some fine-quality stones from Bahia, the vast majority are highly included. Most of the mining is done by *garimpeiros*, in the Carnaíba and Socotó areas.

Santa Terezinha de Goiás

Santa Terezinha in Goiás State was an important emerald-producing area from the 1970s through the 1990s, but the last decade has seen little production. One of the advantages of this area was that the emeralds were found by mining the deposit in a straight line. Because the emeralds were fairly evenly distributed, production was consistent and predictable. This is completely different from emerald mining in Itabira/Nova Era, where the gems are locally concentrated and output is more sporadic.

At Santa Terezinha, emeralds were found in talc-carbonate schist as opposed to Nova Era's harder mica schist. This made extraction of the emerald crystals easier.

Cutting and Trading

Brazil's emerald production goes to both domestic cutters and foreign buyers who take the rough back to cutting centers in their own countries. Companies from Jaipur, India, are able to buy entire mine productions because their cutting facilities can handle all sizes and qualities of emerald, and they have a market for the entire range of goods. This gives them a considerable advantage, allowing them to offer a good price for the entire production. Brazilian cutters have higher labor costs, so they must gear their operations toward the product they can sell for a price that absorbs these costs. Rather than purchasing the entire mine production, they must buy a pick of the mine production—and pay a higher price for it. They have become adept at paying just enough to make it enticing for the miners to sell them the better quality and sizes, while staying competitive in the global market. Brazilian cutters have found a niche in fine-quality calibrated goods that are enticing to manufacturers worldwide (figure 6). This enables them to hit a profitable price point, and they can also cut larger, good-quality emeralds.

The Future

There are substantial challenges facing the Brazilian emerald industry. Stricter environmental regulations increase the cost of mining and make future finds less likely. The cost of labor is constantly rising, making it necessary to invest in technology. As the Brazilian real grows stronger against the dollar, the revenue that can be realized is declining while costs are increasing. Yet the potential for emerald production from the Itabira/Nova Era belt remains extremely promising. These deposits may very well warrant the investment needed for exploitation.

With advanced mining technology, plus high-end domestic cutting generating greater revenue and moving mining companies up the value chain, the future of the Brazilian emerald industry looks very encouraging.

Andy Lucas (alucas@gia.edu) is the gemology product manager for GIA Education in Carlsbad.

Figure 6. The wholesale emerald trade in Brazil is quite active. Businesses such as Sergio Martins' Stone World (shown here in his former office at Teofilo Otoni) enjoy a thriving international and domestic market. Photo by A. Lucas.

The Book Reviews and Gemological Abstracts sections appear in the online version of the journal. Below are the titles of the books and articles reviewed, with the reviewer's name indicated in brackets. These sections are freely available on the *G&G* website (gia.edu/gandg) and as part of *G&G* Online (gia.metapress.com), and are paginated separately from the rest of the issue.

Book Reviews

Set in Style: The Jewelry of Van Cleef & Arpels. By Sarah D. Coffi, 2011 [*Delphine Leblanc*]

Paul Flato: Jeweler to the Stars. By Elizabeth Irvine Bray, 2010 [*Delphine Leblanc*]

Collector's Guide to the Beryl Group. By Robert J. Lauf, 2011 [*Michael T. Evans*]

Diamond Inclusions. By Nizam Peters, 2011 [*Nathan Renfro*]

Gemological Abstracts

COLORED STONES AND ORGANIC MATERIALS

Copal vs. amber. By M. C. Pedersen and B. Williams [*Michele Kelley**]

Genesi e classificazione dei diaspri (II parte) [Formation and classification of jasper. Part II]. By M. C. Venuti [*Rolf Tatje**]

Genesi della agate (I parte) [Formation of agate. Part I]. By M. C. Venuti [*Rolf Tatje**]

Getting a feel for organics. By M. C. Pedersen [*Michele Kelley**]

Luminescence of gem opals: a review of intrinsic and extrinsic emission. By E. Gaillou et al. [*Annette Buckley**]

DIAMONDS

Diamond crystals and their mineral inclusions from the Lynx kimberlite dyke complex, central Quebec. By A. D. van Rythoven et al. [*James E. Shigley**]

Peculiarities of diamond from the commercial deposits of Russia. By G. Y. Kriulina et al. [*Kyaw Soe Moe**]

Phosphorescence in type IIb diamonds. By S. Eaton-Magaña and R. Lu [*Guy Lalous**]

GEM LOCALITIES

Alexandrite and colour-change chrysoberyl from the Lake Manyara alexandrite-emerald deposit in northern Tanzania. By K. Schmetzer and A.-R. Malsy [*Edward R. Blomgren**]

Chemical and growth zoning in trapiche tourmaline from Zambia – a re-evaluation. By K. Schmetzer et al. [*Edward R. Blomgren**]

INSTRUMENTS AND TECHNIQUES

Detection and analysis of diamond fingerprinting feature and its application. By X. Li et al. [*Edward R. Blomgren**]

Jade detection and analysis based on optical coherence tomography images. By S. Chang et al. [*Guy Lalous**]

JEWELRY HISTORY

I vaghi di collana in pietra nella storia [Gemstone beads through history]. By M. C. Venuti et al. [*Rolf Tatje**]

JEWELRY RETAILING

Training helps sales force to sparkle. By D. Pollitt [*Russell Shor**]

SYNTHETICS AND SIMULANTS

And now composite chalcedony. By G. Choudhary [*Michele Kelley**]

Characterization of a new synthetic fancy yellow diamond. By V. Rolandi et al. [*Jennifer Stone-Sundberg**]

TREATMENTS

Diffusion of chromium in sapphire: The effects of electron beam irradiation. By Y.-K. Ahn [*Guy Lalous**]

MISCELLANEOUS

Uplifting the Earth: The ethical performance of luxury jewelry brands. By I. Doyle and J. Bendell [*Alexandra Martini*]

* *Member of the Gemological Abstracts Review Board*

In Memoriam: George Bosshart (1943–2012)

The gemological community mourns the passing of George Bosshart, who died January 14 after a long battle with cancer. Mr. Bosshart was one of the world's leading experts on diamond identification and the geographic origin of colored stones.

With a degree in mineralogy from the Swiss Federal Institute of Technology in Zurich, he conducted mineral analysis for Alcan (Aluminum Company of Canada) in the early 1970s. After completing gemological studies at GIA's Santa Monica campus, he became the first director of the SSEF (Swiss Foundation for the Research of Gemstones) laboratory in 1975. In 1992 he joined the Gübelin Gem Lab, where for many years he served as chief gemologist.

Mr. Bosshart was an important contributor to *G&G*. He coauthored the Fall 2000 *G&G* article "GE POL Diamonds: Before and After," which won second place in the journal's Most Valuable Article Awards. Another article he coauthored, "Gem Localities of the 1990s," received third place that same year. He also wrote an article on a cobalt glass imitation of lapis (Winter 1983) and took part in studies of Burmese jadeite (Spring 2000), the historic Star of the South diamond (Spring 2002), serendibite from Sri Lanka (Spring 2002), and poudretteite from Mogok, Myanmar (Spring 2003).

After retiring in 2004, Mr. Bosshart remained active in gemology, traveling to remote localities around the world. His speaking engagements included GIA's 2006 Gemological Research Conference and, most recently, the 2011 International Gemmological Conference. George Bosshart is survived by his wife, Anne.

G&G Online
Book Reviews

EDITORS
Susan B. Johnson
Jana E. Miyahira-Smith

Set in Style: The Jewelry of Van Cleef & Arpels

By Sarah D. Coffin, with contributions by Suzy Menkes and Ruth Peltason, 288 pp., illus., publ. by the Smithsonian Cooper-Hewitt National Design Museum [www.cooperhewitt.org], New York, 2011, $55.00.

After marriage united two families of Dutch jewelers, Van Cleef & Arpels established its first shop on Paris's famed Place Vendôme in 1906. This marked the beginning of what was to become a jewelry brand of international renown. In collaboration with the jeweler, the Smithsonian Cooper-Hewitt National Design Museum in New York exhibited 350 of Van Cleef & Arpels's most striking pieces from February to July 2011. Most of the objects were chosen from the famed Van Cleef & Arpels Collection, although the selection criteria were not disclosed. Others were loaned by private collectors, some anonymous and some world-famous—including Princess Grace of Monaco and Elizabeth Taylor—which added to the appeal of this distinguished showing. For those who did not view the exhibit, this book offers a worthy substitute.

Like the exhibit, the book is organized thematically rather than chronologically. Its 400 illustrations include photos, archival advertisements, original color sketches of jewelry, and select shots of socialites and movie stars wearing Van Cleef & Arpels. Of the six chapters, "Innovation" provides most of the narrative on the company's signature pieces, including invisible settings, minaudières, zipper necklaces, and Art Deco and "Ludo" bracelets. The "Transformations" chapter features elements from original owners (gems or antique carvings) that were reconfigured in new jewelry pieces. One of the best examples is the Aga Khan emerald and diamond choker necklace with pendant, which incorporates 18th century Indian carved emeralds. Another iconic piece is an antique turquoise Chinese carved snuff bottle recycled as a table clock. Transformation also refers to the remarkably practical Van Cleef & Arpels pieces that can be converted from a necklace into two bracelets. While Daisy Fellowes's emerald bead and diamond manchette bracelets offer prime examples of this characteristic, several others are shown as well.

The chapter titled "Nature as Inspiration" highlights magnificent floral and animal motifs. "Exoticism" starts with the Egyptian revival in the 1920s, a decade that also saw a strong Chinese influence manifested in multigem cases, "necessaires," and occasional objects. Van Cleef & Arpels jewelry was also influenced by wealthy Indian patrons, and many pieces with Indian motifs appeared throughout the 1930s and during a revival in the 1970s. The late 1950s and 1960s show a Siamese influence resulting from commissions by Queen Sirikit of Thailand.

The chapter titled "Fashion and Van Cleef & Arpels" is perhaps misleading: One might expect to see jewelry as it was worn with the corresponding fashion of the day. Instead, these pages highlight pieces with a textural quality in their design, such as the "Serge fabric necklace" mimicking the texture of an obliquely woven wool fabric traditionally used in men's fashion and costumes. Another example is the "lace bow brooch," which imitates the fineness and softness of draped lace. Could one surmise that Van Cleef & Arpels's perspective of eternal beauty rises above fashion trends? The last chapter, written by Ruth Peltason, provides a comprehensive notation of Van Cleef & Arpels jewelry owned by celebrities and royalty.

One distinguishing feature of the book is its use of color renderings, which clearly show the vision behind the jewelry designs. Amid the secrecy of the Place Vendôme, it is quite extraordinary that the sketches were published with the jewelry's serial numbers and the names of customers. The jewelry photos are from different sources, however, with varying quality and rendering. They are displayed with different (unspecified) magnifications, making it difficult to get a sense of scale. Jewelry measurements and carat weight are not noted, either. One could conclude that this book serves as more of a coffee-table edition than a museum catalog, which would have included thumbnail photos, detailed descriptions, and measurements.

That said, the book is required reading for gem and jewelry experts to familiarize themselves with the exclusive Van Cleef & Arpels brand and its most special items. It is a fitting tribute to the inspiration, creativity in design, and craftsmanship of one of the world's most elite jewelry houses.

DELPHINE A. LEBLANC
Hoboken, New Jersey

Paul Flato: Jeweler to the Stars

By Elizabeth Irvine Bray, 223 pp., illus., publ. by the Antique Collectors' Club [www.antiquecollectorsclub.com], Woodbridge, Suffolk, UK, 2010, US$85.00.

With this remarkable oversized book, Elizabeth Irvine Bray offers a unique insight into Paul Flato, an American master in jewelry design who has gained renewed popularity over the last decade. In a long life of dizzying

highs and lows, Flato never lost his hope or his passion for jewelry design. He continued to produce inspired pieces in a vast array of materials until the end of his life.

Equal parts jet-setter and trendsetter, the flamboyant Texan was destined to live the high life. He was born in 1900, and a childhood encounter with a gypsy craftsman sparked his fascination with jewelry. In the early 1920s Flato settled in New York and soon became a member of the café society, where he cultivated his diamond brokerage. While he had a reputation for being able to attract a wealthy clientele, mainly women, he often failed to collect payments and amassed considerable debt.

In other ways, though, he displayed business savvy and foresight. For instance, he quickly built an impressive natural pearl collection at a time when they were becoming rare. He set up a store on One East 57th Street and collaborated with Harry Winston on some major sales during the 1930s. At that time, Winston was a high-end dealer without retail space, ironically. He commissioned Flato to sell the Jonker, a 140 ct emerald cut, one of the largest diamonds at the time.

In 1935, Flato branched out from diamond dealing into designing and manufacturing his own pieces. His style is characterized by a rare combination of three-dimensional, whimsical, and realistic qualities. Some of his favorites were floral, hand, shoe, heart, and star motifs. He generated publicity through advertising and creative co-branding endeavors. One was a special Elizabeth Arden nail polish and lipstick limited edition called "Pink Diamond." He subsequently catered to a fashionable clientele of debutantes, socialites, and actresses.

Helped by a French draftsman named Adolphe Klety, Flato designed his own pieces. He assembled a remarkably talented team. Staff member and socialite Millicent Rogers Balcom provided creative input for a heart brooch collection and helped attract a clientele of affluent heiresses. Josephine Forrestal, a former *Vogue* fashion editor, was brought on to capture more of the elite class. He briefly employed the legendary Fulco de Verdura, who had just arrived in the United States.

After the Depression, Flato ventured out to the West Coast. Fascinated by leading ladies and the fledgling motion picture industry, he was the first jeweler ever credited in a movie. For the romantic comedy *Holiday* (1938), actresses Doris Nolan and Katharine Hepburn wore his splendid adornments. Following this auspicious debut, he opened a store on Sunset Boulevard.

Flato then experienced a string of setbacks, including a $200,000 theft at his Sunset Boulevard store, America's declaration of war in December 1941, and the loss of a consigned 17 ct emerald-cut diamond at his New York store. The uncertain state of his finances led him to desperate measures that resulted in a conviction for grand larceny. He served 18 months in Sing Sing prison starting in December 1943.

Flato's parole ended in 1947, allowing him to reopen for business as a maker of affordable gold and gem compacts designed for a "working girl" clientele. At the same time, he was designing luxury pens for Parker. Susceptible to less-than-scrupulous dealings, he fell under the spell of a fortune teller who led him back into financial trouble. He managed to escape criminal conviction by fleeing to Central America before he was finally captured. After serving time in a Mexican prison, he returned to Sing Sing.

In 1970, he opened his last jewelry store, in Mexico City's affluent Zona Rosa neighborhood. There he designed gold and silver jewelry in his signature style, while incorporating Mayan influences and adapting to the 1970s and 1980s fashions. By that time, Flato had learned to be his own draftsman and would sketch for his customers before having the pieces manufactured by local craftsmen. (Out of respect for them, he signed pieces only upon customer request.) Emeralds, Mexican opals, and lapis lazuli were his gems of choice. The book's final chapter, "Flato's Legacy," recounts the jeweler's return to prominence through a Christie's auction before his death in 1999.

This detailed biography retraces Flato's life and works, shedding a candid light on his accomplishments and his undoings. Illustrations are a strong point of the book, lavishly displaying magnificent jewelry pieces, though very little information is included. Most evocative are the photos of celebrities wearing Flato's iconic pieces, rekindling a "classic Hollywood glamour" and showing how brooches and other pieces were actually worn, sometimes in the most flamboyant way. The book is a must-have for jewelry historians who want to know all about Flato and 1930s style.

DELPHINE A. LEBLANC

Collector's Guide to the Beryl Group

By Robert J. Lauf, 93 pp., illus., publ. by Schiffer Publishing Ltd. [www.schifferbooks.com], Atglen, PA, 2011, $19.99.

This book, volume 11 in the Schiffer Earth Science Monograph series, focuses on the small but very important beryl group. The introduction gives a general history of beryl, its mining, and general uses. This is followed by a gemology section with simple definitions of the gem varieties, causes of color, treatments, and synthetic growth.

The "Taxonomy" section presents beryl's crystal structure, morphology, and chemical composition (in relation to color). The accepted species (bazzite, beryl, indialite, pezzottaite, and stoppaniite) and their formulas are provided. The crystal structure of beryl appears in colorful diagrams; another diagram of Cs-rich beryl looking down the c-axis shows the positions of Cs^{+} ions lying within the

channels formed by silicate rings. There are also some diagrams of beryl crystals from Goldschmidt's *Atlas Der Krystallforen*. The chromophores, and in some instances the color centers, that make this group so colorful are discussed.

Beryl in igneous rocks, metamorphic rocks, alteration, and pseudomorphs are the subtopics of "Formation and Geochemistry." Famous LCT (lithium, cesium, and tantalum) pegmatites like those of Brazil, Pakistan, Afghanistan, California, and New England are covered. The vanadium-colored emeralds of Dyakou, China, forming in quartz and pegmatite veins are cited. The author also describes the unusual Sakavalana pegmatite in Madagascar, a mixture of some characteristics of both LCT and NYF (niobium, yttrium, and fluorine) pegmatites, home of the recently described species pezzottaite. Topaz rhyolites of the western United States and Mexico are the host rock of the beryl variety bixbite (red beryl), whose formation is briefly covered. Emerald deposits of Colombia, Austria, Russia, Zambia, and Zimbabwe are presented as examples of beryl in metamorphic and metamorphic-hydrothermal deposits. Paralava, a high-temperature metamorphic rock heated by naturally burning coal seams, is the host of indialite, whose unique formation is described as well. The alteration of beryl to kaolinite and the replacement of beryl by epididymite and milarite are briefly mentioned under "Alteration and Pseudomorphs." Also named are a few other species that are associated with beryl alteration.

The last section, "The Minerals," is the heart of the book, where all the group's species are covered individually. Of these, beryl itself is given the greatest attention. Common beryl, emerald, aquamarine, heliodor, morganite, goshenite, and bixbite varieties are featured, as are their inclusions, etching, and surface features.

The Collector's Guide to the Beryl Group is intended more for mineral collectors than for gemologists or geologists. The gemological description of the beryl group is quite brief, with an overemphasis on trapiche emerald and synthetic beryl growth. It should have included some description of the green color (hue, tone, saturation) required for a stone to be designated as emerald. And while the use of colorless oil to hide cracks in emerald is considered acceptable in the trade, especially compared to the use of green fillers to enhance color, it is still a treatment that should be fully disclosed. Meanwhile, figure 15 shows a heliodor crystal described as "yellowish green." Shouldn't it be classified as green beryl since green is the dominant hue? In the taxonomy chapter and elsewhere, the use of a z-axis instead of a c-axis could cause some confusion.

The book's greatest strengths lies in the many color photos of the various beryl-group species and varieties from important international localities (except San Diego County, California) showing various forms and associated species. The photos of inclusions in beryl and of etched beryl specimens add further interest. If you collect beryl and perhaps the other members of the group, then this book has just the right amount of technical information to deepen your appreciation of your treasured specimens, while serving as a helpful reference in recognizing a sample's identity and locale.

MICHAEL T. EVANS
Gemological Institute of America
Carlsbad, California

OTHER BOOKS RECEIVED

Diamond Inclusions. *By Nizam Peters, 208 pp., illus., publ. by American Institute of Diamond Cutting Inc. [diamondschool.com], Deerfield Beach, FL, 2011, $135.00.* Although the title of this book implies that it will address inclusions in diamonds or the occurrence of diamond inclusions in other gems, those hungry for technical explanations of diamond inclusions may not be satisfied. For basic explanations of common clarity characteristics seen in diamonds, it is satisfactory. Overall, the content serves as a reference for basic diamond inclusions. Its photos show a variety of surface and internal features commonly seen in rough and finished diamonds. For a more comprehensive work on diamond grading, interested parties may want to consult Gary Roskin's *Photo Masters for Diamond Grading.* For a more technical and scientific resource on inclusions in diamonds, readers may prefer *The MicroWorld of Diamonds* by John I. Koivula.

NATHAN RENFRO
Gemological Institute of America
Carlsbad, California

EDITOR

Brendan M. Laurs
GIA, Carlsbad

REVIEW BOARD

Edward R. Blomgren
Asheville, North Carolina

Annette Buckley
Austin, Texas

Jo Ellen Cole
Vista, California

R. A. Howie
Royal Holloway, University of London

Edward Johnson
GIA, London

Michele Kelley
Monmouth Beach, New Jersey

Guy Lalous
Academy for Mineralogy, Antwerp, Belgium

Kyaw Soe Moe
GIA, New York

Keith A. Mychaluk
Calgary, Alberta, Canada

Joshua Sheby
New York, New York

James E. Shigley
GIA, Carlsbad

Russell Shor
GIA, Carlsbad

Jennifer Stone-Sundberg
Portland, Oregon

Rolf Tatje
Duisburg, Germany

Dennis A. Zwigart
State College, Pennsylvania

COLORED STONES AND ORGANIC MATERIALS

Copal vs. amber. M. C. Pedersen [maggiecp@btinternet.com] and B. Williams, *Gems & Jewellery*, Vol. 20, No. 2, 2011, pp. 20–24.

Correctly identifying copal and amber can be difficult, as standard gemological tests are not very useful for resins. In addition, the treatments they may undergo are complex and numerous. Understanding the differences between these resins, as well as their treatments, is vital to ensuring proper disclosure. In this article, the characteristics of natural/treated amber and copal are reported from gemological tests specific to organics, as well as more advanced FTIR, Raman, and cross-polarized filter testing. A discussion of the results helps provide insight as to which tests can correctly identify an unknown specimen and any possible treatments. *MK*

Genesi e classificazione dei diaspri (II parte) [Formation and classification of jasper (Part II)]. M. C. Venuti, *Rivista Gemmologica Italiana*, Vol. 5, No. 2, 2010, pp. 133–158 [in Italian].

Today's nomenclature of jasper is a motley collection of varietal and trade names rather than a well-ordered classification system. The author proposes a classification based on formation, surroundings, and processes. He distinguishes four types: *Oceanic jasper* (formed by organic sedimentation), *volcanic jasper* (silicification of volcanic rocks), *pseudomorphous jasper* (silicification after fossils), and *chemical jasper* (chemical precipitation from silicic solutions and gels). For all four types, various sequences of formation are described. Generally, they include different mechanisms of silica concentration, from single molecules resolved in aqueous solution to the crystallization of jasper (in most cases including opal as a transitional stage). As formation conditions can vary widely and the pro-

This section is designed to provide as complete a record as practical of the recent literature on gems and gemology. Articles are selected for abstracting solely at the discretion of the section editors and their abstractors, and space limitations may require that we include only those articles that we feel will be of greatest interest to our readership.

Requests for reprints of articles abstracted must be addressed to the author or publisher of the original material.

The abstractor of each article is identified by his or her initials at the end of each abstract. Guest abstractors are identified by their full names. Opinions expressed in an abstract belong to the abstractor and in no way reflect the position of Gems & Gemology *or GIA.*

© 2012 Gemological Institute of America

cesses (especially hydration and dehydration) can be repeated or reversed several times, jaspers accordingly show many different patterns and colors. *RT*

Genesi della agate (I parte) [Formation of agate (Part I)]. M. C. Venuti, *Rivista Gemmologica Italiana*, Vol. 5, No. 3, 2010, pp. 213–225 [in Italian].

The diversity of agates makes their classification difficult. The author's investigations reveal four types of layers that comprise all agates. The first type is a clear chalcedony layer that forms the outer part of every specimen. It is always the first layer to form, and is generally transparent and nonbanded, with a spherulitic texture. It can be as thin as 1 mm or fill the entire cavity. Only within this layer do features develop such as moss, plumes, and dendrites. The second type consists of the banded layers characteristic of agates. They can be concentric, parallel ("Uruguay type"), or hemispherical. The third type is rare and forms white, often interrupted horizontal bands or massive parts of the agate. The fourth consists of macrocrystalline quartz, sometimes amethyst. While the clear chalcedony layer always occurs, but only once, the other layers may form consecutively or simultaneously and be repeated several times in the same agate. *RT*

Getting a feel for organics. M. C. Pedersen [maggiecp@btinternet.com], *Gems & Jewellery*, Vol. 19, No. 3, 2010, pp. 14–15.

Organic gems and their imitations have been around for countless years, and this article explains how general observations and common sense can help in the identification process. While sight is the sense most often relied upon, touch, smell, and sound can also be helpful as long as there is some basic knowledge of organic gems. Provenance can also help distinguish some organic gems. Yet the author cautions that there will be times when more sophisticated testing or a gemological laboratory may be required for conclusive identification. *MK*

Luminescence of gem opals: A review of intrinsic and extrinsic emission. E. Gaillou, E. Fritsch, and F. Massuyeau, *Australian Gemmologist*, Vol. 24, No. 8, 2011, pp. 200–201.

Not all opals display luminescence, but when they do their emission colors are typically green or a chalky white to blue. Rarer orange emission is restricted to opal with a pink bodycolor. The researchers examined 20 strongly luminescent opals from a range of localities using a Fluorolog 3 spectrofluorometer to determine the cause(s) of their luminescence.

Blue emission resulted from "the nano-structured nature of silica in opal, offering abundant surface with dangling bonds." Green emission, often seen in common opal, was related to extrinsic uranium impurities, and specimens exhibited emission bands characteristic of the "uranyl group in a phosphate environment." Orange emission was caused by quinones, or "fossil organic molecules" that are absorbed into phyllosilicate inclusions in the opal.

For all three types of luminescence, concentrations of iron ranging from 1000 to 2000 ppm will suppress emissions. Furthermore, all three basic emissions have the capacity to mix in different proportions and subsequently exhibit various combined colors. *AB*

DIAMONDS

Diamond crystals and their mineral inclusions from the Lynx kimberlite dyke complex, central Quebec. A. D. van Rythoven, T. E. McCandless, D. J. Schulze, A. Bellis, L. A. Taylor, and Y. Liu, *Canadian Mineralogist*, Vol. 49, No. 3, 2011, pp. 691–706.

The Lynx kimberlite is located in the Otish Mountains of central Quebec, within 2 km of the Renard kimberlite cluster. Yet diamonds from these two deposits differ in physical characteristics, mineral inclusions, and geologic ages. Test sampling of ~500 tons of Lynx kimberlite ore yielded nearly 6,600 macrodiamonds. A 22 ct pale brown octahedron is the largest crystal found to date in the province. There were two main diamond morphologies, with 41% being octahedra and the remainder being partially resorbed tetrahexahedra. Typical colors include brown, gray, and colorless. Cathodoluminescence imaging of flat plates cut from 20 crystals revealed various patterns of deformation and resorption, as well as oscillatory growth zoning. Primary mineral inclusions consisted of olivine, Cr-diopside, Cr-pyrope, orthopyroxene, omphacite, and sulfide minerals. Data obtained from these inclusions suggest the diamonds formed at a depth of 180–190 km in the lithospheric mantle. *JES*

Peculiarities of diamond from the commercial deposits of Russia. G. Y. Kriulina [galinadiamond@gmail.com], V. K. Garanin, A. Y. Rotman, and O. E. Koval'chuk, *Moscow University Geology Bulletin*, Vol. 66, No. 3, pp. 171–183.

This comprehensive article presents morphological and spectroscopic characteristics of more than 12,000 diamond crystals from several Russian deposits in the Arkhangelsk diamond province (ADP) and the Yakutia diamond province (YDP). Most had type I morphology according to Orlov's classification. Dodecahedral crystals were dominant in the ADP, while octahedral crystals were more common in the YDP. A rhombic-dodecahedral habit characterized diamonds from the Lomonosov deposit (ADP). The Zolotitskoe field and the Grib pipe (both ADP) had a higher percentage of cubic crystals. About half of the diamonds from the ADP were structurally homogenous, featuring a single growth habit. Some crystals from Lomonosov showed multiple growth habits, trending from

octahedral to cubic to fibrous; the opposite trend was observed in diamonds from the YDP.

Many rounded dodecahedral crystals from the Karpinsky-1 pipe and the Zolotitskoe field showed oxidizing dissolution traces, indicating their formation in saline fluids. However, crystals from the Grib pipe showed poorly developed resorption features with negative trigons, and reflect a less oxidative diamond-forming environment. Large crystals with numerous deep cavities were prevalent in the Snegurochka, Kol'tsovskaya, and Pervomaiskaya pipes.

Diamonds from the Arkhangelskaya, Karpinsky-1, and Karpinsky-2 pipes exhibited yellow and yellow-green luminescence. Most crystals from the Lomonosov, Pionerskaya, and Grib pipes and from the Mirninskoe field displayed unevenly distributed blue and violet luminescence. Some Mirninskoe diamonds also showed green luminescence with a pink peripheral zone. Most samples from the Nakyn field and the Botuobinskaya pipe exhibited violet luminescence. A small percentage of diamonds from the Jubileynaya (Yubileinaya) and Komsomolskaya pipes showed pink luminescence, while very few showed orange. The authors also observed a relationship between crystal habit and luminescence. For example, octahedrons from the Mir pipe tended to have pink luminescence while dodecahedrons fluoresced blue; for crystals that combined these two habits, the luminescence was yellow-green.

Electron paramagnetic resonance (EPR) spectroscopy revealed that diamonds from Internationalnaya, Lomonosov, and Pionerskaya possess similar paramagnetic centers—mainly P1, resulting from single-substituted nitrogen atoms. The P2 center, which is related to aggregated nitrogen atoms, was observed in most of the Grib diamonds. The N2 center, related to plastic deformation, was abundant in Grib diamonds but absent from the Pomorskaya samples. The M2 center, also related to plastic deformation, was found in pink-violet diamonds from the Internationalnaya pipe. Nickel-related paramagnetic centers such as NE1, NE2, and M1 were detected only in diamonds from Jubileynaya.

Based on their IR spectra, the YDP diamonds contained higher concentrations of nitrogen B-aggregates than those from the ADP. The Lomonosov and Grib diamonds were rich in hydrogen and platelets but contained fewer nitrogen aggregates. Samples from Pomorskaya, Karpinsky-1, and Arkhangelskaya had the highest concentrations of nitrogen A-aggregates (1,200, 1,100, and 950 ppm, respectively). The hydrogen, platelet, and B-aggregate concentrations in stones from the Mir pipe were similar to those from Internationalnaya and Butuobinskaya. Diamonds from the Komsomolskaya pipe contained A-aggregates with strong platelet bands but very weak or nonexistent hydrogen bands. The strongest platelet and hydrogen bands were observed in Jubileynaya crystals.

KSM

Phosphorescence in type IIb diamonds. S. Eaton-Magaña [smagana@gia.edu] and R. Lu, *Diamond and Related Materials*, Vol. 20, No. 7, 2011, pp. 983–989, http://dx.doi.org/10.1016/j.diamond.2011.05.007.

Phosphorescence spectroscopy was performed on 354 type IIb and seven type IIa diamonds, along with 24 HPHT-treated diamonds and 18 HPHT-grown synthetics. The phosphorescence in type IIb diamonds is due to a donor (most likely nitrogen) and acceptor (boron) pair recombination. In this mechanism, holes bound to acceptors and electrons bound to donors recombine and emit light with an energy corresponding to the difference between the energies of the isolated donor and acceptor, plus an electrostatic correction.

The only phosphorescence bands observed in the natural diamonds were centered at 500 and 660 nm. The relative intensity and half-life of these measured bands corresponded well to their boron concentration. None of the treated or synthetic diamonds showed the 660 nm band. However, these samples did have the 500 nm band, with a much higher intensity in the synthetics. The phosphorescence spectra were correlated to data collected from infrared absorption and photoluminescence spectroscopy, and these results provide additional evidence for the mechanism responsible for the observed phosphorescence.

GL

GEM LOCALITIES

Alexandrite and colour-change chrysoberyl from the Lake Manyara alexandrite–emerald deposit in northern Tanzania. K. Schmetzer [schmetzerkarl@hotmail.com] and A.-R. Malsy, *Journal of Gemmology*, Vol. 32, No. 5–8, 2011, pp. 179–209.

Trace amounts of Cr are the principal cause of the green color in emerald and the color change in alexandrite; Cr often predominates over V by a factor of five. Both gems require the simultaneous presence of Be and Cr for their formation, and it is not uncommon for them to occur in proximity to one another (but not in contact).

In the Lake Manyara mining area, emeralds are associated with pegmatitic intrusions and alexandrite crystals are found in adjacent phlogopite-bearing schist that formed from the metasomatism of mafic or ultramafic rocks by the pegmatites. This metamorphic-metasomatic geologic setting is similar to that found in the alexandrite-emerald belt of the Russian Urals and Novello, Zimbabwe. Due to overlapping concentrations, contents of Cr, V, and Fe in these gems should not be considered distinctive criteria for source determination.

Lake Manyara alexandrite shows enormous variability in morphology, including the presence of single crystals and a wide range of twins (e.g., contact, penetration, and cyclic twins, called *trillings*) developed in two major habits: one tabular parallel to the *a* pinacoid, the other

columnar along the a-axis. Dozens of color photomicrographs and schematic drawings illustrate not only these external morphologies but also their corresponding growth structures in both reflected and transmitted light. Numerous inclusions are discussed, including phlogopite, apatite, and zircon (surrounded by tension cracks), as well as partially healed fractures with residual fluid inclusions and two-phase inclusions within negative crystals. Milky white zones were caused by channels running parallel to the a-axis, occasionally in combination with negative crystals along the *a* plane.

The complexity of alexandrite's color-change phenomenon was studied in relation to colorimetric issues using the CIELAB color circle. The color changes observed in alexandrite and color-change chrysoberyl—and what distinguishes them from one another—are controversial and of great interest to the trade. They are extremely variable and relate directly to Cr contents and the orientation of the table facet with respect to the crystallographic axes. *ERB*

Chemical and growth zoning in trapiche tourmaline from Zambia – A re-evaluation. K. Schmetzer [schmetzerkarl@hotmail.com], H.-J. Bernhardt, and T. Hainschwang, *Journal of Gemmology*, Vol. 32, No. 5–8, 2011, pp. 151–173.

In the last several years, tourmaline has been added to the short list of trapiche minerals, the most commonly known being emerald from Colombia and ruby from Mong Hsu, Myanmar. When slices of Zambian trapiche tourmaline are cut perpendicular to the c-axis, two different patterns can result—a three-rayed fixed star with three transparent sectors between the rays, or (most commonly) a three-rayed pattern in the center of the slice surrounded by six transparent sectors, with six boundaries between the center and the rim and between the six sectors of the rim.

The complex chemical and structural trapiche pattern is consistent with the formation of tourmaline crystals in a two-step process: the skeletal growth of Na-rich dravite in the first phase and subsequent layer-by-layer growth of a second tourmaline generation beginning with Ca-rich fluor-uvite followed sequentially by more Na-rich dravite.

The dominant external crystal forms of the trapiche tourmaline include the hexagonal prism *a* $\{11\bar{2}0\}$, the positive pyramids *r* $\{10\bar{1}1\}$ and *o* $\{02\bar{2}1\}$, and the negative pyramid *–r* $\{01\bar{1}1\}$. The trapiche pattern occurs when high concentrations of liquid and mineral inclusions are trapped along narrow growth boundaries between pyramidal and prismatic growth sectors, and where elongated channels or voids extend into the surrounding tourmaline sectors perpendicular to the dominant crystal forms mentioned above. They are chemically zoned with isomorphic substitutions of Ca by Na and Mg by Al (which is characteristic for tourmalines of the uvite-dravite solid-solution series); Na increases while Ca decreases from core to rim. However, at the boundaries between different growth sectors (forming the trapiche pattern), compositions were found with higher Na and lower Ca than in the adjacent pyramidal and prismatic growth sectors. The green coloration of the tourmaline is caused by minor amounts of V and Cr.

The article contains dozens of annotated color photos, illustrations, and graphical analyses that are helpful for understanding the complexities of the chemical and growth zoning. *ERB*

INSTRUMENTS AND TECHNIQUES

Detection and analysis of diamond fingerprinting feature and its application. X. Li, G. Huang [tshgl@tsinghua.edu.cn], Q. Li, and S. Chen, *Journal of Physics: Conference Series*, Vol. 277, 2011, pp. 1–9, http://dx.doi.org/10.1088/1742-6596/277/1/012018.

This article presents an innovative theoretical and tested model for fingerprinting faceted diamonds, and notes two major improvements over a space-frequency-based approach. The authors detail how a diamond's fingerprint is obtained by directing parallel light beams toward the table facet. Using an arrangement of concave-convex lenses, Fourier transform methods, and an efficient software interface, a unique spatial frequency spectral analysis of a diamond's surface structure of reflected light is computed—its "fingerprint."

The authors discuss key formulas for the superposition relationships between complex amplitude distributions on diffraction and back focal planes, the coaxial light intensity distributions, the actual mathematical model of the fingerprinting map, and the assessment and control of image signal-to-noise issues. The software platform is VC2003 (Visual Studio 2003) linking to the OpenCV library, which allows customization for real-time image collection and preview, analysis, and archiving with additional information (owner, carat weight, provenance, etc.), as well as background noise removal (to generate clearer fingerprints). The authors provide an algorithm for accurate analysis of diamond spectral data by a "radius comparison method," using compared sequences of mean square error (MSE) and maximum error (ME).

The model's multi-sampled robustness is tested by employing MSE and ME, which yields good specificity and space-invariance. In other words, there is minimal variance from positional changes of a diamond placed within the apparatus (measured on axes called *center translation invariance* and *rotation invariance*), resulting in reliable fingerprinting.

The usefulness of the findings is discussed in terms of a real-time, accurate, and relatively simple technology to aid in countering smuggling, theft, and other security issues where diamond fingerprinting is useful. *ERB*

Jade detection and analysis based on optical coherence tomography images. S. Chang [shoude.chang@nrc.ca], Y. Mao, G. Chang, and C. Flueraru, *Optical Engineering*, Vol. 49, No. 6, 2010, pp. 1–8, http://dx.doi.org/10.1117/1.3449112.

Optical coherence tomography (OCT) is a fundamentally new type of optical sensing technology that can perform high-resolution, cross-sectional sensing of the internal structure of materials. Advantages over other volume-sensing systems include: higher resolution, non-invasive noncontact, speed, fiber-optic delivery, and no harmful radiation. The micron-level resolution makes it unique among tomographic imaging technologies. Jade is almost translucent to IR wavelengths and has various types of internal textures. The textural features of various jades were analyzed using their OCT signals. Six parameters were used to numerically describe their texture patterns. 3-D volume data were generated through swept-source OCT with a depth resolution of 4 μm and penetration range of 5 mm. OCT can be used for the detection, classification, counterfeit recognition, and guided artistic carving of jade. *GL*

JEWELRY HISTORY

I vaghi di collana in pietra nella storia [Gemstone beads through history]. M. C. Venuti, A. Garuti, and G. Romiti. *Rivista Gemmologica Italiana*, Vol. 5, No. 3, 2010, pp. 197–212 [in Italian].

The authors survey the use of beads in jewelry. About 100,000 years ago, snail shells were used for bead chains, but 9,000 years ago they were replaced by quartz, followed by agate, chalcedony, jasper, and others. Parallelling human migration, beads spread from Africa to the Middle East, India, and eventually the rest of the world from East Asia to the Mediterranean Sea. Over the course of time, the methods of bead production (drilling, polishing, and dyeing) became increasingly sophisticated. An important production center is India, especially Khambar, where this ancient tradition lives on.

The authors also discuss different types of beads, ancient versus modern beads, and the identification of treatments and imitations. *RT*

JEWELRY RETAILING

Training helps sales force to sparkle. D. Pollitt, *Human Resource Management International Digest*, Vol. 19, No. 1, 2011, pp. 15–16.

British-based Aurum, a luxury jewelry retail chain, improved year-on-year sales by revamping its sales training from a product-based approach to one that developed customer interaction skills. The transformation encompassed the entire buying experience, not just the sales close. This meant listening to customers to gauge their needs and help them gain confidence in their decision before attempting to close. The program, developed by a consultant, consisted of a two-day e-learning module for all 1,600 employees, followed by support meetings with senior and regional management. *RS*

SYNTHETICS AND SIMULANTS

And now composite chalcedony. G. Choudhary [gagan@gjepcindia.com], *Gems & Jewellery*, Vol. 19, No. 4, 2010, pp. 28–30.

This article briefly reports on the examination and identification of three chalcedony composites held together in a polymer-based matrix. The specimens varied in color: dark green with a gold matrix, light green with a silvery white matrix, and orange with a silvery white matrix. These pieces, which were submitted to the author's gem testing laboratory for identification, underwent standard gemological testing as well as FTIR and EDXRF analysis. Key properties are listed, and the study concluded that these specimens are similar in nature to composite turquoise with metallic veins (described by the author in the Summer 2010 *G&G*, pp. 106–113). *MK*

Characterization of a new synthetic fancy yellow diamond. V. Rolandi, A. Brajkovic [anna.brajkovic@unimib.it], A. Giorgioni, A. Malossi, R. Scotti, *Gemmologie: Zeitschrift der Deutschen Gemmologischen Gesellschaft*, Vol. 60, No. 1–2, 2011, pp. 9–24.

Malossi Gemmecreate, an Italian company from Milan, is marketing faceted gem-quality yellow synthetic diamonds in the 1–2 ct range. This report provides some details of the crystal growth method and the results of gemological and spectroscopic measurements for identification purposes.

Malossi synthetic diamonds are produced in eastern Europe using an HPHT technique with a split-sphere or BARS press. After growth, they are annealed at high temperature and pressure. The growth method employs a truncated tetragonal bipyramidal growth cell rather than a cubic growth cell, to more closely approximate the crystal habit adopted during natural diamond formation, resulting in minimal weight loss during cutting. The exact growth process is a Malossi trade secret, but some details are revealed. The growth temperature ranges from 1360°C to 1680°C, at a pressure of 60–70 kbar. The flux is composed of alkali carbonates and the carbon source is pure graphite, to which nickel and other metal growth catalysts are added. The finished crystals weigh ~3.0 ct and take about 72 hours to grow. The post-growth processing for improving color and transparency includes heating the crystals to between 1800°C and 2000°C for 10–15 hours while cycling the pressure as high as 80 kbar.

Gemological characterization of the finished stones showed a specific gravity value identical to that of natural diamond, with uniform color and clarity ranging from IF to VS. The samples displayed cloud-like inclusions of oriented and arranged pinpoint and needle-like diamond crystals, weak anomalous double refraction, and uniform bright green UV fluorescence with a pattern common to synthetic diamonds grown with a nickel catalyst. Spectroscopic techniques employed included FTIR, UV-Vis-NIR, photoluminescence, and electron spin resonance spectroscopy as well as cathodoluminescence imaging. These techniques revealed characteristic nickel signatures and identified the synthetic diamonds as almost exclusively type IaA. *JS-S*

TREATMENTS

Diffusion of chromium in sapphire: The effects of electron beam irradiation. Y.-K. Ahn, J.-G. Seo, and J.-W. Park [jwpark@hanyang.ac.kr], *Journal of Crystal Growth*, Vol. 326, No. 1, 2011, pp. 45–49, http://dx.doi.org/10.1016/j.jcrysgro.2011.01.049.

This study evaluated chromium diffusion of sapphire using different treatment methods. Two samples were irradiated with 10 MeV of electrons at fluences of 2×10^{17} cm^{-2} for one hour. One of the samples was coated with Cr^{3+} prior to irradiation. Annealing experiments were performed on these, as well as an untreated and uncoated sapphire, at temperatures ranging from 1,773 to 1,923 K for 200 hours under an oxidation condition of 1 atm. The diffusion of chromium in sapphire was profiled using SEM-EDX spectroscopy, and Arrhenius equations for the diffusion coefficient were obtained.

Chromium penetrated deepest within the coated and electron beam–irradiated sapphire, followed by the uncoated electron beam–irradiated sample, and finally the uncoated non-irradiated sapphire. Photoluminescence spectroscopy showed that samples irradiated with electron beams had higher peak intensities than the non-irradiated sample, indicating a greater abundance of anion and cation vacancies. Irradiated samples therefore showed deeper diffusion of chromium. It also became evident that an even coating of chromium on the sapphire enhanced diffusion. *GL*

MISCELLANEOUS

Uplifting the Earth: The ethical performance of luxury jewelry brands. I. Doyle [idoyle@lifeworth.com] and J. Bendell, *Lifeworth Consulting*, June 2011, pp. 1–58, www.lifeworth.com/consult/wp-content/uploads/2011/06/UpliftingTheEarth.pdf.

Consumer concerns over the ethical sourcing of gemstones and precious metals have pushed brands to redefine their business practice. This is the first study to benchmark luxury jewelry brands on their corporate responsibility. Ten of them were analyzed for their ethical, social, and environmental performance, with particular attention on the ethical sourcing of raw materials. The brands, selected for their renown and focus on fine gemstones, provided a cross-section of this sector: Boucheron, Buccellati, Bulgari, Cartier, Chanel, Chopard, Graff, Harry Winston, Piaget, and Van Cleef & Arpels.

The study revealed that Boucheron and Cartier are the brands most active in addressing corporate responsibility throughout the supply chain, while the others are either inactive or only partially active. (Although not part of the study, Tiffany & Co. was commended for its practices.) By examining efforts of responsible jewelry pioneers, this report outlines a vision of ethical excellence in luxury jewelry where brands can "uplift the earth" by providing decent work, building community, and restoring environments.

In-depth analysis suggests that the industry has yet to genuinely integrate corporate responsibility as part of its strategy. Brands will need to broaden their focus to one that is opportunity-based, and move from risk management to ethical excellence. This report illustrates how greater corporate responsibility can shape organizational qualities, inspire new business approaches, and create opportunities to use materials that contribute to sustainable development. *Alexandra Martini*

JEWELS OF THE TRADE

Sooner or later, the world's most extraordinary gems will cross paths with

RAHUL KADAKIA.

Here, Christie's Senior VP, Head of Jewelry Americas, shares priceless insight into the jewelry business and the value of an expert education.

A master eye for gems ... born or made? Coming from four generations of jewelers undoubtedly piqued my interest in this great business. But one needs to constantly train their eye by looking at gems – the more you learn, the better you will be at identifying and pricing gems, as well as being an effective salesperson and well-rounded businessman.

Something most people don't know about you. GIA is what brought me to Christie's. After studying in Santa Monica, I attended a GIA Career Fair where I had my first interview with the company.

Ok. Definitely a story there? I started work when I was 17 and five years into it, I thought I knew pretty much everything there was to know ... until I enrolled at GIA. The Institute's meticulous training and high standards exposed me to a whole new world of expertise.

Ultimate sales edge ... emotion or expertise? Jewelry is an emotional shopping experience, but expertise plays a decisive role. It's wonderful to show people a brilliant diamond, but it means more when you can follow up with a skillful explanation of the 4Cs exemplified in that particular gem.

Lean economy. Less jewelry? At the nexus of the downturn in late 2008, we sold the Wittelsbach Blue Diamond for $24 million, a world record price back then for any gem ever sold at auction. When you have great gems and jewels, the money makes itself available.

Any advice to the up and coming? Don't lose the passion that brought you to this business, and above all, keep learning every day.

GIA gratefully acknowledges those who, for 80 years, have used our resources to further world expertise in gems. Invest in your success at **WWW.GIA.EDU**

GIA®